CHANNEL-IMPOSED FUSION: A SIMPLE YET EFFECTIVE METHOD FOR MEDICAL TIME SERIES CLASSIFICATION

Anonymous authors
Paper under double-blind review

ABSTRACT

Medical time series (MedTS) such as EEG and ECG are critical for clinical diagnosis, yet existing deep learning approaches often struggle with two key challenges: the misalignment between domain-specific physiological knowledge and generic architectures, and the inherent low signal-to-noise ratio (SNR) of MedTS. To address these limitations, we shift from a conventional model-centric paradigm toward a data-centric perspective grounded in physiological principles. We propose Channel-Imposed Fusion (CIF), a method that explicitly encodes causal inter-channel relationships by linearly combining signals under domain-informed constraints, thereby enabling interpretable signal enhancement and noise suppression. To further demonstrate the effectiveness of data-centric design, we develop a simple yet powerful model, Hidden-layer Mixed Bidirectional Temporal Convolutional Network (HM-BiTCN), which, when combined with CIF, consistently outperforms Transformer-based approaches on multiple MedTS benchmarks and achieves new state-of-the-art performance on general time series classification datasets. Moreover, CIF is architecture-agnostic and can be seamlessly integrated into mainstream models such as Transformers, enhancing their adaptability to medical scenarios. Our work highlights the necessity of rethinking MedTS classification from a data-centric perspective and establishes a transferable framework for bridging physiological priors with modern deep learning architectures. The complete source code supporting this study is publicly available at the following anonymous repository: anonymous link.

1 INTRODUCTION

Medical time series (MedTS) data, such as electroencephalogram (EEG) and electrocardiogram (ECG) signals, are widely used in clinical settings to monitor patient health and play a crucial role in diagnosing neurological and cardiovascular diseases Arif et al. (2024); Xiao et al. (2023); Zhu et al. (2025); Wang et al. (2024b; 2025b). Accurate classification of these signals enables early anomaly detection, personalized treatment, and optimized therapy planning, ultimately improving patient outcomes and healthcare efficiency Liu et al. (2024a); Tian et al. (2023). With advances in deep learning, CNN-based models like EEGNet Lawhern et al. (2018) can automatically extract informative features from raw signals, significantly improving classification performance.

In recent years, Transformer models Vaswani et al. (2017), originally inspired by the self-attention mechanism Bahdanau et al. (2014), have achieved remarkable progress in time series modeling, particularly in capturing long-range dependencies and global contextual information Liu et al. (2021); Zhou et al. (2021). By mapping sequential data into high-dimensional token embeddings, Transformers are able to implicitly model complex temporal dependencies. Despite their success across a wide range of time series tasks, applying Transformer architectures to MedTS classification still faces several challenges, which can be summarized as follows: **(1) Misalignment between domain-specific knowledge and generic architectures.** Mainstream time series models, such as Autoformer Wu et al. (2021), Crossformer Zhang & Yan (2022), and Reformer Kitaev et al. (2019), have demonstrated strong performance in general domains such as weather forecasting and finance. However, as illustrated in Fig. 1, these approaches fail to achieve comparable effectiveness in MedTS classification tasks. This raises the urgent question of how to enhance the applicability of general-purpose models

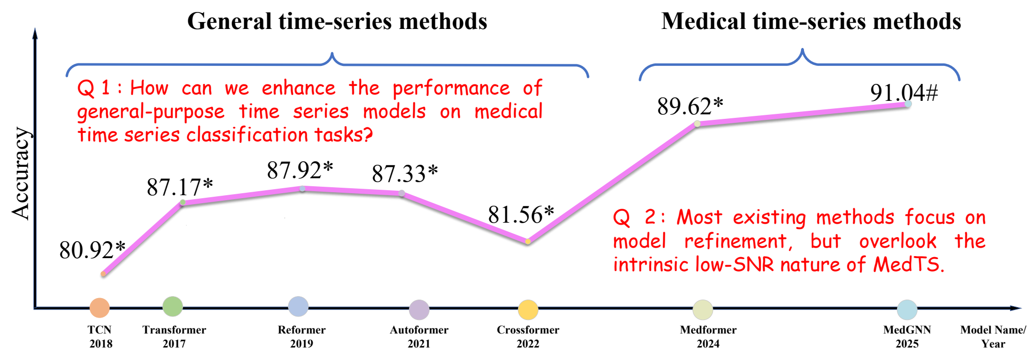

Figure 1: The results of various methods on the TDBrain dataset (EEG) are presented, where $*$ indicates results reported by *Medformer Wang et al. (2024a)*, and # indicates results reported by *MedGNN Fan et al. (2025)*. In addition, we highlight two main motivations of this work (Q1 and Q2).

in medical scenarios. Moreover, MedTS often encode critical physiological characteristics—for example, conduction delays across ECG leads Auricchio et al. (2014) and rhythmic synchrony in EEG signals Palva & Palva (2014); Fries (2015)—which inherently reflect *channel-level relationships*. Unfortunately, such physiological dependencies are rarely considered in generic time series modeling frameworks. **(2) Overemphasis on model optimization while neglecting the intrinsic low SNR of MedTS.** Unlike general-purpose time series tasks, MedTS are characterized by pronounced low-SNR conditions Del Rio et al. (2011); Sraitih et al. (2022); Sharma (2017); Mohd Apandi et al. (2020); Jia et al. (2024), where noise and artifacts can easily overshadow critical physiological features. In such conditions, complex Transformer architectures do not always succeed in stably extracting effective representations, while simpler models (e.g., TCNs Bai et al. (2018)) may also experience more severe performance degradation. Indeed, recent Transformer-based methods tailored for MedTS, such as MedGNN Fan et al. (2025) and Medformer Wang et al. (2024a), primarily rely on architectural innovations, yet they fall short in fundamentally addressing the low-SNR challenge. This raises a key question: should breakthroughs in MedTS classification come from increasingly complex architectures, or from more principled data processing and representation strategies?

To address the aforementioned limitations, we depart from the traditional *model-centric* paradigm that relies on increasingly complex architectures to capture temporal dependencies, and instead propose a **data-centric** approach grounded in the physiological properties of medical time series. Following this principle, we introduce the *Channel-Imposed Fusion (CIF)* method, which explicitly encodes prior causal structures into feature representations. Specifically, CIF constructs new features through a linear combination of signals from different channels:

$$x_{\text{new}} = ax + by, \tag{1}$$

where x and y denote signals from two distinct channels, and a and b are coefficients predefined based on domain knowledge. When a and b take fixed values, they are not learned directly from patient data, but instead derived from two domain-specific prior hypotheses: **(1) Physiological Coupling Hypothesis.** For ECG signals, when two leads are highly correlated (e.g., P-wave polarity and morphology are consistent Platonov (2012)), setting $a = b = 1$ achieves in-phase summation, thereby enhancing target signal components and improving the SNR. **(2) Noise Suppression Hypothesis.** In EEG recordings, ocular artifacts such as blinks often appear highly correlated in frontal electrodes Fp1 and Fp2 Croft & Barry (2000). To suppress such noise, we set $a = 1, b = -1$, applying a differential fusion strategy to cancel common-mode interference. Here, the coefficients a and b serve as symbolic encodings of interpretable physiological principles, rather than exact data-driven estimates. When treated as learnable parameters, they can be fine-tuned under symbolic constraints imposed by prior knowledge (e.g., enforcing $a > 0, b > 0$ under coupling, and $a > 0, b < 0$ under noise suppression). This design maintains the interpretability of directional relationships (e.g., signal enhancement or cancellation) while allowing the model to adaptively adjust the magnitude of each coefficient based on the training data.

To emphasize the importance of data-centric approaches, we deliberately designed a simple yet effective model—the Hidden-layer Mixed Bidirectional Temporal Convolutional Network (HM-BiTCN)—to demonstrate that excellent performance does not necessarily require model complexity. The combination of CIF and HM-BiTCN not only outperforms Transformer-based methods on multiple medical datasets but also achieves new state-of-the-art (SOTA) results on general time series classification benchmarks. More importantly, the CIF method is not limited to the HM-BiTCN architecture itself; it exhibits strong transferability and can be seamlessly integrated into existing Transformer architectures, enhancing their adaptability to MedTS data. Our main contributions are:

- **Proposal of Channel-Imposed Fusion (CIF).** We introduce CIF to explicitly model inter-channel relationships in medical time series, particularly suitable for signals with well-defined physiological structures such as EEG and ECG.
- **Design of HM-BiTCN based on CIF.** By integrating CIF into HM-BiTCN, our method consistently outperforms existing SOTA models across multiple publicly available medical and non-medical time series classification datasets.
- **Methodological transferability.** CIF is architecture-agnostic and can be seamlessly integrated into mainstream models such as Transformers, compensating for the limitations of traditional positional encodings in modeling channel-level correlations, and highlighting the paradigm shift from a *model-centric* to a *data-centric* perspective.

2 Related Work

Medical Time Series Classification. Medical time series analysis diverges fundamentally from general time series forecasting Wu et al. (2022a); Lu et al. (2024) by prioritizing pathological signature decoding over temporal extrapolation, with modalities like EEG Tang et al. (2021); Yang et al. (2023); Qu et al. (2020), ECG Xiao et al. (2023); Wang et al. (2023); Kiyasseh et al. (2021), and EMG [Xiong et al. (2021); Dai et al. (2022)] encoding distinct clinical semantics. Early methods were dominated by compact CNNs such as EEGNet Lawhern et al. (2018), which employs depthwise separable convolutions to efficiently extract spatio–temporal features while providing preliminary interpretability via feature-map visualization. Subsequently, temporal convolutional networks (TCNs) Bai et al. (2018); Lin et al. (2019) leveraging dilated causal convolutions achieved parallelizable computation and extended receptive fields, surpassing LSTM-based approaches Zhou et al. (2016); Shen & Lee (2016); Hochreiter & Schmidhuber (1997) on multiple medical signal classification benchmarks. Hybrid architectures such as EEG-Conformer Song et al. (2022) combined convolutional front-ends with Transformer self-attention to capture both local and global dependencies and enabled attention-based interpretability. More recently, fine-grained Transformer models such as Medformer Wang et al. (2024a) introduced cross-channel tokenization and dual-stage self-attention, setting new SOTA accuracy on several public datasets. The latest MedGNN Fan et al. (2025) further augments attention mechanisms with multi-resolution graph learning to jointly model spatial multi-scale channel dependencies and temporal dynamics.

Model-centric Transformer-based time series methods. In time series analysis, Transformer-based models learn complex dependencies through diversified architectural designs: the vanilla Transformer Vaswani et al. (2017) first introduced multi-head self-attention and sinusoidal positional encoding to model temporal correlations globally; Informer Zhou et al. (2021) employs ProbSparse attention to select key time steps and compress sequence length, thereby reducing the computational cost of long-range dependencies; Reformer Kitaev et al. (2019) incorporates Locality-Sensitive Hashing (LSH) to reduce attention complexity to $\mathcal{O}(L \log L)$, making it suitable for ultra-long sequences; Autoformer Wu et al. (2021) proposes an Auto-Correlation mechanism that aggregates periodic subsequences to enhance the implicit capture of cyclic patterns; FEDformer Zhou et al. (2022) performs seasonal–trend decomposition in the frequency domain and uses compressed Fourier coefficients to enable cross-frequency attention interactions; Crossformer Zhang & Yan (2022) designs a two-stage attention mechanism across time and feature dimensions to implicitly fuse multivariate spatiotemporal couplings; iTransformer Liu et al. (2024b) innovatively treats time steps as channel dimensions and applies standard attention to implicitly learn nonlinear inter-variable relationships; PatchTST Nie et al. (2023) segments continuous time steps into patch-based tokens and uses a combination of local and global attention to capture multi-scale temporal patterns; Medformer Wang et al. (2024a) introduces multi-granularity patch embeddings and cross-channel attention for medical signals, implicitly modeling the heterogeneous couplings of physiological metrics; and MedGNN Fan et al. (2025) combines graph attention with frequency-differential networks to incorporate medical topological priors into implicit spatiotemporal dependency learning.

3 METHOD

3.1 CHANNEL-IMPOSED FUSION

As shown in Eq. 1, a linear combination of two channels can incorporate physiological priors to construct more meaningful feature representations. For multi-channel data with N channels, we select two subsets X and Y, each containing $n \leq N$ channels. Each corresponding channel pair X_i and Y_i is linearly fused to produce

$$X_i^{\text{new}} = a_i X_i + b_i Y_i, \quad i = 1, 2, \ldots, n, \tag{2}$$

where a_i and b_i are the linear combination coefficients for the i-th pair of channels. Consequently, this multi-channel fusion scheme requires n coefficients a_i and n coefficients b_i in total. By leveraging physiological priors through such linear combinations across multiple channels, the model can enhance its capability to capture salient physiological patterns .

SNR Improvement via Linear Channel Fusion. Details in Appendix A Consider two observed signals $x_1 = s_1 + \epsilon_1$ and $x_2 = s_2 + \epsilon_2$, with zero-mean, mutually uncorrelated signal and noise components. The CIF module performs a linear combination $y = ax_1 + bx_2 = as_1 + bs_2 + a\epsilon_1 + b\epsilon_2$, whose output SNR can be expressed as $\text{SNR}_{\text{out}} = \text{Var}(as_1 + bs_2)/\text{Var}(a\epsilon_1 + b\epsilon_2)$.

In the simple case where the signals and noises have equal variances σ_s^2 and σ_ϵ^2, and correlations ρ and γ, this reduces to $\text{SNR}_{\text{out}} = \text{SNR}_{\text{in}} \cdot (a^2 + b^2 + 2ab\rho)/(a^2 + b^2 + 2ab\gamma)$. Maximizing this ratio yields two canonical modes: *cooperative mode* ($\rho > \gamma$) with $a = b$, which amplifies correlated signals, and *differential mode* ($\rho < \gamma$) with $a = -b$, which suppresses correlated noise.

In the general case where signal and noise variances are unequal and may both be correlated, let the signal vector $[s_1, s_2]^T$ and noise vector $[\epsilon_1, \epsilon_2]^T$ have covariance matrices $\mathbf{S} = \begin{bmatrix} \sigma_{s1}^2 & \rho\sigma_{s1}\sigma_{s2} \\ \rho\sigma_{s1}\sigma_{s2} & \sigma_{s2}^2 \end{bmatrix}$ and $\mathbf{N} = \begin{bmatrix} \sigma_{\epsilon 1}^2 & \gamma\sigma_{\epsilon 1}\sigma_{\epsilon 2} \\ \gamma\sigma_{\epsilon 1}\sigma_{\epsilon 2} & \sigma_{\epsilon 2}^2 \end{bmatrix}$, respectively, and let the linear combination coefficients be $\mathbf{w} = [a, b]^T$. The output SNR is then $\text{SNR}(\mathbf{w}) = (\mathbf{w}^T\mathbf{S}\mathbf{w})/(\mathbf{w}^T\mathbf{N}\mathbf{w})$. Taking the derivative with respect to $\mathbf{w}$ and setting it to zero yields the generalized eigenvalue problem $\mathbf{S}\mathbf{w} = \lambda\mathbf{N}\mathbf{w}$, where the eigenvalue λ represents an achievable SNR. In the two-channel case, λ satisfies the quadratic equation $A\lambda^2 + B\lambda + C = 0$, with $A = \sigma_{\epsilon 1}^2\sigma_{\epsilon 2}^2(1 - \gamma^2)$, $B = -\left(\sigma_{s1}^2\sigma_{\epsilon 2}^2 + \sigma_{s2}^2\sigma_{\epsilon 1}^2 - 2\rho\gamma\sigma_{s1}\sigma_{s2}\sigma_{\epsilon 1}\sigma_{\epsilon 2}\right)$, and $C = \sigma_{s1}^2\sigma_{s2}^2(1 - \rho^2)$. The maximum output SNR is therefore $\text{SNR}_{\max} = \lambda_{\max} = [-B + \sqrt{B^2 - 4AC}]/(2A)$, and the corresponding optimal coefficient ratio is $(b/a) = (\lambda_{\max}\sigma_{\epsilon 1}^2 - \sigma_{s1}^2)/(\rho\sigma_{s1}\sigma_{s2} - \lambda_{\max}\gamma\sigma_{\epsilon 1}\sigma_{\epsilon 2})$. This two-channel SNR maximization framework can be directly extended to multi-channel recordings by grouping channels into corresponding pairs (x_{i_k}, x_{j_k}), constructing for each pair the signal and noise covariance matrices $\mathbf{S}_k$ and $\mathbf{N}_k$, and solving $\mathbf{S}_k\mathbf{w}_k = \lambda_k\mathbf{N}_k\mathbf{w}_k$ to obtain the optimal fusion coefficients $\mathbf{w}_k = [a_k, b_k]^T$, which define the fused channel $y_k = a_k x_{i_k} + b_k x_{j_k}$. Such pairwise optimal linear fusion exploits inter-channel signal correlations while suppressing correlated noise, thereby achieving simultaneous SNR enhancement across all channels in a multi-channel system .

However, despite the fact that designing independent coefficients (a_i, b_i) for each channel pair can maximize physiological interpretability and enhance the signal-to-noise ratio, this approach still faces several practical challenges in real-world applications. The total number of parameters scales linearly with the number of channels, reaching $2n$, which can make parameter management and optimization cumbersome as n increases. Moreover, if the coefficients are not learnable, each pair must be manually adjusted, substantially increasing the workload and introducing potential human bias. In addition, when the coefficients are uncertain or need to be searched over a range of candidate values, the number of possible configurations grows exponentially (i.e., K^{2n} for K candidate values per coefficient), rendering exhaustive optimization practically infeasible.

To alleviate these issues, we adopt a simplified strategy in which a single coefficient a is applied uniformly to the first n channels and a single coefficient b is applied to the remaining n channels, reducing the total number of parameters from $2n$ to 2. This substantially decreases the manual adjustment and computational cost while retaining the core advantages of linear fusion. The simplified fusion can be expressed as

$$X_i^{\text{new}} = aX_i + bY_i, \quad i = 1, \ldots, n. \tag{3}$$

Although this strategy significantly reduces the parameter space and improves practical usability, it comes with a trade-off: replacing pairwise coefficients (a_i, b_i) with global coefficients (a, b) reduces micro-level interpretability and may limit the ability to selectively enhance high-signal channels. Overall, this design provides a practical compromise between physiological fidelity, parameter efficiency, and computational feasibility. For applications that require more fine-grained modeling, intermediate strategies such as group-wise coefficients or learnable parameters can be employed to balance interpretability and parameter efficiency.

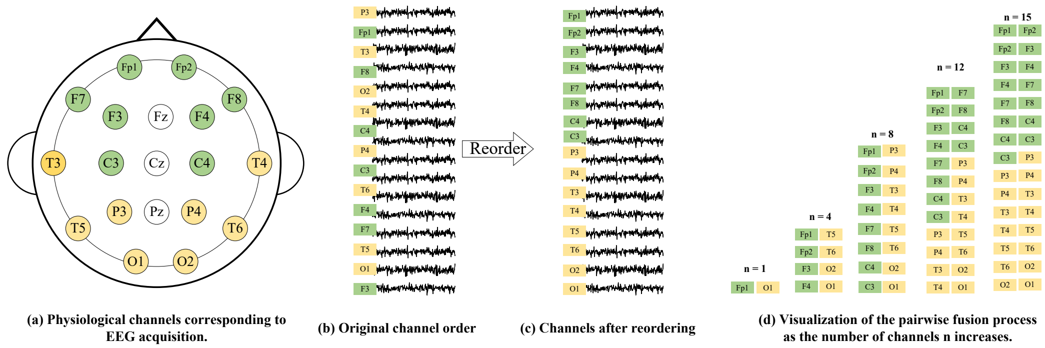

Figure 2: Reorders the channels , placing electrodes from the same functional region adjacently along the input dimension to create an “functional region fusion” input layout. Panel (d) visualizes the pairwise channel fusion process as the number of channels n varies.

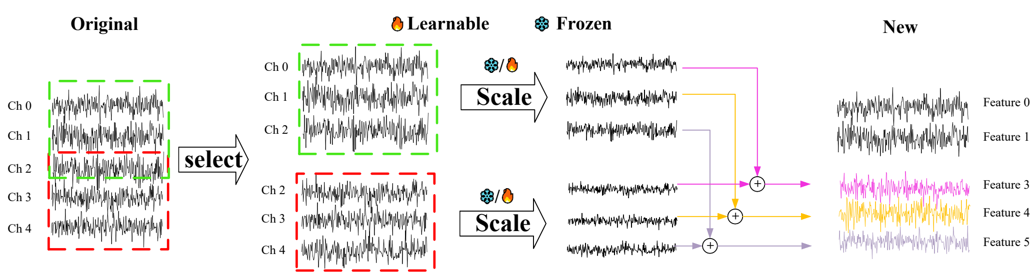

Figure 3: The implementation process of the Channel-Imposed Fusion method.

To align with the use of global coefficients (a, b), the subsequent stage of the CIF module reorders channels according to physiological priors, ensuring that linear fusion operates on a physiologically meaningful sequence and preserves functional relationships. In the first step, input channels are reordered as shown in Figure 2(b) to explicitly encode the physiological priors depicted in Figure 2(a). For EEG, channels are grouped by functional regions following the international 10–20 system Klem (1999), with anterior regions (frontopolar and frontal) placed at the beginning and posterior regions (parietal and occipital) at the end, while preserving local spatial neighborhoods within each region as much as possible. This "anterior-to-posterior" ordering is independent of specific electrode montages, allowing application across datasets and enhancing the capture of spatial patterns related to the brain’s anterior–posterior organization. For ECG, channels are grouped according to cardiac physiology: limb leads (I, II, III) and augmented leads (aVR, aVL, aVF) are placed first, precordial leads (V1–V6) in the middle, and other derived or vector leads (Vx, Vy, Vz) last. The precordial and vector leads roughly follow the thoracic spatial trajectory—from proximal to distal, right to left, and anterior to posterior—ensuring adjacent placement of leads capturing related cardiac activity, thereby enabling effective fusion across functional regions or lead groups. This process, referred to as *functional region fusion* (FRF), allows the CIF module to fully exploit cross-region spatial dependencies.

In Figure 2 (d), we illustrate the specific physiological channel fusion relationships as the number of channels n varies; for clarity, Figure 3 provides a simplified schematic of this process. Specifically, the anterior and posterior brain regions are first arranged according to physiological order, and then the first n channels are fused with the last n channels. When n is less than half of the total number of channels, fusion occurs across different functional regions; when n exceeds half, fusion occurs within the same functional region. This approach relies on only a few tunable parameters—n, a, and b—which control the number of channels affected by the CIF module. As n increases, more channels are influenced while maintaining physiological diversity across channels. This flexible fusion strategy provides a foundation for systematically exploring different channel subsets and integrating additional physiological features, while also supporting subsequent parameter optimization.

3.2 HM-BiTCN Structure Design and Theoretical Analysis

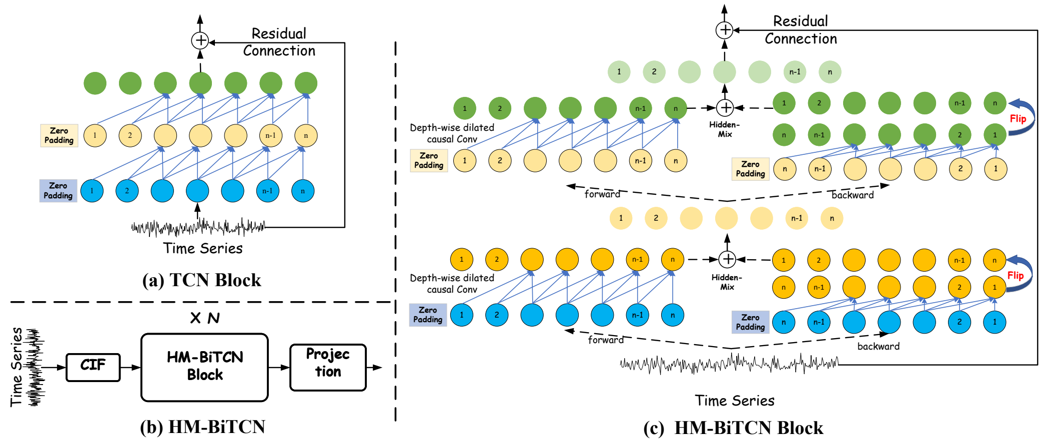

Figure 4: HM-BiTCN Architecture Diagram.

To demonstrate the advantages of data-centric approaches and to show that simple models can achieve strong performance, as illustrated in Figure 4 (a), the conventional TCN only models unidirectional causal relationships in time series. In contrast, our proposed HM-BiTCN (Figure 4 (c)) extends the traditional TCN by introducing bidirectional feature mixing, allowing each layer to capture both forward and backward temporal dependencies. This design is complementary to CIF's enhancement along the channel dimension: CIF focuses on capturing inter-channel spatial relationships and improving the signal-to-noise ratio, while HM-BiTCN strengthens feature extraction along the temporal dimension. The combined enhancement across both channel and temporal dimensions enables CIF+HM-BiTCN to more fully exploit the information contained in the data, achieving superior performance. Importantly, when the parameters a and b in CIF are set to be learnable, they are optimized jointly with HM-BiTCN's structural parameters in an end-to-end training process, thereby enabling unified channel- and time-domain feature enhancement. For further details, please refer to Appendix D and Appendix E.

4 Experiments

Medical Time Series Datasets. (1) **APAVA** Escudero et al. (2006) is an EEG dataset where each sample is assigned a binary label indicating whether the subject has Alzheimer's disease. (2) **TDBrain** van Dijk et al. (2022) is an EEG dataset with a binary label assigned to each sample, indicating whether the subject has Parkinson's disease. (3) **ADFTD** Miltiadous et al. (2023b;a) is an EEG dataset with a three-class label for each sample, categorizing the subject as Healthy, having Frontotemporal Dementia, or Alzheimer's disease. (4) **PTB** PhysioBank (2000) is an ECG dataset where each sample is labeled with a binary indicator of Myocardial Infarction. (5) **PTB-XL** Wagner et al. (2020) is an ECG dataset with a five-class label for each sample, representing various heart conditions. Table 5 provides information on the processed datasets.The data processing methodology is the same as that of Medformer Wang et al. (2024a) and MedGNN Fan et al. (2025).

Baselines. We compare with 12 state-of-the-art time series transformer methods: Autoformer Wu et al. (2021), Crossformer Zhang & Yan (2022), FEDformer Zhou et al. (2022), Informer Zhou et al. (2021), iTransformer Liu et al. (2024b), MTST Zhang et al. (2024), Nonformer Liu et al. (2022), PatchTST Nie et al. (2023), Reformer Kitaev et al. (2019), vanilla Transformer Vaswani et al. (2017), Medformer Wang et al. (2024a), MedGNN Fan et al. (2025).

Implementation. We employ six evaluation metrics: accuracy, precision (macro-averaged), recall (macro-averaged), F1 score (macro-averaged), AUROC (macro-averaged), and AUPRC (macro-averaged). The training process is conducted with five random seeds (41-45) on fixed training, validation, and test sets to compute the mean and standard deviation of the models. All experiments were conducted using an NVIDIA RTX 3090 GPU and implemented with PyTorch version 1.11.0 Paszke et al. (2017). Following Medformer Wang et al. (2024a) and MedGNN Fan et al. (2025), we consider two dataset partitioning strategies: (i) **Subject-Dependent Split**, where samples from the same subject may appear in both training and test sets, potentially causing information leakage; and (ii) **Subject-Independent Split**, where each subject appears only in one of the train, validation, or test sets, simulating real-world diagnostic scenarios while introducing inter-subject variability challenges. The model is trained to minimize the supervised loss $\mathcal{L} = \frac{1}{N}\sum_{i=1}^{N} \ell(\hat{y}_i, y_i)$, where $\ell(\hat{y}_i, y_i)$ measures the discrepancy between the predicted labels $\hat{y}_i$ and the ground-truth labels y_i. Specifically, the encoder $f_\theta : \mathbb{R}^{T\times C} \to \mathbb{R}^d$ maps each input x_i to a latent representation $h_i = f_\theta(x_i)$, which is then passed to the classifier g_ϕ to produce the prediction $\hat{y}_i = g_\phi(h_i)$.

4.1 Results of Subject-Dependent

Table 1: **Results of Subject-Dependent Setup.** Results of the ADFTD dataset under this setup are presented here.The best result is highlighted in **bold**, and the second-best is underlined.

Datasets	Models	Accuracy ↑	Precision ↑	Recall ↑	F1 score ↑	AUROC ↑	AUPRC ↑
ADFTD (3-Classes) Reported	**Autoformer**	87.83±1.62	87.63±1.66	87.22±1.97	87.38±1.79	96.59±0.88	93.82±1.64
	Crossformer	89.35±1.32	89.00±1.44	88.79±1.37	88.88±1.40	97.52±0.58	95.45±1.03
	FEDformer	77.63±2.37	76.76±2.17	76.68±2.48	76.60±2.46	91.67±1.34	84.94±2.11
	Informer	90.93±0.90	90.74±0.71	90.50±1.14	90.60±0.94	98.19±0.27	96.51±0.49
	iTransformer	64.90±0.25	62.53±0.27	62.21±0.26	62.25±0.33	81.52±0.29	68.87±0.49
	MTST	65.08±0.69	63.85±0.80	62.71±0.64	63.03±0.58	81.36±0.56	69.34±0.89
	Nonformer	96.12±0.47	95.94±0.56	95.99±0.38	95.96±0.47	99.59±0.09	99.08±0.16
	PatchTST	66.26±0.40	65.08±0.41	64.97±0.51	64.95±0.42	83.07±0.45	71.70±0.61
	Reformer	91.51±1.75	91.15±1.79	91.65±1.56	91.14±1.83	98.85±0.35	97.88±0.60
	Transformer	97.00±0.43	96.87±0.53	96.86±0.36	96.86±0.44	99.75±0.04	99.42±0.07
	Medformer	97.62±0.34	97.53±0.33	97.48±0.40	97.50±0.36	99.83±0.05	99.62±0.12
	MedGNN	98.42±0.04	98.31±0.02	98.29±0.05	98.30±0.12	99.93±0.11	-
	Medformer + CIF	<u>98.87±0.26</u>	<u>98.77±0.27</u>	<u>98.86±0.27</u>	<u>98.81±0.27</u>	<u>99.96±0.01</u>	<u>99.92±0.03</u>
	MedGNN + CIF	**99.60±0.09**	**99.60±0.11**	**99.58±0.09**	**99.59±0.10**	**99.99±0.01**	**99.97±0.01**

Following Medformer Wang et al. (2024a), in this setup, the training, validation, and test sets are split at the sample level. All samples from all subjects are randomly shuffled and assigned to the three sets according to a predetermined ratio, so that samples from the same subject may appear simultaneously in the training, validation, and test sets. This setup has limited applicability for MedTS-based disease diagnosis in real-world scenarios and is typically used to quickly assess whether the dataset exhibits cross-subject features. Results obtained under this setup are generally much higher than those from the subject-independent setup, reflecting the upper bound of the dataset's learnability.

We reproduced 12 baselines. Table 1 lists their reported results, and Table 10 in Appendix I shows our reproduced results. Experimental results show that integrating the CIF method into MedGNN and Medformer outperforms existing approaches, fully demonstrating its effectiveness and superiority.

4.2 Results of Subject-Independent

Following Medformer Wang et al. (2024a), in this setup, the training, validation, and test sets are split based on subjects. All subjects and their corresponding samples are assigned to the training, validation, and test sets according to a predetermined ratio or subject IDs, ensuring that samples from the same subject appear in only one of these sets. This simulates real-world MedTS-based disease diagnosis, aiming to train a model on subjects with known labels and then test it on unseen subjects to determine whether they have a specific disease. All five datasets are evaluated using this setup.

Table 2: **Results of Subject-Independent Setup.** The results we compare include those reported by Medforme Wang et al. (2024a) and MedGNN Fan et al. (2025). Additionally, we have reproduced all the methods in the Table 11 to ensure a **fairer comparison**.The best result is highlighted in **bold**, and the second-best is underlined.

Datasets	Models	Accuracy ↑	Precision ↑	Recall ↑	F1 score ↑	AUROC ↑	AUPRC ↑
APAVA (2-Classes) Reported	**Autoformer**	68.64±1.82	68.48±2.10	68.77±2.27	68.06±1.94	75.94±3.61	74.38±4.05
	Crossformer	73.77±1.95	79.29±4.36	68.86±1.70	68.93±1.85	72.39±3.33	72.05±3.65
	FEDformer	74.94±2.15	74.59±1.50	73.56±3.55	73.51±3.39	83.72±1.97	82.94±2.37
	Informer	73.11±4.40	75.17±6.06	69.17±4.56	69.47±5.06	70.46±4.91	70.75±5.27
	iTransformer	74.55±1.66	74.77±2.10	71.76±1.72	72.30±1.79	85.59±1.55	84.39±1.57
	MTST	71.14±1.59	79.30±0.97	65.27±2.28	64.01±3.16	68.87±2.34	71.06±1.60
	Nonformer	71.89±3.81	71.80±4.58	69.44±3.56	69.74±3.84	70.55±2.96	70.78±4.08
	PatchTST	67.03±1.65	78.76±1.28	59.91±2.02	55.97±3.10	65.65±0.28	67.99±0.76
	Reformer	78.70±2.00	82.50±3.95	75.00±1.61	75.93±1.82	73.94±1.40	76.04±1.14
	Transformer	76.30±4.72	77.64±5.95	73.09±5.01	73.75±5.38	72.50±6.60	73.23±7.60
	Medformer	78.74±0.64	81.11±0.84	75.40±0.66	76.31±0.71	83.20±0.91	83.66±0.92
	MedGNN	82.60±0.35	**87.70±0.22**	78.93±0.09	80.25±0.16	85.93±0.26	-
	HM-BiTCN + CIF	**86.30±1.05**	**86.16±1.09**	**85.47±1.12**	**85.71±1.09**	**94.26±0.54**	**94.42±0.49**
TDBrain (2-Classes) Reported	**Autoformer**	87.33±3.79	88.06±3.56	87.33±3.79	87.26±3.84	93.81±2.26	93.32±2.42
	Crossformer	81.56±2.19	81.97±2.19	81.56±2.19	81.50±2.20	91.20±1.78	91.51±1.71
	FEDformer	78.13±1.98	78.52±1.91	78.13±1.98	78.04±2.01	86.56±1.86	86.48±1.99
	Informer	89.02±2.50	89.43±2.14	89.02±2.50	88.98±2.54	96.64±0.68	96.75±0.63
	iTransformer	74.67±1.06	74.71±1.06	74.67±1.06	74.65±1.06	83.37±1.14	83.73±1.27
	MTST	76.96±3.76	77.24±3.59	76.96±3.76	76.88±3.83	85.27±4.46	82.81±5.64
	Nonformer	87.88±2.48	88.86±1.84	87.88±2.48	87.78±2.56	97.05±0.68	96.99±0.68
	PatchTST	79.25±3.79	79.60±4.09	79.25±3.79	79.20±3.77	87.95±4.96	86.36±6.67
	Reformer	87.92±2.01	88.64±1.40	87.92±2.01	87.85±2.08	96.30±0.54	96.40±0.45
	Transformer	87.17±1.67	87.99±1.68	87.17±1.67	87.10±1.68	96.28±0.92	96.34±0.81
	Medformer	89.62±0.81	89.68±0.78	89.62±0.81	89.62±0.81	96.41±0.35	96.51±0.33
	MedGNN	91.04±0.09	91.15±0.12	91.04±0.20	91.04±0.08	96.74±0.04	-
	HM-BiTCN + CIF	**93.13±1.41**	**93.33±1.37**	**93.13±1.41**	**93.12±1.42**	**98.62±0.66**	**98.68±0.63**
ADFTD (3-Classes) Reported	**Autoformer**	45.25±1.48	43.67±1.94	42.96±2.03	42.59±1.85	61.02±1.82	43.10±2.30
	Crossformer	50.45±2.31	45.57±1.63	45.88±1.82	45.50±1.70	66.45±2.03	48.33±2.05
	FEDformer	46.30±0.59	46.05±0.76	44.22±1.38	43.91±1.37	62.62±1.75	46.11±1.44
	Informer	48.45±1.96	46.54±1.68	46.06±1.84	45.74±1.38	65.87±1.27	47.60±1.30
	iTransformer	52.60±1.59	46.79±1.27	47.28±1.29	46.79±1.13	67.26±1.16	49.53±1.21
	MTST	45.60±2.03	44.70±1.33	45.05±1.30	44.31±1.74	62.50±0.81	45.16±0.85
	Nonformer	49.95±1.05	47.71±0.97	47.46±1.50	46.96±1.35	66.23±1.37	47.33±1.78
	PatchTST	44.37±0.95	42.40±1.13	42.06±1.48	41.97±1.37	60.08±1.50	42.49±1.79
	Reformer	50.78±1.17	49.64±1.49	49.89±1.67	47.94±0.69	69.17±1.58	51.73±1.94
	Transformer	50.47±2.14	49.13±1.83	48.01±1.53	48.09±1.59	67.93±1.59	48.93±2.02
	Medformer	53.27±1.54	51.02±1.57	50.71±1.55	50.65±1.51	70.93±1.19	51.21±1.32
	MedGNN	56.12±0.11	55.07±0.09	55.47±0.34	55.00±0.24	74.68±0.33	-
	HM-BiTCN + CIF	**58.56±0.93**	**55.65±0.81**	**55.86±0.79**	**55.42±0.82**	**76.07±0.59**	**59.75±0.67**
PTB (2-Classes) Reported	**Autoformer**	73.35±2.10	72.11±2.89	63.24±3.17	63.69±3.84	78.54±3.48	74.25±3.53
	Crossformer	80.17±3.79	85.04±1.83	71.25±6.29	72.75±7.19	88.55±3.45	87.31±3.25
	FEDformer	76.05±2.54	77.58±3.61	66.10±3.55	67.14±4.37	85.93±4.31	82.59±5.42
	Informer	78.69±1.68	82.87±1.02	69.19±2.90	70.84±3.47	92.09±0.53	90.02±0.60
	iTransformer	83.89±0.71	88.25±1.18	76.39±1.01	79.06±1.06	91.18±1.16	90.93±0.98
	MTST	76.59±1.90	79.88±1.90	66.31±2.95	67.38±3.71	86.86±2.75	83.75±2.84
	Nonformer	78.66±0.49	82.77±0.86	69.12±0.87	70.90±1.00	89.37±2.51	86.67±2.38
	PatchTST	74.74±1.62	76.94±1.51	63.89±2.71	64.36±3.38	88.79±0.91	83.39±0.96
	Reformer	77.96±2.13	81.72±1.61	68.20±3.35	69.65±3.88	91.13±0.74	88.42±1.30
	Transformer	77.37±1.02	81.84±0.66	67.14±1.80	68.47±2.19	90.08±1.76	87.22±1.68
	Medformer	83.50±2.01	85.19±0.94	77.11±3.39	79.18±3.31	92.81±1.48	90.32±1.54
	MedGNN	84.53±0.28	87.35±0.45	77.90±0.66	80.40±0.62	93.31±0.46	-
	HM-BiTCN + CIF	**88.29±1.45**	**90.66±1.48**	**83.21±2.02**	**85.59±1.96**	**94.28±0.93**	**93.78±1.11**
PTB-XL (5-Classes) Reported	**Autoformer**	61.68±2.72	51.60±1.64	49.10±1.52	48.85±2.27	82.04±1.44	51.93±1.71
	Crossformer	73.30±0.14	65.06±0.35	**61.23±0.33**	62.59±0.14	90.02±0.06	67.43±0.22
	FEDformer	57.20±9.47	52.38±6.09	49.04±7.26	47.89±8.44	82.13±4.17	52.31±7.03
	Informer	71.43±0.32	62.64±0.60	59.12±0.47	60.44±0.43	88.65±0.09	64.76±0.17
	iTransformer	69.28±0.22	59.59±0.45	54.62±0.18	56.20±0.19	86.71±0.10	60.27±0.21
	MTST	72.14±0.27	63.84±0.72	60.01±0.81	61.43±0.38	88.97±0.33	65.83±0.51
	Nonformer	70.56±0.55	61.57±0.66	57.75±0.72	59.10±0.66	88.32±0.36	63.40±0.79
	PatchTST	73.23±0.25	65.70±0.64	60.82±0.76	**62.61±0.34**	89.74±0.19	67.32±0.22
	Reformer	71.72±0.43	63.12±1.02	59.20±0.75	60.69±0.18	88.80±0.24	64.72±0.47
	Transformer	70.59±0.44	61.57±0.65	57.62±0.35	59.05±0.25	88.21±0.16	63.36±0.29
	Medformer	72.87±0.23	64.14±0.42	60.60±0.46	62.02±0.37	89.66±0.13	66.39±0.22
	MedGNN	**73.87±0.18**	**66.26±0.29**	61.13±0.29	62.54±0.20	90.21±0.15	-
	HM-BiTCN + CIF	73.73±0.30	65.41±0.67	60.70±1.08	61.89±0.91	**90.53±0.22**	**67.75±0.75**

Table 2 presents the results **reported** by various methods in the subject-independent setting, while Table 11 shows the results of our **reproduction** of these methods. Our method achieves the highest average scores across six metrics on four out of the five datasets. On PTB-XL, our method tops AUROC and AUPRC and ranks second in Accuracy versus reported results, and ranks first in Accuracy, Precision, AUROC, AUPRC, and second in Recall versus our reproduced results. Additionally, it is worth noting that in the subject-independent, the F1 score of ADFTD is 55.42%, which is significantly lower than the 99.59% achieved in the subject-dependent setup. This comparison highlights the challenges of the subject-independent setup, **which better simulates real-world scenarios**.

4.2.1 Efficiency Analysis

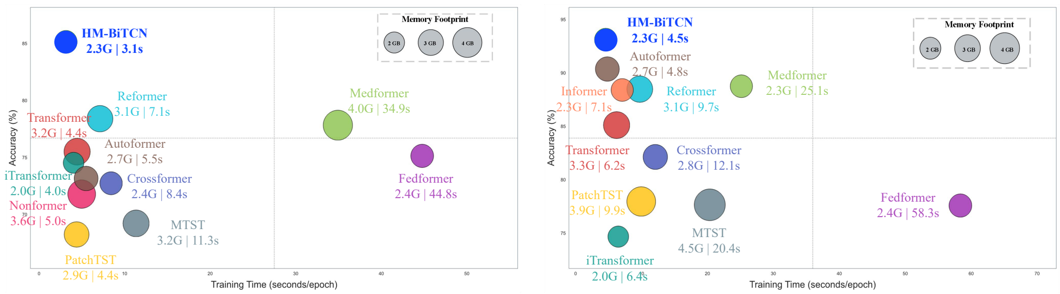

(a) APAVA (b) TDBRAIN

Figure 5: Effectiveness and efficiency on two datasets (subject-based).

We evaluate the model efficiency in terms of accuracy, training speed, and memory footprint using two datasets: APAVA and TDBRAIN. In Figure 5, a marker closer to the upper-left corner indicates higher accuracy and faster training speed, while a smaller marker area corresponds to lower memory usage. The results show that HM-BiTCN achieves the best overall performance among all baseline methods, demonstrating its high efficiency and reliability across different application scenarios.

4.3 Ablation Study

(1) Effectiveness of CIF: Table 3 demonstrates the excellent performance of combining HM-BiTCN with CIF, confirming the compatibility of the HM-BiTCN with CIF. See Appendix J.1 for details. Appendix F presents ablation studies on the HM-BiTCN architecture, the performance improvements from integrating CIF into its components, and comparisons with the vanilla TCN structure.

Table 3: Exploring the Integration of HM-BiTCN Structure with CIF.

Datasets	APAVA		ADFTD		PTB		TDBRAIN		PTB-XL	
Metrics	Accuracy	F1 Score	Accuracy	F1 Score	Accuracy	F1 Score	Accuracy	F1 Score	Accuracy	F1 Score
w/ CIF	86.30±1.05	85.71±1.09	58.56±0.93	55.42±0.82	88.29±1.45	85.59±1.96	93.13±1.41	93.12±1.42	73.73±0.30	61.89±0.91
w/o CIF	82.49±1.40	81.60±1.39	52.05±2.22	49.48±2.70	81.87±1.87	75.84±3.20	84.90±2.60	84.76±2.74	72.92±0.88	61.49±0.82
Improvement	**+3.81%**	**+4.11%**	**+6.51%**	**+5.94%**	**+6.42%**	**+9.75%**	**+8.23%**	**+8.36%**	**+0.81%**	**+0.40%**

(2) Hyperparameter Transfer and Adaptation: We evaluate the transferability of key hyperparameters (e.g., a, b, n) from HM-BiTCN to other models. If transferred settings underperform, we further fine-tune them for adaptation. See Appendices J.2 and J.3. Figure 6 illustrates the outstanding performance of CIF when combined with other models.

(3) Exploring alternative fusion strategies: In Appendix G, we systematically evaluate several fusion approaches, including the fusion using only the Fp1 and Fp2 channels mentioned in the Introduction, the fusion of a reduced set of left-right symmetric channels, and our further exploration using canonical correlation analysis (CCA) for fusion. The experimental results demonstrate that CIF exhibits strong scalability, maintaining performance advantages across different fusion strategies.

(4)Results on general time series classification tasks

To evaluate the performance of our method on general time series, we follow the design of Medformer Wang et al. (2024a) and test it on two human activity recognition (HAR) datasets: FLAAP(13,123 samples, 10 classes) Kumar & Suresh (2022) and UCI-HAR(10,299 samples, 6 classes) Anguita et al. (2013). Additionally, to conduct a more comprehensive evaluation, following TimeMixer++ Wang et al. (2025a), we used 10 multivariate datasets from the UEA Time Series Classification Archive (2018) for the assessment of classification tasks.

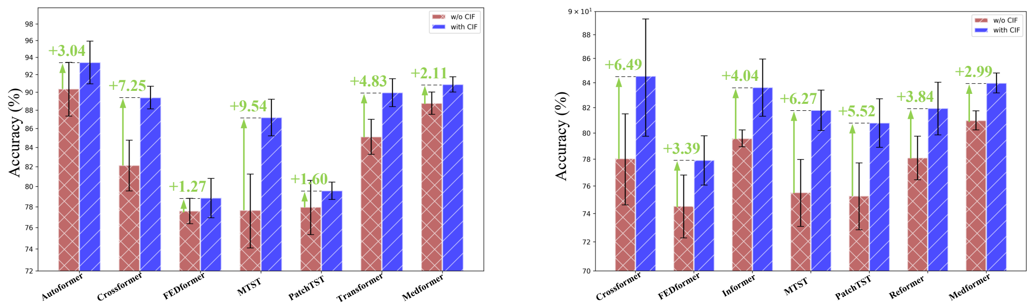

(a) TDBRAIN-Subject (b) PTB-Subject

Figure 6: The improvements achieved by various baselines when combined with the CIF method.

Table 4: Performance on the HAR and UCI-HAR non-medical time series datasets. Bold numbers indicate the best results. * denotes the results reported by Medformer.

Dataset / Metric		Crossformer * Zhang & Yan (2022)	Reformer * Kitaev et al. (2019)	Transformer * Vaswani et al. (2017)	TCN * Bai et al. (2018)	ModernTCN * Luo & Wang (2024)	Mamba * Gu & Dao (2023)	Medformer * Wang et al. (2024a)	HM-BiTCN (This work)	HM-BiTCN + CIF (This work)
FLAAP *(10 Classes)*	Accuracy	75.84±0.52	71.65±1.27	74.96±1.25	66.48±1.66	74.80±0.96	64.87±2.78	76.44±0.64	76.08±0.81	**76.82**±1.32
	F1 Score	75.52±0.66	71.14±1.45	74.49±1.39	65.29±1.74	74.35±0.85	64.14±2.70	76.25±0.65	75.54±0.94	**76.39**±1.18
UCI-HAR *(6 Classes)*	Accuracy	89.74±1.08	88.44±2.02	88.86±1.65	93.08±0.95	91.44±1.01	87.78±1.10	91.65±0.74	93.72±0.73	**93.78**±0.32
	F1 Score	89.70±1.10	88.34±1.98	88.80±1.67	93.19±0.88	91.47±0.98	87.72±1.10	91.61±0.75	93.69±0.76	**93.74**±0.34

As shown in Table 4, and Fig. 7, the combination of HM-BiTCN and CIF consistently outperforms other architectures in general time series classification, achieving a 5.5% improvement over the original TCN and surpassing current SOTA methods. Although CIF was originally designed for MedTS, its integration with HM-BiTCN significantly outperforms Transformer-based models in both medical and general time series classification tasks, demonstrating the effectiveness of our data-centric approach.

The results in Tables 4, 9, 3 and Figure 6 show that CIF achieves significant improvements in MedTS classification, while the gains on non-medical data are relatively limited. This observation further demonstrates that a data-driven perspective is particularly effective for MedTS classification with physiological characteristics.

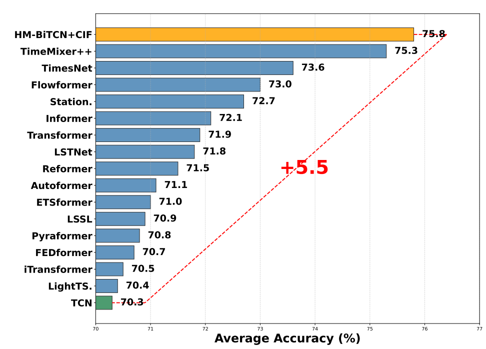

Figure 7: Average accuracy of various methods on the UEA dataset. More details in Appendix H.

5 Conclusion

In this work, we propose a simple and effective method for medical time series classification, *Channel-Imposed Fusion* (CIF), which explicitly encodes physiological causal relationships between channels in the feature representations while enhancing the SNR of the original signals. Combined with the simple HM-BiTCN architecture, CIF surpasses existing SOTA methods on multiple medical datasets and performs strongly on general time series classification tasks, demonstrating that data-centric design enables simple models to outperform more complex architectures. More importantly, CIF exemplifies the shift from the traditional *model-centric* paradigm to a *data-centric* perspective, where structured representations grounded in physiological priors are both efficient and scalable for medical time series classification. CIF also exhibits strong transferability and can be seamlessly integrated into mainstream models such as Transformers, enhancing their applicability in medical scenarios. We hope this work encourages the community to reconsider the core of medical time series classification: should it be driven primarily by *data-centric strategies* or by *model-centric design* or both?

REFERENCES

Davide Anguita, Alessandro Ghio, Luca Oneto, Xavier Parra, Jorge Luis Reyes-Ortiz, et al. A public domain dataset for human activity recognition using smartphones. In *Esann*, volume 3, pp. 3, 2013.

Aniqa Arif, Yihe Wang, Rui Yin, Xiang Zhang, and Ahmed Helmy. Ef-net: Mental state recognition by analyzing multimodal eeg-fnirs via cnn. *Sensors*, 24(6):1889, 2024.

Angelo Auricchio, Joost Lumens, and Frits W Prinzen. Does cardiac resynchronization therapy benefit patients with right bundle branch block: cardiac resynchronization therapy has a role in patients with right bundle branch block. *Circulation: Arrhythmia and Electrophysiology*, 7(3): 532–542, 2014.

Anthony Bagnall, Hoang Anh Dau, Jason Lines, Michael Flynn, James Large, Aaron Bostrom, Paul Southam, and Eamonn Keogh. The uea multivariate time series classification archive, 2018. *arXiv preprint arXiv:1811.00075*, 2018.

Dzmitry Bahdanau, Kyunghyun Cho, and Yoshua Bengio. Neural machine translation by jointly learning to align and translate. *arXiv preprint arXiv:1409.0473*, 2014.

Shaojie Bai, J Zico Kolter, and Vladlen Koltun. An empirical evaluation of generic convolutional and recurrent networks for sequence modeling. *arXiv preprint arXiv:1803.01271*, 2018.

Rodney J Croft and Robert J Barry. Removal of ocular artifact from the eeg: a review. *Neurophysiologie Clinique/Clinical Neurophysiology*, 30(1):5–19, 2000.

Yuanchao Dai, Jing Wu, Yuanzhao Fan, Jin Wang, Jianwei Niu, Fei Gu, and Shigen Shen. Mseva: A musculoskeletal rehabilitation evaluation system based on emg signals. *ACM Transactions on Sensor Networks*, 19(1):1–23, 2022.

Abhimanyu Das, Weihao Kong, Andrew Leach, Shaan K Mathur, Rajat Sen, and Rose Yu. Long-term forecasting with tiDE: Time-series dense encoder. *Transactions on Machine Learning Research*, 2023. ISSN 2835-8856.

B Aldecoa Sanchez Del Rio, T Lopetegi, and I Romero. Assessment of different methods to estimate electrocardiogram signal quality. In *2011 Computing in Cardiology*, pp. 609–612. IEEE, 2011.

J Escudero, Daniel Abásolo, Roberto Hornero, Pedro Espino, and Miguel López. Analysis of electroencephalograms in alzheimer's disease patients with multiscale entropy. *Physiological measurement*, 27(11):1091, 2006.

Wei Fan, Jingru Fei, Dingyu Guo, Kun Yi, Xiaozhuang Song, Haolong Xiang, Hangting Ye, and Min Li. Towards multi-resolution spatiotemporal graph learning for medical time series classification. In *Proceedings of the ACM on Web Conference 2025*, pp. 5054–5064, 2025.

Jean-Yves Franceschi, Aymeric Dieuleveut, and Martin Jaggi. Unsupervised scalable representation learning for multivariate time series. *Advances in neural information processing systems*, 32, 2019.

Pascal Fries. Rhythms for cognition: communication through coherence. *Neuron*, 88(1):220–235, 2015.

Albert Gu and Tri Dao. Mamba: Linear-time sequence modeling with selective state spaces. *arXiv preprint arXiv:2312.00752*, 2023.

Albert Gu, Karan Goel, and Christopher Ré. Efficiently modeling long sequences with structured state spaces. In *ICLR*, 2022.

Alex Hanson, Koutilya Pnvr, Sanjukta Krishnagopal, and Larry Davis. Bidirectional convolutional lstm for the detection of violence in videos. In *Proceedings of the European conference on computer vision (ECCV) workshops*, pp. 0–0, 2018.

Simon S Haykin. *Adaptive filter theory*. Pearson Education India, 2002.

Kaiming He, Xiangyu Zhang, Shaoqing Ren, and Jian Sun. Deep residual learning for image recognition. In *Proceedings of the IEEE conference on computer vision and pattern recognition*, pp. 770–778, 2016.

Sepp Hochreiter and Jürgen Schmidhuber. Long short-term memory. *Neural computation*, 9(8): 1735–1780, 1997.

Harold Hotelling. Relations between two sets of variates. In *Breakthroughs in statistics: methodology and distribution*, pp. 162–190. Springer, 1992.

Ming Hu, Jianfu Yin, Jing Wang, Yuqi Wang, Bingliang Hu, and Quan Wang. Specslice-convlstm: Medical hyperspectral image segmentation using spectral slicing and convlstm. In *International Conference on Pattern Recognition*, pp. 211–225. Springer, 2024.

Ming Hu, Jianfu Yin, Zhuangzhuang Ma, Jianheng Ma, Feiyu Zhu, Bingbing Wu, Ya Wen, Meng Wu, Cong Hu, Bingliang Hu, et al. beta-fft: Nonlinear interpolation and differentiated training strategies for semi-supervised medical image segmentation. In *Proceedings of the Computer Vision and Pattern Recognition Conference*, pp. 30839–30849, 2025.

Yifan Jia, Hongyu Pei, Jiaqi Liang, Yuheng Zhou, Yanfei Yang, Yangyang Cui, and Min Xiang. Preprocessing and denoising techniques for electrocardiography and magnetocardiography: A review. *Bioengineering*, 11(11):1109, 2024.

Steven M Kay. *Fundamentals of statistical signal processing: estimation theory*. Prentice-Hall, Inc., 1993.

Nikita Kitaev, Lukasz Kaiser, and Anselm Levskaya. Reformer: The efficient transformer. In *International Conference on Learning Representations*, 2019.

Dani Kiyasseh, Tingting Zhu, and David A Clifton. Clocs: Contrastive learning of cardiac signals across space, time, and patients. In *International Conference on Machine Learning*, pp. 5606–5615. PMLR, 2021.

George H Klem. The ten-twenty electrode system of the international federation. the international federation of clinical neurophysiology. *Electroencephalogr. Clin. Neurophysiol. Suppl.*, 52:3–6, 1999.

Prabhat Kumar and S Suresh. Flaap: An open human activity recognition (har) dataset for learning and finding the associated activity patterns. *Procedia Computer Science*, 212:64–73, 2022.

Guokun Lai, Wei-Cheng Chang, Yiming Yang, and Hanxiao Liu. Modeling long-and short-term temporal patterns with deep neural networks. In *SIGIR*, 2018.

Vernon J Lawhern, Amelia J Solon, Nicholas R Waytowich, Stephen M Gordon, Chou P Hung, and Brent J Lance. Eegnet: a compact convolutional neural network for eeg-based brain–computer interfaces. *Journal of neural engineering*, 15(5):056013, 2018.

Yann LeCun, Bernhard Boser, John S Denker, Donnie Henderson, Richard E Howard, Wayne Hubbard, and Lawrence D Jackel. Backpropagation applied to handwritten zip code recognition. *Neural computation*, 1(4):541–551, 1989.

Lei Lin, Beilei Xu, Wencheng Wu, Trevor W Richardson, and Edgar A Bernal. Medical time series classification with hierarchical attention-based temporal convolutional networks: A case study of myotonic dystrophy diagnosis. In *CVPR workshops*, volume 2, 2019.

Shizhan Liu, Hang Yu, Cong Liao, Jianguo Li, Weiyao Lin, Alex X Liu, and Schahram Dustdar. Pyraformer: Low-complexity pyramidal attention for long-range time series modeling and forecasting. In *International conference on learning representations*, 2021.

Xi Liu, Xinming Zhang, Tao Yu, Ruochen Dang, Jian Li, Bingliang Hu, Quan Wang, and Rong Luo. Classification of self-limited epilepsy with centrotemporal spikes by classical machine learning and deep learning based on electroencephalogram data. *Brain Research*, 1830:148813, 2024a.

Yong Liu, Haixu Wu, Jianmin Wang, and Mingsheng Long. Non-stationary transformers: Exploring the stationarity in time series forecasting. *Advances in Neural Information Processing Systems*, 35: 9881–9893, 2022.

Yong Liu, Tengge Hu, Haoran Zhang, Haixu Wu, Shiyu Wang, Lintao Ma, and Mingsheng Long. itransformer: Inverted transformers are effective for time series forecasting. *International Conference on Learning Representations*, 2024b.

Jiecheng Lu, Xu Han, Yan Sun, and Shihao Yang. Cats: Enhancing multivariate time series forecasting by constructing auxiliary time series as exogenous variables. *arXiv preprint arXiv:2403.01673*, 2024.

Donghao Luo and Xue Wang. Moderntcn: A modern pure convolution structure for general time series analysis. In *The Twelfth International Conference on Learning Representations*, 2024.

Andreas Miltiadous, Emmanouil Gionanidis, Katerina D Tzimourta, Nikolaos Giannakeas, and Alexandros T Tzallas. Dice-net: a novel convolution-transformer architecture for alzheimer detection in eeg signals. *IEEE Access*, 2023a.

Andreas Miltiadous, Katerina D Tzimourta, Theodora Afrantou, Panagiotis Ioannidis, Nikolaos Grigoriadis, Dimitrios G Tsalikakis, Pantelis Angelidis, Markos G Tsipouras, Euripidis Glavas, Nikolaos Giannakeas, et al. A dataset of scalp eeg recordings of alzheimer's disease, frontotemporal dementia and healthy subjects from routine eeg. *Data*, 8(6):95, 2023b.

Ziti Fariha Mohd Apandi, Ryojun Ikeura, Soichiro Hayakawa, and Shigeyoshi Tsutsumi. An analysis of the effects of noisy electrocardiogram signal on heartbeat detection performance. *Bioengineering*, 7(2):53, 2020.

Guy P Nason and Rainer von Sachs. Wavelets in time-series analysis. *Philosophical transactions of the royal society of London. Series A: Mathematical, Physical and Engineering Sciences*, 357 (1760):2511–2526, 1999.

Yuqi Nie, Nam H Nguyen, Phanwadee Sinthong, and Jayant Kalagnanam. A time series is worth 64 words: Long-term forecasting with transformers. *ICLR*, 2023.

Jaakko Matias Palva and Satu Palva. The correlation of the neuronal long-range temporal correlations, avalanche dynamics with the behavioral scaling laws and interindividual variability. *Criticality in Neural Systems*, pp. 105–126, 2014.

Adam Paszke, Sam Gross, Soumith Chintala, Gregory Chanan, Edward Yang, Zachary DeVito, Zeming Lin, Alban Desmaison, Luca Antiga, and Adam Lerer. Automatic differentiation in pytorch. 2017.

Bo Peng, Eric Alcaide, Quentin Anthony, Alon Albalak, Samuel Arcadinho, Stella Biderman, Huanqi Cao, Xin Cheng, Michael Chung, Matteo Grella, et al. Rwkv: Reinventing rnns for the transformer era. In *Findings of the Association for Computational Linguistics: EMNLP 2023*, pp. 936–951, 2023. URL `https://aclanthology.org/2023.findings-emnlp.936/`.

PhysioToolkit PhysioBank. Physionet: components of a new research resource for complex physiologic signals. *Circulation*, 101(23):e215–e220, 2000.

Pyotr G Platonov. P-wave morphology: underlying mechanisms and clinical implications. *Annals of Noninvasive Electrocardiology*, 17(3):161–169, 2012.

Xiaodong Qu, Zepeng Hu, Zhaonan Li, and Timothy J Hickey. Ensemble methods and lstm outperformed other eight machine learning classifiers in an eeg-based bci experiment. In *International Conference on Learning Representations*, 2020.

David E Rumelhart, Geoffrey E Hinton, and Ronald J Williams. Learning representations by back-propagating errors. *Nature*, 323(6088):533–536, 1986.

Nand Sharma. Single-trial p300 classification using pca with lda, qda and neural networks. *arXiv preprint arXiv:1712.01977*, 2017.

Sheng-syun Shen and Hung-yi Lee. Neural attention models for sequence classification: Analysis and application to key term extraction and dialogue act detection. *arXiv preprint arXiv:1604.00077*, 2016.

Yonghao Song, Qingqing Zheng, Bingchuan Liu, and Xiaorong Gao. Eeg conformer: Convolutional transformer for eeg decoding and visualization. *IEEE Transactions on Neural Systems and Rehabilitation Engineering*, 31:710–719, 2022.

Mohamed Sraitih, Younes Jabrane, and Amir Hajjam El Hassani. A robustness evaluation of machine learning algorithms for ecg myocardial infarction detection. *Journal of Clinical Medicine*, 11(17): 4935, 2022.

Siyi Tang, Jared Dunnmon, Khaled Kamal Saab, Xuan Zhang, Qianying Huang, Florian Dubost, Daniel Rubin, and Christopher Lee-Messer. Self-supervised graph neural networks for improved electroencephalographic seizure analysis. In *International Conference on Learning Representations*, 2021.

Ziwei Tian, Bingliang Hu, Yang Si, and Quan Wang. Automatic seizure detection and prediction based on brain connectivity features and a cnns meet transformers classifier. *Brain Sciences*, 13(5): 820, 2023.

Hanneke van Dijk, Guido van Wingen, Damiaan Denys, Sebastian Olbrich, Rosalinde van Ruth, and Martijn Arns. The two decades brainclinics research archive for insights in neurophysiology (tdbrain) database. *Scientific data*, 9(1):333, 2022.

Ashish Vaswani, Noam Shazeer, Niki Parmar, Jakob Uszkoreit, Llion Jones, Aidan N Gomez, Łukasz Kaiser, and Illia Polosukhin. Attention is all you need. *Advances in neural information processing systems*, 30, 2017.

Patrick Wagner, Nils Strodthoff, Ralf-Dieter Bousseljot, Dieter Kreiseler, Fatima I Lunze, Wojciech Samek, and Tobias Schaeffter. Ptb-xl, a large publicly available electrocardiography dataset. *Scientific data*, 7(1):1–15, 2020.

Shiyu Wang, Jiawei Li, Xiaoming Shi, Zhou Ye, Baichuan Mo, Wenze Lin, Ju Shengtong, Zhixuan Chu, and Ming Jin. Timemixer++: A general time series pattern machine for universal predictive analysis. In *ICLR 2025: The Thirteenth International Conference on Learning Representations*. International Conference on Learning Representations, 2025a.

Yihe Wang, Nan Huang, Taida Li, Yujun Yan, and Xiang Zhang. Medformer: A multi-granularity patching transformer for medical time-series classification. *arXiv preprint arXiv:2405.19363*, 2024a.

Yihe Wang, Nadia Mammone, Darina Petrovsky, Alexandros T Tzallas, Francesco C Morabito, and Xiang Zhang. Adformer: A multi-granularity transformer for eeg-based alzheimer's disease assessment. *arXiv preprint arXiv:2409.00032*, 2024b.

Yihe Wang, Nan Huang, Nadia Mammone, Marco Cecchi, and Xiang Zhang. Lead: Large foundation model for eeg-based alzheimer's disease detection. *arXiv preprint arXiv:2502.01678*, 2025b.

Zekai Wang, Stavros Stavrakis, and Bing Yao. Hierarchical deep learning with generative adversarial network for automatic cardiac diagnosis from ecg signals. *Computers in Biology and Medicine*, 155:106641, 2023.

Gerald Woo, Chenghao Liu, Doyen Sahoo, Akshat Kumar, and Steven Hoi. Etsformer: Exponential smoothing transformers for time-series forecasting. *arXiv preprint arXiv:2202.01381*, 2022.

Haixu Wu, Jiehui Xu, Jianmin Wang, and Mingsheng Long. Autoformer: Decomposition transformers with auto-correlation for long-term series forecasting. *Advances in Neural Information Processing Systems*, 34:22419–22430, 2021.

Haixu Wu, Tengge Hu, Yong Liu, Hang Zhou, Jianmin Wang, and Mingsheng Long. Timesnet: Temporal 2d-variation modeling for general time series analysis. *arXiv preprint arXiv:2210.02186*, 2022a.

Haixu Wu, Jialong Wu, Jiehui Xu, Jianmin Wang, and Mingsheng Long. Flowformer: Linearizing transformers with conservation flows. In *ICML*, 2022b.

Haixu Wu, Tengge Hu, Yong Liu, Hang Zhou, Jianmin Wang, and Mingsheng Long. Timesnet: Temporal 2d-variation modeling for general time series analysis. In *International Conference on Learning Representations*, 2023.

Qiao Xiao, Khuan Lee, Siti Aisah Mokhtar, Iskasymar Ismail, Ahmad Luqman bin Md Pauzi, Qiuxia Zhang, and Poh Ying Lim. Deep learning-based ecg arrhythmia classification: A systematic review. *Applied Sciences*, 13(8):4964, 2023.

Dezhen Xiong, Daohui Zhang, Xingang Zhao, and Yiwen Zhao. Deep learning for emg-based human-machine interaction: A review. *IEEE/CAA Journal of Automatica Sinica*, 8(3):512–533, 2021.

Chaoqi Yang, M Brandon Westover, and Jimeng Sun. Manydg: Many-domain generalization for healthcare applications. In *The Eleventh International Conference on Learning Representations*, 2023.

Kun Yi, Qi Zhang, Wei Fan, Longbing Cao, Shoujin Wang, Hui He, Guodong Long, Liang Hu, Qingsong Wen, and Hui Xiong. A survey on deep learning based time series analysis with frequency transformation. In *Proceedings of the 31st ACM SIGKDD Conference on Knowledge Discovery and Data Mining V. 2*, pp. 6206–6215, 2025.

Jianfu Yin, Nan Wang, Binliang Hu, Yao Wang, and Quan Wang. Degradation-aware deep unfolding network with transformer prior for video compressive imaging. *Signal Processing*, 227:109660, 2025.

Fisher Yu and Vladlen Koltun. Multi-scale context aggregation by dilated convolutions. *arXiv preprint arXiv:1511.07122*, 2015.

Ailing Zeng, Muxi Chen, Lei Zhang, and Qiang Xu. Are transformers effective for time series forecasting? *AAAI*, 2023.

Tianping Zhang, Yizhuo Zhang, Wei Cao, Jiang Bian, Xiaohan Yi, Shun Zheng, and Jian Li. Less is more: Fast multivariate time series forecasting with light sampling-oriented mlp structures. *arXiv preprint arXiv:2207.01186*, 2022.

Yitian Zhang, Liheng Ma, Soumyasundar Pal, Yingxue Zhang, and Mark Coates. Multi-resolution time-series transformer for long-term forecasting. In *International Conference on Artificial Intelligence and Statistics*, pp. 4222–4230. PMLR, 2024.

Yunhao Zhang and Junchi Yan. Crossformer: Transformer utilizing cross-dimension dependency for multivariate time series forecasting. In *The Eleventh International Conference on Learning Representations*, 2022.

Haoyi Zhou, Shanghang Zhang, Jieqi Peng, Shuai Zhang, Jianxin Li, Hui Xiong, and Wancai Zhang. Informer: Beyond efficient transformer for long sequence time-series forecasting. In *Proceedings of the AAAI conference on artificial intelligence*, volume 35, pp. 11106–11115, 2021.

Peng Zhou, Wei Shi, Jun Tian, Zhenyu Qi, Bingchen Li, Hongwei Hao, and Bo Xu. Attention-based bidirectional long short-term memory networks for relation classification. In *Proceedings of the 54th annual meeting of the association for computational linguistics (volume 2: Short papers)*, pp. 207–212, 2016.

Tian Zhou, Ziqing Ma, Qingsong Wen, Xue Wang, Liang Sun, and Rong Jin. Fedformer: Frequency enhanced decomposed transformer for long-term series forecasting. In *International Conference on Machine Learning*, pp. 27268–27286. PMLR, 2022.

Feiyu Zhu, Jing Zhang, Ruochen Dang, Bingliang Hu, and Quan Wang. Mtnet: Multimodal transformer network for mild depression detection through fusion of eeg and eye tracking. *Biomedical Signal Processing and Control*, 100:106996, 2025.

APPENDIX

THE USE OF LLM AND REPRODUCIBILITY STATEMENT

Large language models are only used for writing refinement. The complete source code supporting this study is publicly available at the following anonymous repository: anonymous link.

A EXPLANATION OF SNR OPTIMIZATION VIA CIF.

In analyzing the SNR improvement process of the CIF module, we consider two scenarios for the two-channel signals: the first scenario assumes equal signal variances and equal noise variances across the channels, while the second scenario represents the more general case where the signal and noise variances differ between the two channels.

SCENARIO 1: EQUAL SIGNAL AND NOISE VARIANCES

Consider the linear combination of the two observed signals:

$$y = ax_1 + bx_2, \tag{4}$$

where a and b are real coefficients. The observed signals are given by

$$x_1 = s_1 + \epsilon_1, \quad x_2 = s_2 + \epsilon_2, \tag{5}$$

with zero-mean signal and noise components:

$$\mathbb{E}[s_i] = \mathbb{E}[\epsilon_i] = 0, \quad i = 1, 2,$$

and mutually uncorrelated signal and noise components: $\mathrm{Cov}(s_i, \epsilon_j) = 0$.

The power of a zero-mean random signal is given by its variance:

$$P_s = \mathrm{Var}[s] = \mathbb{E}[(s - \mathbb{E}[s])^2] = \mathbb{E}[s^2]. \tag{6}$$

This is why, for zero-mean signals, the SNR can be expressed as a ratio of variances (or mean-square values) Kay (1993).

For the linear combination of signals:

$$\begin{aligned} \mathrm{Var}(as_1 + bs_2) &= a^2\mathrm{Var}(s_1) + b^2\mathrm{Var}(s_2) + 2ab\,\mathrm{Cov}(s_1, s_2) \\ &= a^2\sigma_s^2 + b^2\sigma_s^2 + 2ab(\rho\sigma_s^2) \\ &= \sigma_s^2\big(a^2 + b^2 + 2ab\rho\big), \end{aligned} \tag{7}$$

where $\rho = \mathrm{Corr}(s_1, s_2)$.

Similarly, the noise power of the linear combination is:

$$\begin{aligned} \mathrm{Var}(a\epsilon_1 + b\epsilon_2) &= a^2\mathrm{Var}(\epsilon_1) + b^2\mathrm{Var}(\epsilon_2) + 2ab\,\mathrm{Cov}(\epsilon_1, \epsilon_2) \\ &= a^2\sigma_\epsilon^2 + b^2\sigma_\epsilon^2 + 2ab(\gamma\sigma_\epsilon^2) \\ &= \sigma_\epsilon^2\big(a^2 + b^2 + 2ab\gamma\big), \end{aligned} \tag{8}$$

where $\gamma = \mathrm{Corr}(\epsilon_1, \epsilon_2)$.

Using the definition of SNR as the ratio of signal power to noise power:

$$\mathrm{SNR}_{\text{out}} = \frac{\mathrm{Var}(as_1 + bs_2)}{\mathrm{Var}(a\epsilon_1 + b\epsilon_2)} = \frac{\sigma_s^2(a^2 + b^2 + 2ab\rho)}{\sigma_\epsilon^2(a^2 + b^2 + 2ab\gamma)} = \mathrm{SNR}_{\text{in}} \cdot \frac{a^2 + b^2 + 2ab\rho}{a^2 + b^2 + 2ab\gamma}, \tag{9}$$

where $\mathrm{SNR}_{\text{in}} = \sigma_s^2/\sigma_\epsilon^2$.

> *Remark:* The zero-mean property ensures that the variance equals the mean-square value, which is why SNR can be expressed as a ratio of variances Kay (1993); Haykin (2002).

For SNR improvement relative to individual channels:

$$\frac{a^2 + b^2 + 2ab\rho}{a^2 + b^2 + 2ab\gamma} > 1 \quad \Rightarrow \quad 2ab(\rho - \gamma) > 0. \tag{10}$$

- **Difference Mode** ($ab < 0$): $\rho < \gamma$ — suppress correlated noise while possibly attenuating some correlated signal.
- **Cooperative Mode** ($ab > 0$): $\rho > \gamma$ — amplify correlated signals relative to less-correlated noise.

Optimization via the ratio $k = a/b$ (explicit choice of a, b)

Because the output SNR

$$\mathrm{SNR}_{\mathrm{out}} = \mathrm{SNR}_{\mathrm{in}} \cdot \frac{a^2 + b^2 + 2ab\rho}{a^2 + b^2 + 2ab\gamma} \tag{11}$$

is homogeneous of degree zero in (a, b) (i.e. invariant under common scaling $(a, b) \mapsto (ca, cb)$, $c \neq 0$), only the ratio $k = a/b$ matters. Assume $b \neq 0$ and set

$$k = \frac{a}{b}. \tag{12}$$

Define

$$F(k) \;=\; \frac{a^2 + b^2 + 2ab\rho}{a^2 + b^2 + 2ab\gamma} \;=\; \frac{k^2 + 1 + 2k\rho}{k^2 + 1 + 2k\gamma}, \tag{13}$$

so that

$$\mathrm{SNR}_{\mathrm{out}} = \mathrm{SNR}_{\mathrm{in}} \cdot F(k). \tag{14}$$

We therefore study extrema of $F(k)$ to determine favorable relative weights $a : b$.

Let

$$N(k) = k^2 + 1 + 2k\rho, \qquad D(k) = k^2 + 1 + 2k\gamma, \tag{15}$$

so $F(k) = N(k)/D(k)$. Then

$$N'(k) = 2k + 2\rho, \qquad D'(k) = 2k + 2\gamma. \tag{16}$$

Using the quotient rule,

$$F'(k) = \frac{N'(k)D(k) - N(k)D'(k)}{D(k)^2}. \tag{17}$$

The numerator simplifies and factorizes as

$$N'(k)D(k) - N(k)D'(k) = 2(\gamma - \rho)(k - 1)(k + 1), \tag{18}$$

so we obtain

$$F'(k) = \frac{2(\gamma - \rho)(k - 1)(k + 1)}{(k^2 + 1 + 2k\gamma)^2}. \tag{19}$$

Critical points and their nature

From equation 19, the critical points satisfy

$$F'(k) = 0 \iff k = -1,\; k = +1 \quad \text{or} \quad \rho = \gamma. \tag{20}$$

- If $\rho > \gamma$ (so $\gamma - \rho < 0$), then $(k - 1)(k + 1) < 0$ for $k \in (-1, 1)$ and $(k - 1)(k + 1) > 0$ for $k > 1$ or $k < -1$. Hence $F'(k) > 0$ on $(-1, 1)$ and $F'(k) < 0$ outside, so

$$k = 1 \text{ is a local maximum}, \qquad k = -1 \text{ is a local minimum}. \tag{21}$$

- If $\rho < \gamma$ (so $\gamma - \rho > 0$), the inequalities reverse: $F'(k) < 0$ on $(-1, 1)$ and $F'(k) > 0$ for $|k| > 1$, thus

$$k = -1 \text{ is a local maximum}, \qquad k = 1 \text{ is a local minimum}. \tag{22}$$

- If $\rho = \gamma$, then from equation 13 we have

$$F(k) \equiv 1, \quad \forall k \in \mathbb{R}, \tag{23}$$

so no choice of k changes the SNR.

Interpretation in terms of a, b and explicit choice

Recall from equation 12 that $k = a/b$. The critical ratios $k = \pm 1$ correspond to equal-magnitude weights:

$$k = +1 \iff a = b, \qquad k = -1 \iff a = -b. \tag{24}$$

Since $\mathrm{SNR}_{\mathrm{out}}$ in equation 11 is invariant to a common scaling of (a, b), we may fix a convenient normalization:

Fix $b = 1$. Then $k = a$ and the recommended choices are

$$\text{Cooperative mode } (\rho > \gamma): \quad (a, b) = (1, 1), \tag{25}$$

$$\text{Differential mode } (\rho < \gamma): \quad (a, b) = (-1, 1). \tag{26}$$

Fix $b = -1$. Then $k = a$ and the recommended choices are

$$\text{Cooperative mode } (\rho > \gamma): \quad (a, b) = (-1, -1), \tag{27}$$

$$\text{Differential mode } (\rho < \gamma): \quad (a, b) = (1, -1). \tag{28}$$

Degenerate and neutral cases

- If $\rho = \gamma$, then by equation 23 we have

$$\mathrm{SNR}_{\mathrm{out}} = \mathrm{SNR}_{\mathrm{in}}, \quad \forall (a, b) \neq (0, 0), \tag{29}$$

  i.e. the linear combination cannot improve SNR (except for singular noise-cancellation cases).
- The denominator in equation 13 vanishes when

$$k^2 + 1 + 2k\gamma = 0, \tag{30}$$

  which corresponds to zero output noise variance. This is a nongeneric, degenerate configuration (perfect noise cancellation).

From equation 21–equation 22 and equation 24, we conclude:

- If $\rho > \gamma$: the SNR is maximized (among equal-variance combinations) by equal-phase combining $a = b$ (cooperative mode).
- If $\rho < \gamma$: the SNR is maximized by equal-magnitude opposite-phase combining $a = -b$ (differential mode).
- If $\rho = \gamma$: $F(k) \equiv 1$ and no linear combining improves SNR, up to degenerate cases.

Remarks on the choice of (a, b) ranges. If the goal is to find the SNR extremum points, it is sufficient to consider (a, b) combinations where a and b are either of the same sign (both positive or both negative) or of opposite signs. For example, exploring (a, b) within the rectangle $[-1, 1] \times [-1, 1]$ already includes the critical ratios $k = \pm 1$ and thus captures the SNR maxima and minima. While this rectangle does not cover all possible k values (i.e., all real ratios a/b), it is enough to determine the locations of the extremal points, thanks to the homogeneity of SNR in (a, b).

Scenario 2: Unequal Signal and Noise Variances

Consider the general case with potentially unequal variances and nonzero correlations:

$$\begin{aligned} &\mathrm{Var}(s_1) = \sigma_{s1}^2, \qquad \mathrm{Var}(s_2) = \sigma_{s2}^2, \qquad \mathrm{Cov}(s_1, s_2) = \rho\, \sigma_{s1}\sigma_{s2}, \\ &\mathrm{Var}(\epsilon_1) = \sigma_{\epsilon 1}^2, \qquad \mathrm{Var}(\epsilon_2) = \sigma_{\epsilon 2}^2, \qquad \mathrm{Cov}(\epsilon_1, \epsilon_2) = \gamma\, \sigma_{\epsilon 1}\sigma_{\epsilon 2}. \end{aligned} \tag{31}$$

where:

- Signal and noise components are mutually uncorrelated

Consider two observed signals

$$y = as_1 + bs_2 + a\epsilon_1 + b\epsilon_2 = s_y + \epsilon_y \tag{32}$$

where the signal vector $[s_1, s_2]^T$ has covariance

$$\mathbf{S} = \begin{bmatrix} \sigma_{s1}^2 & \rho\sigma_{s1}\sigma_{s2} \\ \rho\sigma_{s1}\sigma_{s2} & \sigma_{s2}^2 \end{bmatrix} \tag{33}$$

and the noise vector $[\epsilon_1, \epsilon_2]^T$ has covariance

$$\mathbf{N} = \begin{bmatrix} \sigma_{\epsilon1}^2 & \gamma\sigma_{\epsilon1}\sigma_{\epsilon2} \\ \gamma\sigma_{\epsilon1}\sigma_{\epsilon2} & \sigma_{\epsilon2}^2 \end{bmatrix}, \tag{34}$$

with signal and noise mutually uncorrelated. Define the coefficient vector

$$\mathbf{w} = \begin{bmatrix} a \\ b \end{bmatrix}. \tag{35}$$

The output signal-to-noise ratio (SNR) is

$$\mathrm{SNR}(\mathbf{w}) = \frac{\mathrm{Var}(s_y)}{\mathrm{Var}(\epsilon_y)} = \frac{\mathbf{w}^T\mathbf{S}\mathbf{w}}{\mathbf{w}^T\mathbf{N}\mathbf{w}}. \tag{36}$$

To maximize the SNR, we consider the derivative with respect to $\mathbf{w}$:

$$\frac{\partial}{\partial \mathbf{w}}\mathrm{SNR} = \frac{2\mathbf{S}\mathbf{w}(\mathbf{w}^T\mathbf{N}\mathbf{w}) - 2\mathbf{N}\mathbf{w}(\mathbf{w}^T\mathbf{S}\mathbf{w})}{(\mathbf{w}^T\mathbf{N}\mathbf{w})^2} = 0 \tag{37}$$

which leads to the generalized eigenvalue problem

$$\mathbf{S}\mathbf{w} = \lambda\mathbf{N}\mathbf{w}, \quad \lambda = \mathrm{SNR}. \tag{38}$$

For the 2×2 matrices, this can be written explicitly as

$$\begin{bmatrix} \sigma_{s1}^2 & \rho\sigma_{s1}\sigma_{s2} \\ \rho\sigma_{s1}\sigma_{s2} & \sigma_{s2}^2 \end{bmatrix} \begin{bmatrix} a \\ b \end{bmatrix} = \lambda \begin{bmatrix} \sigma_{\epsilon1}^2 & \gamma\sigma_{\epsilon1}\sigma_{\epsilon2} \\ \gamma\sigma_{\epsilon1}\sigma_{\epsilon2} & \sigma_{\epsilon2}^2 \end{bmatrix} \begin{bmatrix} a \\ b \end{bmatrix}, \tag{39}$$

which yields

$$a\sigma_{s1}^2 + b\rho\sigma_{s1}\sigma_{s2} = \lambda(a\sigma_{\epsilon1}^2 + b\gamma\sigma_{\epsilon1}\sigma_{\epsilon2}) \tag{40}$$

$$a\rho\sigma_{s1}\sigma_{s2} + b\sigma_{s2}^2 = \lambda(a\gamma\sigma_{\epsilon1}\sigma_{\epsilon2} + b\sigma_{\epsilon2}^2). \tag{41}$$

The condition for a nontrivial solution $(a, b) \neq 0$ is

$$\det(\mathbf{S} - \lambda\mathbf{N}) = 0, \tag{42}$$

which explicitly reads

$$(\sigma_{s1}^2 - \lambda\sigma_{\epsilon1}^2)(\sigma_{s2}^2 - \lambda\sigma_{\epsilon2}^2) - (\rho\sigma_{s1}\sigma_{s2} - \lambda\gamma\sigma_{\epsilon1}\sigma_{\epsilon2})^2 = 0. \tag{43}$$

Expanding the determinant, we obtain

$$\begin{aligned} &\sigma_{s1}^2\sigma_{s2}^2 - \sigma_{s1}^2\lambda\sigma_{\epsilon2}^2 - \sigma_{s2}^2\lambda\sigma_{\epsilon1}^2 + \lambda^2\sigma_{\epsilon1}^2\sigma_{\epsilon2}^2 \\ &\quad - \rho^2\sigma_{s1}^2\sigma_{s2}^2 + 2\rho\gamma\lambda\sigma_{s1}\sigma_{s2}\sigma_{\epsilon1}\sigma_{\epsilon2} - \lambda^2\gamma^2\sigma_{\epsilon1}^2\sigma_{\epsilon2}^2 = 0. \end{aligned} \tag{44}$$

Combining like terms yields the quadratic equation in λ:

$$\lambda^2\sigma_{\epsilon1}^2\sigma_{\epsilon2}^2(1-\gamma^2) - \lambda(\sigma_{s1}^2\sigma_{\epsilon2}^2 + \sigma_{s2}^2\sigma_{\epsilon1}^2 - 2\rho\gamma\sigma_{s1}\sigma_{s2}\sigma_{\epsilon1}\sigma_{\epsilon2}) + \sigma_{s1}^2\sigma_{s2}^2(1-\rho^2) = 0. \tag{45}$$

Define

$$A = \sigma_{\epsilon1}^2\,\sigma_{\epsilon2}^2(1-\gamma^2), \tag{46}$$

$$B = -\big(\sigma_{s1}^2\,\sigma_{\epsilon2}^2 + \sigma_{s2}^2\,\sigma_{\epsilon1}^2 - 2\rho\gamma\,\sigma_{s1}\sigma_{s2}\sigma_{\epsilon1}\sigma_{\epsilon2}\big), \tag{47}$$

$$C = \sigma_{s1}^2\,\sigma_{s2}^2(1-\rho^2). \tag{48}$$

The generalized eigenvalue problem leads to the quadratic equation

$$A\lambda^2 + B\lambda + C = 0, \tag{49}$$

whose solution is

$$\lambda = \frac{-B \pm \sqrt{B^2 - 4AC}}{2A}. \tag{50}$$

Taking the positive sign yields the maximum output SNR:

$$\mathrm{SNR}_{\max} = \lambda_{\max} = \frac{-B + \sqrt{B^2 - 4AC}}{2A}. \tag{51}$$

The optimal linear combination coefficients $[a, b]^T = \mathbf{w}_{\text{opt}}$ satisfy

$$\frac{b}{a} = \frac{\lambda_{\max}\sigma_{\epsilon 1}^2 - \sigma_{s1}^2}{\rho\sigma_{s1}\sigma_{s2} - \lambda_{\max}\gamma\sigma_{\epsilon 1}\sigma_{\epsilon 2}}, \quad \mathbf{w}_{\text{opt}} = a \begin{bmatrix} 1 \\ b/a \end{bmatrix}, \; a \neq 0. \tag{52}$$

Multi-Channel Linear Fusion for SNR Enhancement

As shown in equation , the two-channel SNR maximization framework can be directly extended to multi-channel recordings by performing *corresponding pairwise fusion* across multiple channel subsets. Consider two subsets of n channels each,

$$\mathbf{x}_A = [x_{i_1}, \ldots, x_{i_n}]^T, \quad \mathbf{x}_B = [x_{j_1}, \ldots, x_{j_n}]^T, \tag{53}$$

where each channel may have correlated signal and noise components across channels.

For each corresponding channel pair (x_{i_k}, x_{j_k}), $k = 1, \ldots, n$, the optimal linear fusion coefficients

$$\mathbf{w}_k = [a_k, b_k]^T \tag{54}$$

are determined exactly as in the two-channel case by solving the generalized eigenvalue problem:

$$\mathbf{S}_k \mathbf{w}_k = \lambda_k \mathbf{N}_k \mathbf{w}_k, \tag{55}$$

where $\mathbf{S}_k$ and $\mathbf{N}_k$ are the signal and noise covariance matrices for the k-th pair, and λ_k corresponds to the maximum achievable SNR for that fused channel. The fused channel is then constructed as

$$y_k = a_k x_{i_k} + b_k x_{j_k}. \tag{56}$$

By applying this *pairwise optimal fusion* to all n channel pairs, each channel independently reaches its maximum SNR, ensuring that the multi-channel system as a whole achieves a *simultaneous SNR enhancement across all channels*.

B Data Preprocessing

Table 5: **The information of processed datasets.** The table shows the number of subjects, samples, classes, channels, sampling rate, sample timestamps, modality of MedTS, and file size. Here, **#-Timestamps** indicates the number of timestamps per sample.All data processing procedures follow those of Medformer Wang et al. (2024a).

Datasets	#-Subject	#-Sample	#-Class	#-Channel	#-Timestamps	Sampling Rate	Modality	File Size
APAVA	23	5,967	2	16	256	256Hz	EEG	186MB
ADFTD	88	69,752	3	19	256	256Hz	EEG	2.52GB
TDBrain	72	6,240	2	33	256	256Hz	EEG	571MB
PTB	198	64,356	2	15	300	250Hz	ECG	2.15GB
PTB-XL	17,596	191,400	5	12	250	250Hz	ECG	4.28GB

Table 6: Datasets and mapping details of UEA dataset (Bagnall et al., 2018).

Dataset	Sample Numbers(train set,test set)	Variable Number	Series Length
EthanolConcentration	(261, 263)	3	1751
FaceDetection	(5890, 3524)	144	62
Handwriting	(150, 850)	3	152
Heartbeat	(204, 205)	61	405
JapaneseVowels	(270, 370)	12	29
PEMSSF	(267, 173)	963	144
SelfRegulationSCP1	(268, 293)	6	896
SelfRegulationSCP2	(200, 180)	7	1152
SpokenArabicDigits	(6599, 2199)	13	93
UWaveGestureLibrary	(120, 320)	3	315

C Implementation Details

We implement our method and all the baselines based on the Time-Series-Library project[1] from Tsinghua University Wu et al. (2023), which integrates all methods under the same framework and training techniques to ensure a relatively fair comparison. The 12 baseline time series transformer methods are Autoformer Wu et al. (2021), Crossformer Zhang & Yan (2022), FEDformer Zhou et al. (2022), Informer Zhou et al. (2021), iTransformer Liu et al. (2024b), MTST Zhang et al. (2024), Nonformer Liu et al. (2022), PatchTST Nie et al. (2023), Reformer Kitaev et al. (2019), vanilla Transformer Vaswani et al. (2017), Medformer Wang et al. (2024a), and MedGNN Fan et al. (2025).

Autoformer Autoformer Wu et al. (2021) employs an auto-correlation mechanism to replace self-attention for time series forecasting. Additionally, they use a time series decomposition block to separate the time series into trend-cyclical and seasonal components for improved learning. The raw source code is available at `https://github.com/thuml/Autoformer`.

Crossformer Crossformer Zhang & Yan (2022) designs a single-channel patching approach for token embedding. They utilize two-stage self-attention to leverage both temporal features and channel correlations. A router mechanism is proposed to reduce time and space complexity during the cross-dimension stage. The raw code is available at `https://github.com/Thinklab-SJTU/Crossformer`.

FEDformer FEDformer Zhou et al. (2022) leverages frequency domain information using the Fourier transform. They introduce frequency-enhanced blocks and frequency-enhanced attention, which are computed in the frequency domain. A novel time series decomposition method replaces the layer norm module in the transformer architecture to improve learning. The raw code is available at `https://github.com/MAZiqing/FEDformer`.

Informer Informer Zhou et al. (2021) is the first paper to employ a one-forward procedure instead of an autoregressive method in time series forecasting tasks. They introduce ProbSparse self-attention to reduce complexity and memory usage. The raw code is available at `https://github.com/zhouhaoyi/Informer2020`.

iTransformer iTransformer Liu et al. (2024b) questions the conventional approach of embedding attention tokens in time series forecasting tasks and proposes an inverted approach by embedding the whole series of channels into a token. They also invert the dimension of other transformer modules, such as the layer norm and feed-forward networks. The raw code is available at `https://github.com/thuml/iTransformer`.

MTST MTST Zhang et al. (2024) uses the same token embedding method as Crossformer and PatchTST. It highlights the importance of different patching lengths in forecasting tasks and designs a method that can take different sizes of patch tokens as input simultaneously. The raw code is available at `https://github.com/networkslab/MTST`.

Nonformer Nonformer Liu et al. (2022) analyzes the impact of non-stationarity in time series forecasting tasks and its significant effect on results. They design a de-stationary attention module

[1] `https://github.com/thuml/Time-Series-Library`

and incorporate normalization and denormalization steps before and after training to alleviate the over-stationarization problem. The raw code is available at `https://github.com/thuml/Nonstationary_Transformers`.

PatchTST PatchTST Nie et al. (2023) embeds a sequence of single-channel timestamps as a patch token to replace the attention token used in the vanilla transformer. This approach enlarges the receptive field and enhances forecasting ability. The raw code is available at `https://github.com/yuqinie98/PatchTST`.

Reformer Reformer Kitaev et al. (2019) replaces dot-product attention with locality-sensitive hashing. They also use a reversible residual layer instead of standard residuals. The raw code is available at `https://github.com/lucidrains/reformer-pytorch`.

Transformer Transformer Vaswani et al. (2017), commonly known as the vanilla transformer, is introduced in the well-known paper "Attention is All You Need." It can also be applied to time series by embedding each timestamp of all channels as an attention token. The PyTorch version of the code is available at `https://github.com/jadore801120/attention-is-all-you-need-pytorch`.

Medformer Medformer Wang et al. (2024a) uses cross-channel patch embedding to model spatiotemporal dependencies.The raw code is available at `https://github.com/DL4mHealth/Medformer`

MedGNN MedGNN Fan et al. (2025) employs multi-resolution spatiotemporal graph learning to extract dynamic features across multiple time scales. The raw code is available at `https://github.com/aikunyi/MedGNN`.

C.1 Evaluation metrics

For all methods, the optimizer used is Adam, with a learning rate of 1e-4. The batch size is set to {32,32,128,128,128} for the datasets APAVA, TDBrain, ADFD, PTB, and PTB-XL, respectively. Training is conducted for 100 epochs, with early stopping triggered after 10 epochs without improvement in the F1 score on the validation set. We save the model with the best F1 score on the validation set and evaluate it on the test set. We employ six evaluation metrics: accuracy, precision (macro-averaged), recall (macro-averaged), F1 score (macro-averaged), AUROC (macro-averaged), and AUPRC (macro-averaged). Both subject-dependent and subject-independent setups are implemented for different datasets. Each experiment is run with 5 random seeds (41-45) and fixed training, validation, and test sets to compute the average results and standard deviations.

To comprehensively and fairly evaluate the performance of each model in the classification task, we select five evaluation metrics: Accuracy, Precision, Recall, F1 score, and AUROC. The definitions and specific calculation formulas for each metric are presented below:

Accuracy measures the proportion of correct predictions out of the total number of predictions. It's calculated as:

$$\text{Accuracy} = \frac{\text{Number of correct predictions}}{\text{Total number of predictions}}. \tag{57}$$

This metric is useful when the classes are balanced but may be misleading in cases of class imbalance.

Precision focuses on the quality of positive predictions and measures the proportion of correctly predicted positive instances out of all instances predicted as positive. It's especially useful when false positives need to be minimized. The formula is:

$$\text{Precision} = \frac{\text{True Positives}}{\text{True Positives} + \text{False Positives}}. \tag{58}$$

Recall measures the proportion of actual positive instances that were correctly identified. It's important when false negatives are costly. The formula is:

$$\text{Recall} = \frac{\text{True Positives}}{\text{True Positives} + \text{False Negatives}}. \tag{59}$$

It shows how well the model captures all relevant instances.

The F1 score is the harmonic mean of precision and recall, balancing the two when one is more important than the other. It's particularly useful when dealing with imbalanced datasets, as it accounts for both false positives and false negatives. The formula is:

$$\text{F1 Score } = 2 \times \frac{\text{Precision } \times \text{ Recall}}{\text{Precision } + \text{ Recall}}. \tag{60}$$

It gives a single metric that reflects both precision and recall performance.

The Area Under the Receiver Operating Characteristic Curve (AUROC) measures the ability of a model to distinguish between classes, defined as

$$\text{AUROC} = \int_0^1 \text{TPR}(\text{FPR})\, d(\text{FPR}), \tag{61}$$

where

$$\text{TPR} = \frac{TP}{TP + FN}, \qquad \text{FPR} = \frac{FP}{FP + TN}.$$

The Area Under the Precision–Recall Curve (AUPRC) summarizes the trade-off between precision and recall across different thresholds, defined as

$$\text{AUPRC} = \int_0^1 \text{Precision}(\text{Recall})\, d(\text{Recall}), \tag{62}$$

where

$$\text{Precision} = \frac{TP}{TP + FP}, \qquad \text{Recall} = \frac{TP}{TP + FN}.$$

D HM-BITCN STRUCTURE DESIGN AND THEORETICAL ANALYSIS

Modeling short-term and long-term dependencies in time series data is challenging. Traditional CNNs excel at capturing local features but have limited receptive fields, hindering long-range dependency learning. Transformer-based methods effectively model long-term dependencies, but their complex design lacks interpretability, which is a key issue in medical time-series classification.To address these limitations, TCNs use causal convolutions for explicit temporal modeling and dilated convolutions to expand the receptive field, overcoming the constraints of traditional CNNs. Building on the advantages of TCN, we propose the HM-BiTCN, which combines the benefits of dilated convolutions, bidirectional causal convolution, and residual connections. This approach allows for better capture of temporal dependencies while preserving causality.

D.1 DILATED CONVOLUTION

Dilated convolution expands the receptive field without significantly increasing computational cost Yu & Koltun (2015). For a 1D input sequence $x = [x_1, x_2, \ldots, x_T]$, its output is defined as $y(t) = \sum_{i=0}^{k-1} x(t + i \cdot d) \cdot w(i)$, where t is the current time step, k is the kernel size, d is the dilation factor, and $w(i)$ is the weight at the i-th position in the kernel. Increasing d effectively enlarges the receptive field, enabling the network to capture longer-term temporal dependencies. When stacking multiple dilated convolutional layers, the receptive field grows progressively. For the l-th layer, the receptive field r_l can be expressed as $r_l = k + (k-1)\sum_{j=1}^{l-1} d_j$, where d_j is the dilation factor of the j-th layer. By gradually increasing d_j, the network captures temporal dependencies across both global and local scales, offering an effective way to model long-term dependencies in time series.

D.2 BIDIRECTIONAL CAUSAL CONVOLUTION STRUCTURE

In addition to dilated convolutions, HM-BiTCN introduces a *bidirectional causal convolution structure*, inspired by prior bidirectional temporal modeling approaches Hanson et al. (2018); Hu et al. (2024); Yin et al. (2025). Unlike traditional TCNs that use only forward causal convolutions, our architecture applies causal convolutions in both forward and backward directions, enabling the model to capture dependencies from both past and future contexts while strictly preserving causality. The *forward causal convolution* processes the input sequence $x(t)$ in chronological order, producing output $y_{\text{forward}}(t) = \sum_{i=0}^{k-1} x(t - i \cdot d) \cdot w_{\text{forward}}(i)$, which depends only on current and past inputs. For the *backward causal convolution*, we first reverse the input sequence as $x_{\text{flip}}(t) = x(T - t)$, and then apply a causal convolution over this flipped sequence. This ensures that the model captures future-directed dependencies without introducing information leakage. The output is given by $y_{\text{backward}}(t) = \sum_{i=0}^{k-1} x(T - (t - i \cdot d)) \cdot w_{\text{backward}}(i)$. These two operations are implemented using separate convolutional layers (convforward and convbackward), and their outputs are summed to form the final bidirectional result: $y_{\text{bi}}(t) = y_{\text{forward}}(t) + \text{flip}(y_{\text{backward}}(t))$. By integrating both directions under strict causality constraints, HM-BiTCN achieves superior temporal dependency modeling compared to unidirectional causal approaches.

D.3 MULTI-SCALE FEATURE LEARNING AND RESIDUAL CONNECTIONS

To further improve the model's capacity to capture dependencies at different temporal scales, HM-BiTCN incorporates *multi-scale feature learning* and *residual connections*. Multi-scale Feature Learning: In HM-BiTCN, we employ a hierarchy of dilation factors that decrease layer by layer to capture temporal dependencies at multiple scales. Lower layers use larger dilation factors to expand the receptive field, aggregating long-range information and smoothing short-term noise in highly redundant medical time series; higher layers use smaller dilation factors to focus on local dependencies and capture fine-grained features. This coarse-to-fine, global-to-local design enables the network to extract broad patterns in its initial layers and refine precise details in its later layers, thereby enhancing adaptability across a wide range of time series tasks. Residual connections: Residual connections He et al. (2016) are introduced between the dilated convolutional layers to facilitate the efficient flow of information through the network. The residual connection is defined as $y = F(x) + x$, where $F(x)$ is the convolutional output, and x is the input. This design alleviates the vanishing gradient problem and improves the overall stability of the network during training.

E Pseudocode of CIF Method and Key Components of HM-BiTCN

Algorithm 1 CIF Module (Channel-Imposed Fusion with Physiological Ordering)

Require: Input $x_{enc} \in \mathbb{R}^{B \times T \times C}$, hyperparameters t, n, a, b ▷ n must satisfy $1 \leq n \leq C$ (i.e., cannot exceed total number of channels)

Step 1: Physiological Channel Reordering (optional) ▷ Only applied if channels have physiology-consistent structure (e.g., ECG, EEG). For general/unstructured data, skip this step.
if PhysiologyStructured(x_{enc}) **then**
    $x_{enc} \leftarrow$ PhysiologyReorder(x_{enc})
end if

Step 2: Split into front and back segments
if $n > C$ **then**
    Error: n cannot exceed total number of channels C
end if
$front \leftarrow x_{enc}[:, :, : n]$ ▷ Front segment: first n channels
$back \leftarrow x_{enc}[:, :, -n :]$ ▷ Back segment: last n channels

Step 3: Fusion
$x_{new} \leftarrow$ Clone(x_{enc})
$added \leftarrow front \cdot a + back \cdot b$
if $t > 0$ **then**
    $x_{new}[:, :, : n] \leftarrow added$
else
    $x_{new}[:, :, -n :] \leftarrow added$
end if
return x_{new}

Algorithm 2 Model with CCA-based Feature Interaction

Require: Encoded input $x_{\text{enc}} \in \mathbb{R}^{B \times L \times D}$, task configs

Initialize encoder and task-specific heads
procedure FORWARD(x_{enc})
    $n \leftarrow$ number of CCA components
    $X_{\text{front}} \leftarrow$ first n features of x_{enc}
    $X_{\text{back}} \leftarrow$ last n features of x_{enc}
    $x_{\text{enc\_new}} \leftarrow x_{\text{enc}}$ (clone)
    $X_{\text{front\_flat}} \leftarrow$ reshape X_{front} to $[B \cdot L, n]$
    $X_{\text{back\_flat}} \leftarrow$ reshape X_{back} to $[B \cdot L, n]$
    Without gradient:
        $\text{CCA}_1 \leftarrow$ `TorchCCA`(n)
        $(X_c^1, Y_c^1) \leftarrow \text{CCA}_1$.fit_transform($X_{\text{front\_flat}}, X_{\text{back\_flat}}$)
        corr_scores $\leftarrow$ correlation coefficients for each canonical component
        $\text{CCA}_2 \leftarrow$ `TorchCCA`(n)
        $(X_c^2, Y_c^2) \leftarrow \text{CCA}_2$.fit_transform($X_{\text{back\_flat}}, X_{\text{front\_flat}}$)
        corr_scores2 $\leftarrow$ correlation coefficients for each canonical component
    $x_{\text{enc\_new}}[:, :, : n] \leftarrow X_{\text{front}} *$ corr_scores $+ X_{\text{back}}$
    $x_{\text{enc\_new}}[:, :, -n :] \leftarrow X_{\text{front}} + X_{\text{back}} *$ corr_scores2
    return $x_{\text{enc\_new}}$
end procedure

Algorithm 3 TorchCCA: PyTorch-style Canonical Correlation Analysis (CCA)

Require: Input datasets $X \in \mathbb{R}^{N \times D_1}, Y \in \mathbb{R}^{N \times D_2}$
Require: Number of components k, scaling flag `scale`, regularization `reg`
Initialize $\texttt{TorchCCA}(k, \texttt{scale}, \texttt{reg})$
procedure FIT(X, Y)
  $X, Y \leftarrow$ CENTER_AND_SCALE(X, Y)
  $N \leftarrow$ number of rows in X
  $C_{xx} \leftarrow \frac{X^\top X}{N-1} + \texttt{reg} \cdot I$
  $C_{yy} \leftarrow \frac{Y^\top Y}{N-1} + \texttt{reg} \cdot I$
  $C_{xy} \leftarrow \frac{X^\top Y}{N-1}$
  $C_{xx}^{-1/2} \leftarrow (\text{Cholesky}(C_{xx})^{-1})^\top$
  $C_{yy}^{-1/2} \leftarrow (\text{Cholesky}(C_{yy})^{-1})^\top$
  $T \leftarrow C_{xx}^{-1/2} C_{xy} C_{yy}^{-1/2\top}$
  $(U, S, V^\top) \leftarrow \text{SVD}(T)$
  `x_weights` $\leftarrow$ first k columns of U
  `y_weights` $\leftarrow$ first k columns of V
  `corr_scores` $\leftarrow$ first k singular values S
end procedure
procedure TRANSFORM(X, Y)
  $X, Y \leftarrow$ CENTER_AND_SCALE(X, Y)
  $X_c \leftarrow X \cdot \texttt{x\_weights}$
  $Y_c \leftarrow Y \cdot \texttt{y\_weights}$
  return X_c, Y_c
end procedure
procedure FIT_TRANSFORM(X, Y)
  FIT(X, Y)
  return TRANSFORM(X, Y)
end procedure
procedure CENTER_AND_SCALE(X, Y)
  $X \leftarrow X - \text{mean}(X)$
  $Y \leftarrow Y - \text{mean}(Y)$
  if scale **then**
    $X \leftarrow X/\text{std}(X)$
    $Y \leftarrow Y/\text{std}(Y)$
  end if
  return X, Y
end procedure

Algorithm 4 BidirectionalCausalConv

Require: Input $x \in \mathbb{R}^{B \times C \times T}$, kernel size k, dilations d_f, d_b
Compute $p_f \leftarrow (k-1) \cdot d_f$
Compute $p_b \leftarrow (k-1) \cdot d_b$
$x_f \leftarrow \text{PadLeft}(x, p_f)$
$x_b \leftarrow \text{PadLeft}(\text{Flip}(x), p_b)$
$y_f \leftarrow \text{Conv1D}(x_f, \text{dilation} = d_f)$
$y_b \leftarrow \text{Flip}(\text{Conv1D}(x_b, \text{dilation} = d_b))$
return $y_f + y_b$

Algorithm 5 BidirectionalDilatedConvBlock

Require: Input x, channels C_{in}, C_{out}, kernel size k, dilation d

if $C_{in} \neq C_{out}$ or final layer **then**
    $res \leftarrow \text{Conv1D}(x, \text{kernel} = 1)$
else
    $res \leftarrow x$
end if
$x \leftarrow \text{GELU}(x)$
$x \leftarrow \text{BidirectionalCausalConv}(x, k, d, d)$
$x \leftarrow \text{GELU}(x)$
$x \leftarrow \text{BidirectionalCausalConv}(x, k, d, d)$
return $x + res$

F Ablation Experiments of the HM-BiTCN Structure

Table 7: The ablation experiments of the HM-BiTCN structure, where "Forward" indicates using only the forward part, and "Backward" indicates using only the backward part.

Datasets	Models	CIF	Forward	Backward	Accuracy ↑	Precision ↑	Recall ↑	F1 score ↑	AUROC ↑	AUPRC ↑
APAVA	**HM-BiTCN**		✓		82.31$\pm$2.34	83.29$\pm$2.50	80.39$\pm$2.65	81.02$\pm$2.63	91.50$\pm$1.80	91.66$\pm$1.82
(2-Classes)	**HM-BiTCN**			✓	79.45$\pm$3.51	80.69$\pm$3.04	77.14$\pm$4.47	77.58$\pm$4.75	87.95$\pm$3.82	88.41$\pm$3.74
	HM-BiTCN		✓	✓	82.49$\pm$1.40	82.38$\pm$1.79	81.20$\pm$1.32	81.60$\pm$1.39	91.10$\pm$1.63	91.30$\pm$1.71
APAVA	**HM-BiTCN**	✓	✓		80.43$\pm$5.60	80.46$\pm$5.23	79.56$\pm$5.98	79.50$\pm$5.97	89.23$\pm$4.44	89.62$\pm$4.25
(2-Classes)	**HM-BiTCN**	✓		✓	79.39$\pm$3.44	79.49$\pm$3.76	78.09$\pm$2.94	78.35$\pm$3.33	87.62$\pm$3.09	88.11$\pm$2.91
	HM-BiTCN	✓	✓	✓	85.16$\pm$1.55	84.76$\pm$1.62	85.33$\pm$1.27	84.82$\pm$1.49	94.06$\pm$1.07	94.21$\pm$0.99
ADFTD	**HM-BiTCN**		✓		53.32$\pm$1.35	52.01$\pm$1.54	51.46$\pm$2.19	51.21$\pm$1.99	70.78$\pm$1.78	53.16$\pm$2.20
(3-Classes)	**HM-BiTCN**			✓	52.80$\pm$1.18	50.16$\pm$0.77	49.23$\pm$1.22	49.24$\pm$1.02	68.65$\pm$0.71	49.95$\pm$0.97
	HM-BiTCN		✓	✓	52.05$\pm$2.22	50.45$\pm$3.00	50.40$\pm$2.55	49.48$\pm$2.70	69.43$\pm$2.84	50.99$\pm$3.15
ADFTD	**HM-BiTCN**	✓	✓		56.06$\pm$0.47	53.21$\pm$1.03	53.54$\pm$1.36	52.82$\pm$1.33	72.93$\pm$0.88	55.71$\pm$1.03
(3-Classes)	**HM-BiTCN**	✓		✓	56.54$\pm$1.33	54.28$\pm$0.96	54.63$\pm$1.06	53.91$\pm$1.11	73.46$\pm$1.17	56.12$\pm$1.61
	HM-BiTCN	✓	✓	✓	58.56$\pm$0.93	55.65$\pm$0.81	55.86$\pm$0.79	55.42$\pm$0.82	76.07$\pm$0.59	59.75$\pm$0.67
TDBrain	**HM-BiTCN**		✓		87.23$\pm$2.87	87.75$\pm$2.48	87.23$\pm$2.87	87.17$\pm$2.93	95.55$\pm$1.69	95.73$\pm$1.60
(2-Classes)	**HM-BiTCN**			✓	86.92$\pm$3.46	87.41$\pm$3.17	86.92$\pm$3.46	86.86$\pm$3.51	95.28$\pm$1.78	95.42$\pm$1.70
	HM-BiTCN		✓	✓	84.90$\pm$2.60	86.02$\pm$2.00	84.90$\pm$2.60	84.76$\pm$2.74	93.94$\pm$1.92	94.20$\pm$1.85
TDBrain	**HM-BiTCN**	✓	✓		93.29$\pm$1.73	93.34$\pm$1.73	93.29$\pm$1.73	93.29$\pm$1.73	98.50$\pm$0.63	98.56$\pm$0.60
(2-Classes)	**HM-BiTCN**	✓		✓	93.69$\pm$1.52	93.83$\pm$1.42	93.69$\pm$1.52	93.68$\pm$1.53	98.56$\pm$0.67	98.59$\pm$0.64
	HM-BiTCN	✓	✓	✓	93.13$\pm$1.41	93.33$\pm$1.37	93.13$\pm$1.41	93.12$\pm$1.42	98.62$\pm$0.66	98.68$\pm$0.63
PTB	**HM-BiTCN**		✓		82.56$\pm$1.74	86.16$\pm$1.51	74.91$\pm$2.88	77.24$\pm$2.92	95.69$\pm$0.64	94.56$\pm$0.76
(2-Classes)	**HM-BiTCN**			✓	81.07$\pm$4.24	85.36$\pm$2.71	72.50$\pm$6.59	74.33$\pm$6.71	92.83$\pm$2.38	91.28$\pm$2.79
	HM-BiTCN		✓	✓	81.87$\pm$1.87	86.50$\pm$1.24	73.49$\pm$2.90	75.84$\pm$3.20	94.20$\pm$0.29	93.04$\pm$0.45
PTB	**HM-BiTCN**	✓	✓		87.33$\pm$1.41	90.26$\pm$1.24	81.64$\pm$2.04	84.19$\pm$1.97	96.21$\pm$1.30	95.67$\pm$1.52
(2-Classes)	**HM-BiTCN**	✓		✓	84.35$\pm$2.28	87.42$\pm$2.07	77.54$\pm$3.30	79.98$\pm$3.41	91.25$\pm$1.92	90.42$\pm$2.28
	HM-BiTCN	✓	✓	✓	88.29$\pm$1.45	90.66$\pm$1.48	83.21$\pm$2.02	85.59$\pm$1.96	94.28$\pm$0.93	93.78$\pm$1.11
FLAAP	**HM-BiTCN**		✓		70.81$\pm$2.31	72.58$\pm$1.33	69.81$\pm$2.79	70.07$\pm$2.24	95.89$\pm$0.28	76.90$\pm$1.21
(10-Classes)	**HM-BiTCN**			✓	70.29$\pm$2.04	72.77$\pm$2.09	68.86$\pm$2.39	69.56$\pm$1.98	95.61$\pm$0.26	76.56$\pm$1.56
	HM-BiTCN		✓	✓	76.08$\pm$0.81	76.05$\pm$0.83	75.95$\pm$0.84	75.54$\pm$0.94	96.49$\pm$0.10	81.19$\pm$0.65
FLAAP	**HM-BiTCN**	✓	✓		72.30$\pm$1.50	72.98$\pm$1.61	71.65$\pm$1.35	71.54$\pm$1.50	95.92$\pm$0.55	77.87$\pm$2.27
(10-Classes)	**HM-BiTCN**	✓		✓	72.81$\pm$1.04	74.05$\pm$0.80	71.86$\pm$1.25	72.12$\pm$1.17	96.20$\pm$0.21	79.22$\pm$1.25
	HM-BiTCN	✓	✓	✓	76.82$\pm$1.32	77.38$\pm$0.85	76.52$\pm$1.24	76.39$\pm$1.18	96.48$\pm$0.06	81.77$\pm$0.81
UCI-HAR	**HM-BiTCN**		✓		91.94$\pm$0.98	92.36$\pm$0.90	92.02$\pm$0.96	91.98$\pm$0.93	99.30$\pm$0.08	97.31$\pm$0.47
(6-Classes)	**HM-BiTCN**			✓	93.03$\pm$0.62	93.28$\pm$0.63	93.12$\pm$0.60	93.05$\pm$0.62	99.36$\pm$0.19	97.72$\pm$0.46
	HM-BiTCN		✓	✓	93.72$\pm$0.73	94.02$\pm$0.72	93.75$\pm$0.70	93.69$\pm$0.76	99.60$\pm$0.09	98.31$\pm$0.40
UCI-HAR	**HM-BiTCN**	✓	✓		92.18$\pm$0.45	92.42$\pm$0.47	92.21$\pm$0.44	92.14$\pm$0.44	99.17$\pm$0.11	97.04$\pm$0.15
(6-Classes)	**HM-BiTCN**	✓		✓	92.62$\pm$0.90	92.88$\pm$0.86	92.68$\pm$0.88	92.63$\pm$0.89	99.25$\pm$0.18	97.15$\pm$0.57
	HM-BiTCN	✓	✓	✓	93.78$\pm$0.32	94.08$\pm$0.26	93.79$\pm$0.32	93.74$\pm$0.34	99.34$\pm$0.19	97.60$\pm$0.46

As described in Section 2 of the Methods, HM-BiTCN is constructed by adding a backward branch to the vanilla TCN architecture; therefore, using only the Forward part is essentially equivalent to the vanilla TCN structure.

From the table 7, it can be observed that when both the Forward and Backward parts of the HM-BiTCN structure are used simultaneously, the performance drops significantly compared to using only one of them individually. We speculate that this is mainly due to the presence of substantial noise within medical time-series data. When both parts of the structure are applied at the same time, it is akin to capturing noise from two different directions simultaneously. Instead of enhancing the representation, this leads to noise accumulation, which ultimately results in degraded performance.

However, after processing the data with CIF to improve the signal-to-noise ratio, the combination of the Forward and Backward parts of the HM-BiTCN structure eventually outperforms the use of either part alone. This result strongly demonstrates the feature-capturing capability of the HM-BiTCN when both directions are utilized together. It indicates that once noise interference is effectively reduced, the bidirectional structure of HM-BiTCN can better leverage its strengths, thereby improving overall performance.

Further observations show that using only the Forward part of HM-BiTCN outperforms the Backward part. This is closely related to the inherent unidirectionality of medical time-series signals such as EEG and ECG, where information typically propagates forward in time (e.g., neural signal transmission in EEG or atrial-to-ventricular activation in ECG). Such characteristics enable the Forward structure to capture key features and temporal evolution more effectively, yielding better performance. This finding not only deepens the understanding of medical signal processing but also provides insights for optimizing HM-BiTCN in related applications.

To evaluate the performance of our method on general time series, we follow the design of Medformer Wang et al. (2024a) and test it on two human activity recognition (HAR) datasets: FLAAP(13,123 samples, 10 classes) Kumar & Suresh (2022) and UCI-HAR(10,299 samples, 6 classes) Anguita et al. (2013).

Additionally, on the non-medical datasets FLAAP and UCI-HAR, we observed that integrating the bidirectional structure significantly improves performance. This indicates that in high-SNR scenarios, bidirectional modeling can more effectively capture both forward and backward feature information, enhancing overall model performance. In contrast, CIF provides relatively limited gains on these high-SNR datasets. This observation further highlights the design advantage of CIF: it is specifically tailored for low-SNR medical time series, explicitly fusing inter-channel physiological information to enhance signal quality and discriminative power, while its marginal benefit is smaller for low-noise non-medical data. Overall, these findings not only reveal the differential adaptability of model architectures under varying data characteristics but also underscore the unique value of CIF in complex medical scenarios.

G FURTHER EXPLORATION OF PHYSIOLOGICAL STRUCTURES

The parameters (a, b, t, n) in CIF are explicit hyperparameters that can be directly set and adjusted based on experience. For example, Figure. 8 shows the corresponding locations of EEG channels on the human brain, we have adjusted the AFAVA dataset, which comprises 16 channels: `C3`, `C4`, `F3`, `F4`, `F7`, `F8`, `Fp1`, `Fp2`, `O1`, `O2`, `P3`, `P4`, `T3`, `T4`, `T5`, and `T6`. For the first six channels, we performed pairwise fusion as follows:

$$
\begin{aligned}
C3_{\text{new}} &= a \cdot C3 + b \cdot C4, \\
F3_{\text{new}} &= a \cdot F3 + b \cdot F4, \\
F7_{\text{new}} &= a \cdot F7 + b \cdot F8.
\end{aligned}
$$

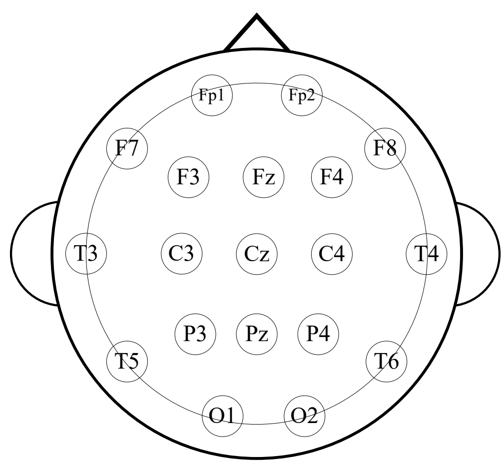

Figure 8: Physiological Placement Diagram of EEG Channels.

Here, the `C3`, `F3`, and `F7` channels correspond to `C4`, `F4`, and `F8`, respectively, exhibiting left–right physiological symmetry, and they also belong to the same functional region. We refer to this type of fusion as *Left–Right Physiological Symmetry Fusion* (LR-PSF). In contrast, the channel fusion strategy introduced earlier in this paper, controlled by the hyperparameter n, reflects fusion across different functional regions, and is therefore termed *Functional Region Fusion* (FRF).

Table 8: **Results of Subject-Independent Setup. APAVA Dataset**

Datasets	Models	Accuracy ↑	Precision ↑	Recall ↑	F1 score ↑	AUROC ↑	AUPRC ↑
APAVA (2-Classes)	HM-BiTCN	82.49±1.40	82.38±1.79	81.20±1.32	81.60±1.39	91.10±1.63	91.30±1.71
	HM-BiTCN + CIF (-Fp1 + Fp2)	82.70±1.90	83.34±1.96	80.73±2.14	81.47±2.13	91.24±2.25	91.62±2.08
	HM-BiTCN + CIF (FRF)	86.30±1.05	86.16±1.09	85.47±1.12	85.71±1.09	94.26±0.54	94.42±0.49
	HM-BiTCN + CIF (LR-PSF)	86.23±2.09	85.82±2.14	**86.04±2.06**	85.83±2.12	94.59±1.08	94.64±1.08
	HM-BiTCN + CIF (CCA)	**87.91**±1.60	**89.81**±0.93	85.85±2.12	**86.93**±1.91	**96.97**±0.52	**96.91**±0.49

Building on these two types of physiologically motivated fusion, we further introduce a data-driven fusion mechanism based on Canonical Correlation Analysis (CCA) Hotelling (1992) (For detailed pseudocode, see Code 2 3.). Specifically, for each input sample we first select the first n channels and the last n channels, denoted as

$$\mathbf{X}^{\text{front}} \in \mathbb{R}^{B\times L\times n}, \qquad \mathbf{X}^{\text{back}} \in \mathbb{R}^{B\times L\times n},$$

where B is the batch size, L is the sequence length, and n is the number of paired channels. We then reshape them into two matrices

$$\mathbf{F} \in \mathbb{R}^{(BL)\times n}, \qquad \mathbf{B} \in \mathbb{R}^{(BL)\times n},$$

by stacking all temporal positions and samples along the first dimension. We apply a CCA module to these two matrices and obtain their canonical projections

$$\mathbf{F}_{\text{c}}, \mathbf{B}_{\text{c}} \in \mathbb{R}^{(BL)\times n}.$$

For each canonical component $i \in \{1, \ldots, n\}$, we compute the Pearson correlation coefficient between the corresponding canonical variables $\mathbf{F}_{\text{c}}^{(i)}$ and $\mathbf{B}_{\text{c}}^{(i)}$, yielding a correlation score vector

$$\boldsymbol{\rho} = (\rho_1, \ldots, \rho_n)^\top \in \mathbb{R}^n.$$

These scores quantify the statistical dependence between the paired channels and are used as adaptive, channel-wise fusion weights. Concretely, we broadcast $\boldsymbol{\rho}$ back to the original tensor shape and construct two fused channel groups:

$$\widetilde{\mathbf{X}}^{\text{front}} = \mathbf{X}^{\text{front}} \odot \boldsymbol{\rho} + \mathbf{X}^{\text{back}}, \qquad \widetilde{\mathbf{X}}^{\text{back}} = \mathbf{X}^{\text{front}} + \mathbf{X}^{\text{back}} \odot \boldsymbol{\rho}',$$

where $\odot$ denotes element-wise (channel-wise) multiplication and $\boldsymbol{\rho}'$ is another correlation score vector obtained by swapping the roles of $\mathbf{F}$ and $\mathbf{B}$ in CCA. The fused tensors $\widetilde{\mathbf{X}}^{\text{front}}$ and $\widetilde{\mathbf{X}}^{\text{back}}$ are then written back to the first and last n channels of the encoder input, respectively.

In this way, the proposed CCA-based fusion adaptively strengthens or attenuates each paired channel according to its learned cross-channel correlation, providing a controllable and data-driven mechanism that complements the physiologically defined LR-PSF and FRF fusion strategies.

We consider that a full theoretical and experimental treatment of CCA would require a more extensive discussion. Therefore, here we present it solely as an exploratory method and do not include its results in the main text.

We also examined the relationship between the `Fp1` and `Fp2` channels, as introduced in the Introduction. For this purpose, we conducted experiments using the following fusion approach:

$$\texttt{Fp1}_{\text{new}} = -1 \cdot \texttt{Fp1} + 1 \cdot \texttt{Fp2},$$

which we refer to as CIF $(-\texttt{Fp1} + \texttt{Fp2})$.

The results in the table 8 reveal that explicit fusion leveraging the prior knowledge of channels can more effectively integrate channel features, thereby yielding more accurate classification outcomes. Many previous methods, especially various general time series models, are unable to incorporate such medical prior knowledge in a "controllable" manner.

H Results on General Time Series

We compared our method with various approaches on the general time series UEA dataset. The results of these methods were provided by TimeMixer++ Wang et al. (2025a). Experimental results show that CIF can enhance the performance of HM-BiTCN on general time series classification tasks. Moreover, the combination of HM-BiTCN with CIF achieves SOTA performance.

Table 9: Full results for the classification task. $*$. in the Transformers indicates the name of $*$former. We report the classification accuracy (%) as the result.

Datasets / Models	RNN			TCN	Transformers										MLP			CNN			
	LSTM (1997)	LSTNet (2018)	LSSL (2022)	TCN (2019)	Trans. (2017)	Re. (2019)	In. (2021)	Pyra. (2021)	Auto. (2021)	Station. (2022)	FED. (2022)	ETS. (2022)	Flow. (2022b)	iTrans. (2024b)	DLinear (2023)	LightTS. (2022)	TiDE (2023)	TimesNet (2022a)	Time Mixer++ (2025a)	**HM-BiTCN (Ours)**	**HM-BiTCN +CIF (Ours)**
EthanolConcentration	32.3	39.9	31.1	28.9	32.7	31.9	31.6	30.8	31.6	32.7	28.1	31.2	33.8	28.1	32.6	29.7	27.1	35.7	39.9	31.9	32.3
FaceDetection	57.7	65.7	66.7	52.8	67.3	68.6	67.0	65.7	68.4	68.0	66.0	66.3	67.6	66.3	68.0	67.5	65.3	68.6	71.8	66.8	67.2
Handwriting	15.2	25.8	24.6	53.3	32.0	27.4	32.8	29.4	36.7	31.6	28.0	32.5	33.8	24.2	27.0	26.1	23.2	32.1	26.5	49.5	51.2
Heartbeat	72.2	77.1	72.7	75.6	76.1	77.1	80.5	75.6	74.6	73.7	73.7	71.2	77.6	75.6	75.1	75.1	74.6	78.0	79.1	74.6	77.5
JapaneseVowels	79.7	98.1	98.4	98.9	98.7	97.8	98.9	98.4	96.2	99.2	98.4	95.9	98.9	96.6	96.2	96.2	95.6	98.4	97.9	97.8	98.3
PEMS-SF	39.9	86.7	86.1	68.8	82.1	82.7	81.5	83.2	82.7	87.3	80.9	86.0	83.8	87.9	75.1	88.4	86.9	89.6	91.0	82.6	86.1
SelfRegulationSCP1	68.9	84.0	90.8	84.6	92.2	90.4	90.1	88.1	84.0	89.4	88.7	89.6	92.5	90.2	87.3	89.8	89.2	91.8	93.1	89.7	91.1
SelfRegulationSCP2	46.6	52.8	52.2	55.6	53.9	56.7	53.3	53.3	50.6	57.2	54.4	55.0	56.1	54.4	50.5	51.1	53.4	57.2	65.6	61.6	62.2
SpokenArabicDigits	31.9	100.0	100.0	95.6	98.4	97.0	100.0	99.6	100.0	100.0	100.0	100.0	98.8	96.0	81.4	100.0	95.0	99.0	99.8	99.5	99.6
UWaveGestureLibrary	41.2	87.8	85.9	88.4	85.6	85.6	85.6	83.4	85.9	87.5	85.3	85.0	86.6	85.9	82.1	80.3	84.9	85.3	88.2	92.1	92.8
Average Accuracy	48.6	71.8	70.9	70.3	71.9	71.5	72.1	70.8	71.1	72.7	70.7	71.0	73.0	70.5	67.5	70.4	69.5	73.6	75.3	74.6	**75.8**

I Reproduced Results of Existing Methods

I.1 Results of Subject-Dependent

In Table 10, we present the results of various models under the *Subject-Dependent Setup* on the ADFTD (3-Classes) dataset. The results indicate that our proposed *CIF method* significantly improves the performance of models, particularly in accuracy, F1 score, AUROC, and AUPRC metrics. Specifically, the combination of *MedGNN + CIF* outperforms *MedGNN* alone across all key performance metrics, and similarly, *Medformer + CIF* surpasses *Medformer* in every critical evaluation metric. These results convincingly demonstrate the effectiveness of the CIF method in enhancing model performance. By integrating the CIF method, not only are the models' performances significantly improved across multiple evaluation metrics, but the broad applicability and substantial benefits of the method across different model architectures are also highlighted. Notably, *MedGNN + CIF* achieves a remarkable Accuracy of 99.60%, far surpassing other models, highlighting the advantage of our approach in handling imbalanced datasets. Furthermore, *MedGNN + CIF* shows significant improvements in F1 score and precision, indicating that the CIF method effectively enhances the model's ability to recognize both positive and negative samples. Thus, our experimental results validate the effectiveness of the CIF method in boosting model generalization and precision.

Table 10: **Results of Subject-Dependent Setup.** The training, validation, and test sets are split based on samples according to a predetermined ratio. Results of the ADFTD dataset under this setup are presented here.

Datasets	Models	Accuracy ↑	Precision ↑	Recall ↑	F1 score ↑	AUROC ↑	AUPRC ↑
ADFTD (3-Classes) Reproduced	**Autoformer**	$87.79_{\pm 2.87}$	$87.63_{\pm 2.95}$	$86.84_{\pm 3.10}$	$87.17_{\pm 3.05}$	$96.45_{\pm 1.15}$	$93.52_{\pm 2.05}$
	Crossformer	$89.27_{\pm 1.19}$	$88.98_{\pm 1.27}$	$88.61_{\pm 1.35}$	$88.77_{\pm 1.29}$	$97.53_{\pm 0.48}$	$95.47_{\pm 0.87}$
	FEDformer	$77.55_{\pm 2.42}$	$76.71_{\pm 2.14}$	$76.46_{\pm 2.52}$	$76.44_{\pm 2.52}$	$91.66_{\pm 1.36}$	$84.99_{\pm 2.15}$
	Informer	$91.72_{\pm 0.13}$	$91.50_{\pm 0.16}$	$91.36_{\pm 0.21}$	$91.42_{\pm 0.14}$	$98.40_{\pm 0.07}$	$96.92_{\pm 0.11}$
	iTransformer	$64.60_{\pm 0.77}$	$62.22_{\pm 0.64}$	$61.95_{\pm 0.35}$	$61.87_{\pm 0.41}$	$81.46_{\pm 0.29}$	$68.81_{\pm 0.39}$
	MTST	$65.43_{\pm 0.79}$	$64.47_{\pm 0.65}$	$63.49_{\pm 0.55}$	$63.71_{\pm 0.55}$	$81.67_{\pm 0.51}$	$69.74_{\pm 0.69}$
	Nonformer	$96.00_{\pm 0.72}$	$95.72_{\pm 0.80}$	$95.90_{\pm 0.69}$	$95.81_{\pm 0.75}$	$99.56_{\pm 0.13}$	$99.02_{\pm 0.23}$
	PatchTST	$66.55_{\pm 0.48}$	$65.61_{\pm 0.60}$	$65.26_{\pm 0.78}$	$65.26_{\pm 0.60}$	$83.27_{\pm 0.33}$	$71.96_{\pm 0.44}$
	Reformer	$90.74_{\pm 2.18}$	$90.87_{\pm 2.15}$	$90.61_{\pm 2.01}$	$90.44_{\pm 2.25}$	$98.69_{\pm 0.50}$	$97.57_{\pm 0.85}$
	Transformer	$96.62_{\pm 0.54}$	$96.46_{\pm 0.54}$	$96.45_{\pm 0.59}$	$96.45_{\pm 0.56}$	$99.69_{\pm 0.08}$	$99.31_{\pm 0.13}$
	Medformer	$95.76_{\pm 1.03}$	$95.54_{\pm 1.10}$	$95.62_{\pm 1.05}$	$95.58_{\pm 1.08}$	$99.53_{\pm 0.18}$	$99.09_{\pm 0.36}$
	Medformer + CIF	$98.87_{\pm 0.26}$	$98.77_{\pm 0.27}$	$98.86_{\pm 0.27}$	$98.81_{\pm 0.27}$	$99.96_{\pm 0.01}$	$99.92_{\pm 0.03}$
	MedGNN	$99.44_{\pm 0.21}$	$99.43_{\pm 0.21}$	$99.41_{\pm 0.22}$	$99.42_{\pm 0.21}$	$99.98_{\pm 0.01}$	$\mathbf{99.97_{\pm 0.01}}$
	MedGNN + CIF	$\mathbf{99.60_{\pm 0.09}}$	$\mathbf{99.60_{\pm 0.11}}$	$\mathbf{99.58_{\pm 0.09}}$	$\mathbf{99.59_{\pm 0.10}}$	$\mathbf{99.99_{\pm 0.01}}$	$\mathbf{99.97_{\pm 0.01}}$

I.2 Results of Subject-Independent

Table 2 presents the results of various methods reported under the subject-independent setup, while Table 11 shows the results of our reproduction of these methods. Our approach achieves the highest scores on six metrics across four out of the five datasets. For the PTB-XL dataset, compared to the

Table 11: **Results of Subject-Independent Setup.** The training, validation, and test sets are distributed based on subjects according to a predetermined ratio/IDs. Results of the APAVA, TDBrain, ADFTD, PTB, and PTB-XL datasets under this setup are presented here. Unfortunately, MedGNN has only released the training parameters for the APAVA and ADFTD datasets.

Datasets	Models	Accuracy ↑	Precision ↑	Recall ↑	F1 score ↑	AUROC ↑	AUPRC ↑
APAVA (2-Classes) Reproduced	**Autoformer**	73.18±7.33	73.87±6.72	73.01±6.10	72.40±7.03	81.64±7.24	81.10±7.75
	Crossformer	72.76±2.04	79.64±2.45	67.41±2.62	66.88±3.61	71.81±4.06	71.64±3.74
	FEDformer	75.16±1.67	74.98±0.69	73.34±2.97	73.50±2.90	83.89±1.54	83.27±1.62
	Informer	72.20±2.78	73.92±4.80	68.48±2.51	68.74±2.70	70.14±3.43	70.84±3.80
	iTransformer	74.55±1.66	74.77±2.10	71.76±1.72	72.30±1.79	85.59±1.55	84.39±1.57
	MTST	69.24±1.24	75.87±2.80	63.28±1.81	61.62±2.75	66.09±3.27	68.08±2.93
	Nonformer	71.81±4.20	71.31±4.40	70.15±3.38	70.38±3.74	71.54±2.73	72.79±2.50
	PatchTST	68.27±2.11	78.56±1.88	61.53±2.60	58.52±4.07	64.61±2.18	67.14±2.06
	Reformer	78.42±2.85	80.89±4.52	75.20±2.28	76.09±2.54	75.48±2.79	77.52±2.64
	Transformer	75.53±4.28	76.90±5.05	72.14±4.87	72.64±5.44	72.30±6.04	73.04±7.15
	Medformer	77.85±2.42	80.31±3.21	74.38±2.49	75.21±2.67	80.85±3.80	81.62±3.24
	MedGNN	77.40±5.77	82.77±4.46	73.24±7.06	73.29±9.01	81.31±2.94	82.80±2.91
	HM-BiTCN + CIF	**85.16±1.55**	**84.76±1.62**	**85.33±1.27**	**84.82±1.49**	**94.06±1.07**	**94.21±0.99**
TDBrain (2-Classes) Reproduced	**Autoformer**	90.38±3.03	91.16±2.42	90.38±3.03	90.31±3.09	95.83±2.14	95.43±2.31
	Crossformer	82.15±2.60	82.81±2.11	82.15±2.60	82.04±2.70	91.20±2.23	91.47±2.16
	FEDformer	77.60±1.23	78.25±1.52	77.60±1.23	77.48±1.19	86.31±1.23	86.48±1.36
	Informer	88.42±2.99	89.01±2.45	88.42±2.99	88.36±3.05	96.54±0.90	96.66±0.85
	iTransformer	74.69±1.02	74.76±1.04	74.69±1.02	74.67±1.02	83.35±1.24	83.65±1.41
	MTST	77.67±3.58	78.97±4.37	77.67±3.58	77.45±3.55	86.47±4.84	84.99±6.43
	Nonformer	88.10±2.39	88.76±1.74	88.10±2.39	88.04±2.47	96.56±0.91	96.36±1.21
	PatchTST	77.98±2.64	79.30±3.73	77.98±2.64	77.76±2.65	86.67±4.03	84.93±5.47
	Reformer	88.50±2.30	89.01±1.80	88.50±2.30	88.45±2.35	96.10±0.63	96.19±0.55
	Transformer	85.13±1.86	86.39±1.56	85.13±1.86	84.99±1.93	95.61±1.05	95.63±0.91
	Medformer	88.77±1.24	88.91±1.11	88.77±1.24	88.76±1.25	96.38±0.34	96.44±0.30
	MedGNN	-	-	-	-	-	-
	HM-BiTCN + CIF	**93.13±1.41**	**93.33±1.37**	**93.13±1.41**	**93.12±1.42**	**98.62±0.66**	**98.68±0.63**
ADFTD (3-Classes) Reproduced	**Autoformer**	46.90±2.89	45.59±2.37	44.91±2.23	44.34±2.52	63.49±2.44	45.63±2.29
	Crossformer	50.18±1.97	45.97±1.84	46.30±1.73	45.90±1.84	66.68±1.67	48.65±1.89
	FEDformer	45.75±0.78	45.71±1.29	44.27±1.28	43.51±1.00	62.64±1.64	45.88±1.35
	Informer	48.42±1.99	46.94±1.60	46.41±0.99	45.76±0.43	65.99±1.14	47.49±1.07
	iTransformer	52.85±1.36	46.97±1.05	47.31±1.03	46.84±0.78	67.46±0.96	49.90±0.89
	MTST	45.77±1.70	44.39±1.73	43.70±1.82	43.36±1.98	61.38±1.57	44.01±1.60
	Nonformer	50.81±1.06	48.71±1.40	48.55±1.47	48.36±1.38	66.95±1.54	48.08±1.82
	PatchTST	43.32±0.53	41.95±0.38	41.45±1.26	40.75±1.62	60.21±0.29	42.49±0.57
	Reformer	51.28±2.60	49.68±2.75	49.64±2.02	48.45±2.06	69.20±2.53	51.74±3.24
	Transformer	50.53±0.94	49.31±0.87	48.57±1.23	48.42±1.28	67.98±0.90	49.07±1.35
	Medformer	53.70±1.18	51.51±1.32	50.49±1.48	50.35±1.53	70.48±1.17	50.91±1.13
	MedGNN	50.22±3.21	48.65±3.72	47.50±4.57	47.33±4.40	67.18±4.39	48.84±4.11
	HM-BiTCN + CIF	**58.56±0.93**	**55.65±0.81**	**55.86±0.79**	**55.42±0.82**	**76.07±0.59**	**59.75±0.67**
PTB (2-Classes) Reproduced	**Autoformer**	71.99±2.74	69.60±3.85	61.50±4.23	61.43±5.07	74.29±1.89	70.26±2.00
	Crossformer	78.06±3.44	81.53±3.13	68.62±5.63	69.76±6.53	88.31±2.07	85.81±2.43
	FEDformer	74.54±2.27	77.99±4.10	63.14±3.29	63.28±4.36	84.63±4.27	80.91±5.55
	Informer	79.59±0.65	83.33±0.77	70.58±0.95	72.58±1.08	92.77±0.48	90.89±0.57
	iTransformer	83.43±1.19	88.06±1.47	75.64±1.55	78.29±1.70	91.38±1.41	91.08±1.30
	MTST	75.53±2.45	78.72±1.87	64.78±4.06	65.30±4.81	87.76±4.09	83.60±3.92
	Nonformer	78.93±1.46	82.48±1.53	69.68±2.15	71.50±2.56	90.54±0.59	87.78±1.46
	PatchTST	75.28±2.44	77.05±2.44	64.86±4.05	65.41±5.28	88.11±2.59	82.65±2.87
	Reformer	78.11±1.65	82.70±0.80	68.17±2.68	69.68±3.34	90.77±1.56	88.14±1.20
	Transformer	76.43±1.98	81.25±1.15	65.64±3.29	66.44±4.39	90.21±1.24	87.28±1.49
	Medformer	80.99±0.75	83.01±0.72	73.35±1.16	75.47±1.21	93.10±1.18	90.69±1.04
	MedGNN	-	-	-	-	-	-
	HM-BiTCN + CIF	**88.29±1.45**	**90.66±1.48**	**83.21±2.02**	**85.59±1.96**	**94.28±0.93**	**93.78±1.11**
PTB-XL (5-Classes) Reproduced	**Autoformer**	60.37±1.72	49.83±0.50	49.17±0.72	48.43±0.47	81.35±0.56	50.83±0.72
	Crossformer	73.15±0.17	64.62±0.31	**61.28±0.45**	**62.49±0.34**	89.94±0.15	67.14±0.29
	FEDformer	56.01±10.27	51.61±5.58	48.77±7.64	47.23±8.76	82.01±4.20	52.23±7.14
	Informer	71.28±0.27	62.28±0.53	59.18±0.54	60.38±0.38	88.57±0.09	64.57±0.18
	iTransformer	69.18±0.33	59.44±0.48	54.84±0.25	56.44±0.23	86.65±0.17	60.27±0.44
	MTST	72.14±0.29	64.01±0.61	59.31±0.27	61.07±0.32	88.82±0.19	65.52±0.52
	Nonformer	70.51±0.79	61.42±1.03	58.15±0.57	59.31±0.63	88.20±0.43	63.33±0.77
	PatchTST	73.13±0.20	65.38±0.54	60.61±0.56	62.39±0.27	89.66±0.16	66.97±0.24
	Reformer	71.24±0.46	61.78±0.79	59.67±0.99	60.51±0.65	88.67±0.21	64.29±0.29
	Transformer	70.46±0.42	61.56±0.58	57.86±0.65	59.16±0.46	88.18±0.14	63.25±0.27
	Medformer	72.94±0.15	64.39±0.32	59.98±0.49	61.61±0.33	89.67±0.10	66.25±0.25
	MedGNN	-	-	-	-	-	-
	HM-BiTCN + CIF	**73.73±0.30**	**65.41±0.67**	60.70±1.08	61.89±0.91	**90.53±0.22**	**67.75±0.75**

results reported by other methods, our method achieves the highest AUROC, with Accuracy ranking second.

In comparison with our reproduced results, our method ranks first in Accuracy, AUROC, and AUPRC, and second in Precision and Recall. Additionally, it is noteworthy that under the subject-independent setup, the F1 score for ADFTD is 55.42%, significantly lower than the 99.59% F1 score achieved under the subject-dependent setup. This comparison highlights the challenge of the subject-independent setup, which better simulates real-world scenarios.

J Ablation Study

J.1 Module Study of CIF

We conduct experiments by integrating our Channel-Imposed Fusion principle with other methods.

In the CIF structure, there are four different hyperparameters. First, t is the switch for forward and backward feature fusion. When $t = 1$, it replaces the forward features with the fused features; when $t = -1$, it replaces the backward features with the fused features. The second hyperparameter, n, determines the number of selected channels. Additionally, there are two scaling factors associated with the channels: a, the scaling factor for the first n channels, and b, the scaling factor for the remaining n channels. Both a and b can either be learnable or fixed parameters. We use 🔥 to represent learnable parameters, and ❄️ to represent non-learnable parameters.

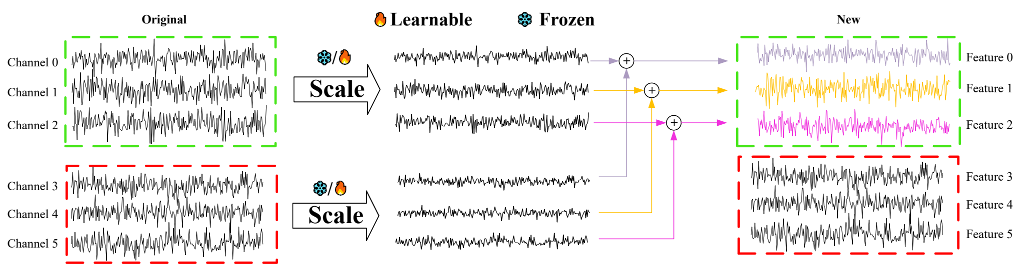

Figure 9: The case of $X_i^{new} = X_{fused}$ is marked by setting $t = 1$.

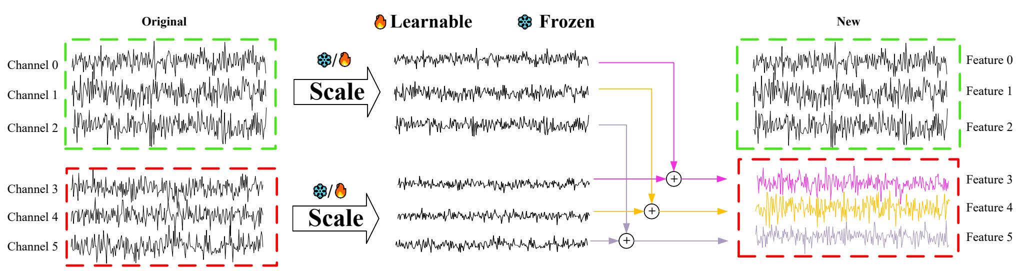

Figure 10: The case of $X_j^{new} = X_{fused}$ is marked by setting $t = -1$.

Following the theoretical analysis of the parameters a and b in Appendix A, we perform an evenly spaced grid search over the range $[-1, 1] \times [-1, 1]$ and report the overall performance trends as these hyperparameters vary.

The ablation study(Table 12 13 14) reveals that the performance of the CIF architecture is highly sensitive to its hyperparameters, with optimal configurations varying significantly across datasets. For the APAVA dataset (16 channels), the best results (86.30% accuracy, 94.26% AUROC) are achieved using backward fusion ($t = -1$) on 9 selected channels ($n = 9$), where the first 7 channels apply fixed reinforcement weights ($a = -0.8$, learnable) and the rest use fixed suppression weights ($b = -0.6$, learnable). Conversely, the ADFTD dataset (19 channels) performs best (58.56% accuracy, 76.07% AUROC) with forward fusion ($t = 1$) over 10 selected channels ($n = 10$) using dynamically learned weights for negative suppression ($a = -0.19$) and positive enhancement ($b = 0.27$). These differences, also observed in PTB (APAVA: 78–85% accuracy vs. ADFTD: 50–58%), emphasize the critical role of dataset-specific tuning. In particular, the number of selected channels (n) and fusion direction (t) are pivotal, while adaptive weighting (a/b) further improves robustness. Overall, the results highlight the necessity of careful hyperparameter optimization—especially in channel selection and fusion strategy—for maximizing CIF performance across diverse medical time series tasks.

Overall, the number of selected channels n and the fusion direction t are the key factors influencing performance, while the adaptive weights a/b further enhance the robustness and generalization ability of the model. Taken together, these results indicate that, for diverse medical time-series tasks, fully leveraging the advantages of CIF requires careful and systematic optimization of hyperparameters such as channel selection and fusion strategy.

Table 12: Ablation study of CIF structure hyperparameters on ADFTD dataset (19 Channels). We use 🔥 to represent learnable parameters, and ❄ to represent non-learnable parameters.

t	n	a	b	Accuracy	Precision	Recall	F1 score	AUROC	AUPRC
-	-	-	-	52.05±2.22	50.45±3.00	50.40±2.55	49.48±2.70	69.43±2.84	50.99±3.15
1	10	-0.20 ❄	-0.30 ❄	57.33±0.95	54.06±1.47	54.44±1.33	53.73±1.47	74.82±1.36	58.24±1.78
1	10	-0.25 ❄	-0.40 ❄	57.08±1.46	53.31±0.98	53.24±1.14	52.87±0.98	73.77±1.28	56.86±1.47
1	11	-0.20 ❄	-0.30 ❄	56.68±1.30	53.04±2.00	53.45±2.03	52.84±2.30	73.81±1.55	57.34±1.46
1	10	-0.19 🔥	-0.27 🔥	**58.56±0.93**	**55.65±0.81**	**55.86±0.79**	**55.42±0.82**	**76.07±0.59**	**59.75±0.67**
1	7	0.20 🔥	-0.60 🔥	56.36±0.58	53.91±1.10	54.34±1.03	53.78±0.91	74.19±0.69	56.62±1.28
1	9	-0.20 🔥	-0.60 🔥	55.20±1.50	53.05±1.14	53.21±1.06	52.76±1.02	73.09±1.13	55.50±1.71
1	10	-0.20 🔥	-0.20 🔥	57.11±0.92	55.04±1.43	55.53±1.57	54.58±1.29	75.13±1.33	58.47±1.43
1	11	-0.20 🔥	-0.30 🔥	57.83±1.16	54.32±1.22	54.51±1.18	54.01±1.21	74.74±1.12	57.96±1.08
1	11	-0.18 🔥	-0.25 🔥	57.00±1.32	53.00±2.28	53.17±1.94	52.32±2.19	73.97±1.89	57.00±1.93
1	7	-1.00 ❄	-1.00 ❄	51.29±1.14	49.72±1.46	49.95±1.65	49.35±1.44	69.13±0.82	51.01±1.19
1	7	-1.00 🔥	-1.00 🔥	50.46±1.57	48.50±1.19	48.68±1.29	48.20±1.38	68.18±1.08	49.73±1.24
1	7	-1.00 ❄	-0.80 ❄	50.62±2.38	49.34±2.17	49.49±2.18	48.97±2.34	68.55±1.78	50.52±2.40
1	7	-1.00 🔥	-0.80 🔥	50.51±2.57	49.04±2.31	49.26±2.60	48.73±2.66	68.32±2.13	50.38±2.53
1	7	-1.00 ❄	-0.60 ❄	51.51±1.56	50.15±1.36	50.35±1.03	49.80±1.24	69.03±0.92	51.09±1.48
1	7	-1.00 🔥	-0.60 🔥	51.09±2.05	49.84±1.97	50.24±2.16	49.33±1.84	69.04±1.83	51.15±2.55
1	7	-1.00 ❄	-0.40 ❄	51.17±1.27	48.47±1.03	48.45±1.36	47.83±1.38	68.20±0.79	49.55±1.06
1	7	-1.00 ❄	-0.40 ❄	53.59±1.01	52.16±2.37	52.16±3.11	51.01±3.24	70.77±2.29	53.17±3.59
1	7	-1.00 🔥	-0.40 🔥	51.27±0.91	48.14±0.91	48.28±1.15	47.66±1.18	67.95±1.05	48.92±1.71
1	7	-1.00 🔥	-0.40 🔥	53.03±1.70	52.41±2.70	51.95±3.09	50.35±3.43	70.69±2.34	52.99±3.58
1	7	-1.00 ❄	-0.20 ❄	51.11±0.61	48.09±0.51	47.88±0.59	47.40±0.59	67.73±0.67	48.74±0.89
1	7	-1.00 ❄	-0.20 ❄	54.26±0.58	52.53±1.78	51.58±2.01	51.31±2.32	70.87±1.43	53.25±2.30
1	7	-1.00 🔥	-0.20 🔥	50.21±2.53	47.75±2.54	47.84±2.62	47.38±2.51	67.34±2.67	48.72±3.07
1	7	-1.00 🔥	-0.20 🔥	54.91±1.15	53.99±1.35	53.54±2.01	53.16±1.56	72.41±1.23	55.67±1.70
1	8	-1.00 ❄	-1.00 ❄	51.22±0.94	49.68±1.50	49.67±2.01	49.18±1.59	68.92±1.00	51.02±1.05
1	8	-1.00 🔥	-1.00 🔥	52.00±1.48	50.10±1.12	49.87±1.43	49.56±1.17	69.38±0.97	51.20±1.26
1	8	-1.00 ❄	-0.80 ❄	52.20±1.50	49.88±1.71	49.90±1.85	49.69±1.75	69.44±1.36	51.39±1.69
1	8	-1.00 🔥	-0.80 🔥	51.19±2.06	47.57±1.30	47.61±1.79	47.18±1.62	67.52±1.78	48.94±1.69
1	8	-1.00 ❄	-0.60 ❄	51.67±1.42	47.79±0.92	47.97±1.22	47.49±1.21	67.89±1.31	49.35±1.62
1	8	-1.00 🔥	-0.60 🔥	51.15±1.78	47.52±0.70	47.29±1.10	46.62±0.71	67.69±1.50	48.90±1.31
1	8	-1.00 ❄	-0.40 ❄	52.58±1.40	49.21±2.48	49.35±1.80	48.50±2.27	68.95±1.57	50.26±2.08
1	8	-1.00 ❄	-0.40 ❄	52.40±0.54	50.11±2.26	49.92±2.13	48.87±2.64	69.13±1.85	50.62±2.47
1	8	-1.00 🔥	-0.40 🔥	52.61±1.20	49.38±2.01	49.07±1.57	48.32±1.97	68.92±1.50	50.01±1.66
1	8	-1.00 🔥	-0.40 🔥	52.47±1.46	49.68±1.96	49.59±1.70	48.30±2.21	68.60±1.70	49.58±2.21
1	8	-1.00 ❄	-0.20 ❄	51.83±1.52	48.65±2.57	48.79±2.05	48.16±2.45	67.83±1.86	49.21±2.17
1	8	-1.00 ❄	-0.20 ❄	52.14±1.35	50.70±2.37	50.25±2.35	49.75±2.07	69.64±1.73	51.02±2.65
1	8	-1.00 🔥	-0.20 🔥	52.70±1.14	50.10±1.76	49.66±1.42	48.99±1.71	69.22±1.06	50.20±1.09

Continued on next page

t	n	a	b	Accuracy	Precision	Recall	F1 score	AUROC	AUPRC
1	8	-1.00 🔥	-0.20 🔥	52.64±0.73	49.69±2.78	50.02±1.94	48.95±2.76	69.15±1.81	50.69±2.16
1	9	-1.00 ❄️	-1.00 ❄️	53.35±1.53	49.43±0.75	49.65±0.54	49.05±1.03	69.05±0.60	51.18±0.44
1	9	-1.00 🔥	-1.00 🔥	53.42±2.39	50.34±1.98	50.23±1.85	49.47±2.21	69.43±1.40	51.76±1.87
1	9	-1.00 ❄️	-0.80 ❄️	52.60±1.52	50.27±0.83	50.10±0.85	49.49±0.70	69.19±0.43	51.16±0.76
1	9	-1.00 🔥	-0.80 🔥	52.41±1.31	49.15±0.81	49.14±1.22	48.13±1.43	68.53±0.45	50.22±0.82
1	9	-1.00 ❄️	-0.60 ❄️	52.18±0.91	49.49±1.11	49.40±1.37	48.90±0.85	68.75±1.16	50.44±1.61
1	9	-1.00 🔥	-0.60 🔥	51.92±1.60	49.03±0.83	48.73±0.78	48.13±0.88	68.31±0.40	49.95±0.46
1	9	-1.00 ❄️	-0.40 ❄️	51.34±0.70	49.72±0.34	49.90±0.42	49.32±0.42	68.67±0.31	50.21±0.90
1	9	-1.00 ❄️	-0.40 ❄️	51.36±2.78	49.89±1.37	49.48±1.07	48.83±1.52	69.11±1.57	50.22±1.88
1	9	-1.00 🔥	-0.40 🔥	52.24±1.09	49.96±0.92	49.42±0.99	49.01±0.85	68.50±0.91	49.71±1.22
1	9	-1.00 🔥	-0.40 🔥	51.23±2.51	50.34±0.95	49.68±0.70	48.94±1.37	69.81±1.24	51.01±1.47
1	9	-1.00 ❄️	-0.20 ❄️	51.30±0.83	49.86±0.96	49.61±0.99	49.00±0.83	68.90±0.99	50.08±1.43
1	9	-1.00 ❄️	-0.20 ❄️	50.63±2.05	49.20±1.98	48.76±1.75	48.08±1.47	68.55±1.89	49.46±2.35
1	9	-1.00 🔥	-0.20 🔥	53.22±2.54	51.76±2.90	50.85±3.02	50.22±3.38	69.92±2.50	51.51±3.36
1	9	-1.00 🔥	-0.20 🔥	51.03±2.23	49.86±1.36	49.59±1.59	49.03±1.66	69.13±1.44	50.35±2.08
1	10	-1.00 ❄️	-1.00 ❄️	51.76±1.87	49.07±2.33	48.94±2.07	48.35±2.23	68.73±1.56	50.36±2.20
1	10	-1.00 🔥	-1.00 🔥	49.94±1.17	47.35±2.22	47.48±1.98	46.89±2.20	67.17±0.98	48.61±1.84
1	10	-1.00 ❄️	-0.80 ❄️	52.94±2.14	50.68±2.19	50.17±2.00	49.79±1.94	69.46±1.79	51.11±2.61
1	10	-1.00 🔥	-0.80 🔥	52.13±2.00	49.49±2.73	49.51±2.54	48.81±2.72	68.65±1.77	50.42±2.08
1	10	-1.00 ❄️	-0.60 ❄️	51.87±2.46	49.68±2.77	49.99±2.84	49.24±2.95	69.18±2.01	51.03±2.77
1	10	-1.00 🔥	-0.60 🔥	51.86±1.69	49.10±1.32	49.76±1.38	48.69±1.49	69.01±1.02	50.41±1.35
1	10	-1.00 ❄️	-0.40 ❄️	52.66±1.03	47.97±1.50	48.38±0.97	47.34±1.41	68.12±1.15	49.01±1.38
1	10	-1.00 ❄️	-0.40 ❄️	52.51±2.82	51.49±3.07	51.10±3.57	50.33±3.43	70.03±3.22	51.80±4.02
1	10	-1.00 🔥	-0.40 🔥	52.41±1.03	48.62±1.93	49.14±1.60	47.99±1.75	68.41±1.13	49.39±1.37
1	10	-1.00 🔥	-0.40 🔥	51.49±1.49	50.82±1.60	50.21±1.68	49.51±1.59	69.39±1.74	50.83±2.24
1	10	-1.00 ❄️	-0.20 ❄️	52.93±0.91	50.09±2.50	49.23±1.64	48.63±1.98	69.06±1.84	50.34±2.30
1	10	-1.00 ❄️	-0.20 ❄️	54.29±2.40	52.85±2.43	51.05±1.91	50.86±2.26	71.26±2.20	53.12±2.65
1	10	-1.00 🔥	-0.20 🔥	53.17±2.38	49.78±3.85	50.04±3.26	49.42±3.77	69.42±3.45	50.81±4.85
1	10	-1.00 🔥	-0.20 🔥	52.73±3.06	51.96±2.78	51.07±2.84	50.37±3.15	70.70±2.84	52.46±3.47
1	11	-1.00 ❄️	-1.00 ❄️	52.58±0.58	48.82±1.37	49.03±1.32	48.54±1.36	68.70±0.98	50.46±1.21
1	11	-1.00 🔥	-1.00 🔥	51.62±1.79	48.69±2.60	48.58±2.66	48.48±2.49	68.51±1.74	50.69±2.33
1	11	-1.00 ❄️	-0.80 ❄️	52.30±1.30	49.28±1.37	48.77±0.61	48.05±1.12	68.63±1.10	50.61±1.37
1	11	-1.00 🔥	-0.80 🔥	53.35±2.23	49.09±2.26	49.08±2.12	47.91±2.25	68.62±1.60	50.38±1.64
1	11	-1.00 ❄️	-0.60 ❄️	51.63±1.71	49.23±1.82	48.99±1.43	48.42±1.59	69.21±1.40	51.41±1.71
1	11	-1.00 🔥	-0.60 🔥	52.79±2.04	48.88±3.26	49.16±2.06	48.29±2.78	68.38±2.51	50.14±2.64
1	11	-1.00 ❄️	-0.40 ❄️	51.21±2.03	48.89±1.47	48.68±0.96	47.98±1.63	68.61±1.26	50.42±1.04
1	11	-1.00 🔥	-0.40 🔥	52.76±1.32	48.29±3.35	48.87±2.77	47.83±3.61	68.48±2.72	50.29±3.06
1	11	-1.00 ❄️	-0.20 ❄️	52.17±2.07	49.95±1.95	49.34±1.79	48.76±2.17	69.64±1.89	51.36±1.79
1	11	-1.00 ❄️	-0.20 ❄️	52.94±1.57	50.48±1.48	50.62±1.19	49.65±1.34	69.49±1.11	50.60±1.77
1	11	-1.00 🔥	-0.20 🔥	52.86±1.18	49.30±2.91	49.10±2.10	48.35±2.69	69.00±1.91	50.58±2.21
1	11	-1.00 🔥	-0.20 🔥	52.79±1.55	50.06±1.70	50.33±1.44	49.25±1.58	69.63±1.11	50.74±1.63
1	12	-1.00 ❄️	-1.00 ❄️	52.23±0.70	49.02±1.30	48.85±1.39	48.42±1.79	69.42±1.28	51.53±1.57
1	12	-1.00 🔥	-1.00 🔥	52.87±0.91	48.84±1.15	48.80±1.09	48.17±1.61	69.83±1.51	51.81±1.39
1	12	-1.00 ❄️	-0.80 ❄️	51.77±1.81	49.15±1.61	48.85±1.60	48.10±1.99	69.28±1.63	51.18±1.62
1	12	-1.00 🔥	-0.80 🔥	51.30±1.90	48.55±2.06	48.64±2.13	48.15±2.30	68.67±1.85	50.49±2.12
1	12	-1.00 ❄️	-0.60 ❄️	51.09±2.09	48.78±1.64	48.58±1.66	48.01±1.97	68.73±1.96	50.50±2.11
1	12	-1.00 🔥	-0.60 🔥	50.75±2.02	48.16±2.49	47.98±2.48	47.38±2.42	68.05±2.19	49.60±2.52
1	12	-1.00 ❄️	-0.40 ❄️	50.24±1.48	47.38±1.71	47.13±1.68	46.79±1.63	67.87±1.12	49.14±1.11
1	12	-1.00 🔥	-0.40 🔥	49.54±2.95	47.32±2.66	47.10±2.16	46.00±2.48	67.31±1.79	48.73±2.04
1	12	-1.00 ❄️	-0.20 ❄️	50.92±1.56	48.17±1.85	48.04±1.63	47.63±1.68	68.12±1.42	49.36±1.84
1	12	-1.00 ❄️	-0.20 ❄️	51.41±2.32	49.46±2.48	49.58±2.61	48.42±2.26	68.68±2.27	49.71±2.82
1	12	-1.00 🔥	-0.20 🔥	51.05±1.58	48.59±2.39	48.22±1.78	47.63±1.73	68.61±1.48	49.90±1.68
1	12	-1.00 🔥	-0.20 🔥	52.52±0.88	49.16±2.35	49.51±2.45	48.47±1.92	69.29±2.02	50.12±2.34

Table 13: Ablation study of CIF structure hyperparameters on PTB dataset (15 Channels). We use 🔥 to represent learnable parameters, and ❄ to represent non-learnable parameters.

t	n	a	b	Accuracy	Precision	Recall	F1 score	AUROC	AUPRC
-	-	-	-	81.87±1.87	86.50±1.24	73.49±2.90	75.84±3.20	94.20±0.29	93.04±0.45
1	8	0.21 ❄	-0.50 ❄	**88.29±1.45**	**90.66±1.48**	**83.21±2.02**	**85.59±1.96**	94.28±0.93	**93.78±1.11**
1	8	0.20 ❄	-0.50 ❄	84.45±2.15	88.34±1.15	77.40±3.52	79.89±3.51	93.15±0.70	91.94±0.67
1	9	0.22 ❄	-0.50 ❄	85.14±0.22	87.42±1.08	79.05±0.52	81.42±0.35	93.82±1.19	92.73±1.27
1	10	0.22 ❄	-0.50 ❄	85.40±2.08	88.17±1.96	79.17±3.12	81.57±3.07	**94.57±1.13**	93.53±1.44
1	11	0.22 ❄	-0.50 ❄	84.47±0.84	88.02±0.59	77.50±1.26	80.10±1.28	92.77±0.89	92.02±0.78
1	8	0.23 ❄	-0.50 ❄	83.96±5.41	87.13±3.96	76.89±8.22	78.66±9.51	92.49±2.91	91.14±3.79
1	8	0.25 ❄	-0.50 ❄	85.56±2.09	88.96±1.77	79.03±3.03	81.61±3.14	93.61±1.11	93.07±1.03
-1	7	-1.00 ❄	-1.00 ❄	82.57±0.88	86.88±0.94	74.58±1.26	77.09±1.35	93.75±1.30	92.74±1.65
-1	7	-1.00 🔥	-1.00 🔥	82.26±3.27	86.11±2.38	74.28±4.93	76.48±5.44	92.94±2.37	91.53±2.75
-1	7	-1.00 ❄	-0.90 ❄	81.49±3.97	86.49±2.89	72.81±6.00	74.78±6.87	93.41±1.80	92.62±2.04
-1	7	-1.00 🔥	-0.90 🔥	78.44±4.44	84.94±2.03	68.22±7.05	69.04±8.81	92.58±2.17	91.48±2.14
-1	7	-1.00 ❄	-0.80 ❄	79.94±3.18	85.35±2.61	70.48±4.79	72.26±6.02	93.43±1.49	92.30±1.61
-1	7	-1.00 🔥	-0.80 🔥	80.57±4.70	85.89±3.20	71.38±7.18	72.86±9.26	92.43±0.59	91.48±1.19
-1	7	-1.00 ❄	-0.70 ❄	81.01±2.74	86.90±0.99	71.93±4.34	73.99±5.25	92.44±2.72	91.70±2.53
-1	7	-1.00 🔥	-0.70 🔥	83.64±1.03	87.21±0.54	76.36±1.71	78.88±1.65	93.50±0.94	92.83±0.73
-1	7	-1.00 ❄	-0.60 ❄	80.22±1.47	86.35±1.48	70.72±2.19	72.82±2.57	92.61±1.47	91.70±1.77
-1	7	-1.00 🔥	-0.60 🔥	81.73±2.77	86.55±1.78	73.24±4.32	75.45±4.82	90.80±1.65	90.14±1.62
-1	8	-1.00 ❄	-1.00 ❄	82.23±3.14	86.39±1.88	74.18±4.86	76.40±5.01	94.31±1.14	93.25±1.17
-1	8	-1.00 🔥	-1.00 🔥	80.07±1.79	84.28±2.52	71.10±2.50	73.16±2.85	93.63±0.95	92.04±1.42
-1	8	-1.00 ❄	-0.90 ❄	81.36±2.30	86.49±1.89	72.62±3.49	74.87±3.81	92.14±2.56	91.19±2.68
-1	8	-1.00 🔥	-0.90 🔥	79.96±1.46	84.20±1.84	70.92±2.02	72.98±2.32	92.00±1.97	90.66±2.01
-1	8	-1.00 ❄	-0.80 ❄	80.34±1.93	86.14±1.65	71.00±3.00	73.07±3.40	91.44±2.64	91.01±2.55
-1	8	-1.00 🔥	-0.80 🔥	77.08±4.30	84.12±3.23	66.14±6.66	66.44±9.24	89.68±3.65	88.73±3.53
-1	8	-1.00 ❄	-0.70 ❄	79.17±2.48	85.39±1.26	69.35±4.22	70.91±5.05	92.43±1.29	91.69±0.98
-1	8	-1.00 🔥	-0.70 🔥	80.03±4.82	85.46±2.00	70.75±7.74	71.98±8.94	91.05±2.98	90.05±3.18
-1	9	-1.00 ❄	-1.00 ❄	81.23±2.67	86.60±1.43	72.39±4.23	74.52±4.64	92.20±1.22	91.55±1.57
-1	9	-1.00 🔥	-1.00 🔥	80.05±4.78	86.50±2.17	70.45±7.40	71.73±9.27	92.73±0.93	91.87±1.14
-1	9	-1.00 ❄	-0.90 ❄	80.89±4.06	87.74±1.78	71.49±6.25	73.24±7.85	93.83±2.39	93.33±2.64
-1	9	-1.00 🔥	-0.90 🔥	82.34±3.22	87.35±2.06	74.12±5.14	76.30±5.62	94.05±2.17	93.54±2.08
-1	9	-1.00 ❄	-0.80 ❄	84.06±3.49	88.91±1.67	76.49±5.44	78.88±5.80	92.73±1.43	92.39±1.26
-1	9	-1.00 🔥	-0.80 🔥	82.50±2.14	88.19±1.12	74.03±3.33	76.51±3.67	94.33±0.84	93.83±1.05
-1	9	-1.00 ❄	-0.70 ❄	81.44±4.04	87.88±1.77	72.37±6.23	74.28±7.32	92.35±1.77	91.86±1.50
-1	9	-1.00 🔥	-0.70 🔥	80.07±3.15	87.48±1.01	70.24±4.97	71.96±6.03	92.83±2.18	92.43±2.24
-1	10	-1.00 ❄	-1.00 ❄	79.43±3.39	85.03±2.12	69.86±5.42	71.34±6.75	90.25±3.82	89.29±4.14
-1	10	-1.00 🔥	-1.00 🔥	82.20±1.03	86.48±1.03	74.07±1.47	76.53±1.61	92.05±2.25	91.29±2.26
-1	10	-1.00 ❄	-0.90 ❄	83.08±3.17	87.22±1.54	75.41±5.02	77.64±5.69	90.27±3.83	89.89±3.83
-1	10	-1.00 🔥	-0.90 🔥	80.74±3.10	86.14±1.21	71.72±4.94	73.63±5.85	92.44±1.50	91.53±1.55
-1	10	-1.00 ❄	-0.80 ❄	78.96±3.54	86.02±2.07	68.75±5.52	70.07±6.74	90.23±3.34	89.36±3.48
-1	10	-1.00 🔥	-0.80 🔥	79.20±3.45	85.98±0.63	69.31±5.83	70.58±6.97	93.24±1.60	92.07±1.78
-1	10	-1.00 ❄	-0.70 ❄	82.37±1.89	87.63±0.88	74.00±3.03	76.44±3.21	93.05±1.90	92.39±1.83
-1	10	-1.00 🔥	-0.70 🔥	77.99±4.51	85.22±0.87	67.50±7.35	67.94±9.84	91.94±3.85	90.81±3.67
-1	11	-1.00 ❄	-1.00 ❄	81.63±3.29	86.31±2.32	73.11±5.00	75.22±5.90	91.76±2.02	90.82±2.04
-1	11	-1.00 🔥	-1.00 🔥	79.09±3.82	86.30±1.79	68.91±5.95	70.15±7.70	91.35±3.78	90.46±3.63
-1	11	-1.00 ❄	-0.90 ❄	79.68±2.84	86.22±1.10	69.89±4.48	71.60±5.35	92.11±1.09	91.33±1.27
-1	11	-1.00 🔥	-0.90 🔥	78.44±3.40	86.20±1.44	67.84±5.36	68.96±6.63	90.75±5.55	90.19±5.31
-1	11	-1.00 ❄	-0.80 ❄	80.05±2.78	87.14±1.09	70.25±4.35	72.08±5.08	92.86±2.82	92.27±2.86
-1	11	-1.00 🔥	-0.80 🔥	82.18±0.99	86.96±1.56	73.88±1.47	76.36±1.56	91.48±3.29	90.85±3.31
-1	11	-1.00 ❄	-0.70 ❄	80.82±2.07	85.72±1.44	71.94±3.23	74.08±3.62	89.25±2.75	88.51±2.83
-1	11	-1.00 🔥	-0.70 🔥	78.20±2.54	84.96±1.72	67.72±3.95	69.00±5.18	90.29±0.65	89.52±0.96

Continued on next page

t	n	a	b	Accuracy	Precision	Recall	F1 score	AUROC	AUPRC
-1	12	-1.00 ❄	-1.00 ❄	78.27±3.04	86.34±1.19	67.54±4.80	68.65±6.04	91.52±2.68	90.92±2.48
-1	12	-1.00 🔥	-1.00 🔥	82.45±1.76	87.85±0.79	74.10±3.00	76.55±3.05	92.78±1.02	92.30±0.82
-1	12	-1.00 ❄	-0.90 ❄	79.49±1.84	85.59±2.16	69.67±2.57	71.57±3.17	91.80±1.78	90.84±1.96
-1	12	-1.00 🔥	-0.90 🔥	82.03±1.90	88.37±0.83	73.22±3.06	75.64±3.42	93.21±1.67	92.67±1.74
-1	12	-1.00 ❄	-0.80 ❄	80.02±2.82	86.84±2.62	70.21±4.03	72.15±4.65	91.42±0.95	90.99±1.27
-1	12	-1.00 🔥	-0.80 🔥	81.67±3.24	87.40±2.30	72.82±4.86	75.00±5.75	92.56±1.50	91.81±1.68
-1	12	-1.00 ❄	-0.70 ❄	80.32±4.95	87.36±2.58	70.62±7.57	72.03±8.91	93.41±3.07	92.78±3.34
-1	12	-1.00 🔥	-0.70 🔥	79.00±1.99	87.52±0.83	68.43±3.05	70.02±3.74	92.27±2.22	92.16±1.82
1	7	-1.00 ❄	-1.00 ❄	85.02±1.35	88.50±1.01	78.27±1.99	80.88±1.99	95.79±0.74	95.11±0.72
1	7	-1.00 🔥	-1.00 🔥	84.81±1.84	88.77±1.20	77.86±3.06	80.43±2.94	96.33±1.03	95.64±1.19
1	7	-1.00 ❄	-0.90 ❄	83.37±2.41	87.74±1.09	75.71±3.86	78.15±4.02	94.66±1.34	93.86±1.44
1	7	-1.00 🔥	-0.90 🔥	83.70±1.62	87.88±1.13	76.19±2.45	78.77±2.47	95.73±0.89	95.00±0.68
1	7	-1.00 ❄	-0.80 ❄	84.10±1.64	88.14±1.54	76.78±2.28	79.40±2.41	95.46±1.68	94.73±1.86
1	7	-1.00 🔥	-0.80 🔥	83.59±2.52	88.30±1.38	75.88±3.99	78.38±4.01	93.55±1.14	93.01±1.42
1	7	-1.00 ❄	-0.70 ❄	82.68±2.56	87.55±1.12	74.56±4.03	76.94±4.37	95.07±1.61	94.34±1.52
1	7	-1.00 🔥	-0.70 🔥	86.59±1.96	89.57±1.34	80.67±3.11	83.14±2.92	95.86±0.99	95.33±1.08
1	7	-1.00 ❄	-0.60 ❄	83.42±3.53	87.76±2.07	75.78±5.45	78.08±5.59	95.23±1.66	94.35±1.82
1	7	-1.00 🔥	-0.60 🔥	84.09±2.80	87.38±1.49	77.12±4.43	79.45±4.54	93.88±1.22	93.14±1.40
1	8	-1.00 ❄	-1.00 ❄	82.84±2.54	84.33±2.58	76.30±3.90	78.32±3.72	94.66±1.53	92.85±1.97
1	8	-1.00 🔥	-1.00 🔥	81.17±1.65	84.79±1.21	72.91±2.68	75.10±2.91	94.65±1.08	92.31±2.18
1	8	-1.00 ❄	-0.90 ❄	83.41±0.89	86.62±1.18	76.22±1.40	78.67±1.40	94.87±1.00	93.35±1.07
1	8	-1.00 🔥	-0.90 🔥	81.23±2.07	84.90±1.55	73.00±3.35	75.14±3.64	94.30±1.54	92.69±2.04
1	8	-1.00 ❄	-0.80 ❄	82.75±2.09	85.86±1.82	75.41±3.40	77.66±3.50	94.49±1.21	92.78±1.69
1	8	-1.00 🔥	-0.80 🔥	83.49±2.10	85.88±2.27	76.66±2.93	78.97±3.02	95.08±2.27	93.62±2.66
1	8	-1.00 ❄	-0.70 ❄	82.14±2.38	85.38±1.66	74.44±3.79	76.63±4.11	94.74±1.66	93.38±1.67
1	8	-1.00 🔥	-0.70 🔥	83.04±1.70	85.52±1.90	76.05±2.52	78.33±2.58	94.25±1.34	92.44±1.50
1	8	-1.00 ❄	-0.60 ❄	83.87±2.61	86.85±2.41	76.95±4.01	79.26±4.08	95.20±2.86	93.94±3.31
1	8	-1.00 🔥	-0.60 🔥	84.24±2.01	87.41±1.67	77.34±2.97	79.81±3.00	94.88±0.96	93.38±1.20
1	9	-1.00 ❄	-1.00 ❄	82.58±3.05	86.28±1.69	74.89±4.91	77.07±4.91	93.56±2.06	92.48±1.79
1	9	-1.00 🔥	-1.00 🔥	81.97±2.26	85.64±1.61	73.99±3.46	76.26±3.77	93.68±1.04	92.21±1.27
1	9	-1.00 ❄	-0.90 ❄	81.24±2.88	84.95±2.58	72.97±4.37	75.05±4.74	94.07±2.15	92.79±2.34
1	9	-1.00 🔥	-0.90 🔥	83.23±1.06	86.49±2.05	75.95±1.17	78.42±1.32	93.78±1.86	92.82±2.05
1	9	-1.00 ❄	-0.80 ❄	81.84±2.15	86.93±1.44	73.30±3.27	75.65±3.53	93.56±0.88	92.60±1.15
1	9	-1.00 🔥	-0.80 🔥	82.90±1.57	86.86±1.99	75.18±2.19	77.67±2.29	94.64±0.85	93.78±0.94
1	9	-1.00 ❄	-0.70 ❄	83.52±2.03	86.44±2.85	76.45±2.50	78.89±2.76	93.94±1.29	92.76±1.71
1	9	-1.00 🔥	-0.70 🔥	79.94±3.23	84.83±2.00	70.69±5.00	72.45±5.82	93.59±1.56	92.47±1.42
1	9	-1.00 ❄	-0.60 ❄	81.79±3.50	87.48±1.74	73.12±5.52	75.20±6.04	94.39±1.57	93.35±2.09
1	9	-1.00 🔥	-0.60 🔥	82.20±1.47	87.39±2.01	73.78±2.18	76.26±2.31	94.56±3.17	93.59±3.93
1	10	-1.00 ❄	-1.00 ❄	82.13±3.26	87.02±1.61	73.82±5.11	75.97±5.88	93.67±1.96	92.80±2.01
1	10	-1.00 🔥	-1.00 🔥	82.69±4.49	86.75±2.85	74.85±7.00	76.75±7.98	94.19±0.91	93.34±0.96
1	10	-1.00 ❄	-0.90 ❄	81.80±2.20	86.99±2.63	73.17±3.06	75.57±3.48	92.92±1.69	92.09±2.04
1	10	-1.00 🔥	-0.90 🔥	86.15±1.41	88.87±0.92	80.15±2.16	82.62±2.05	95.97±0.65	95.32±0.57
1	10	-1.00 ❄	-0.80 ❄	82.52±2.43	87.71±1.90	74.19±3.65	76.64±4.01	93.67±3.19	92.93±3.20
1	10	-1.00 🔥	-0.80 🔥	82.92±1.74	87.86±1.61	74.83±2.52	77.40±2.76	93.42±3.18	92.76±2.99
1	10	-1.00 ❄	-0.70 ❄	84.52±1.47	88.52±0.74	77.38±2.32	80.01±2.38	95.45±1.12	94.74±1.04
1	10	-1.00 🔥	-0.70 🔥	83.00±1.47	87.12±0.99	75.26±2.31	77.76±2.42	94.24±1.35	93.54±1.19
1	11	-1.00 ❄	-1.00 ❄	83.24±2.22	87.34±1.29	75.60±3.43	78.05±3.68	94.73±1.95	93.82±1.85
1	11	-1.00 🔥	-1.00 🔥	82.60±0.88	87.11±0.95	74.55±1.37	77.08±1.43	92.63±1.52	91.79±1.51
1	11	-1.00 ❄	-0.90 ❄	80.82±2.45	85.77±1.59	71.90±3.72	74.02±4.24	93.53±1.82	92.37±1.58
1	11	-1.00 🔥	-0.90 🔥	81.41±3.01	86.76±2.08	72.68±4.66	74.78±5.44	94.61±1.16	93.24±1.68
1	11	-1.00 ❄	-0.80 ❄	82.73±2.62	87.66±2.10	74.59±3.93	77.01±4.30	94.59±0.65	93.61±0.69
1	11	-1.00 🔥	-0.80 🔥	77.98±2.41	85.65±1.32	67.28±4.08	68.40±4.92	92.95±3.27	92.12±3.26
1	11	-1.00 ❄	-0.70 ❄	83.28±3.98	87.98±2.44	75.47±6.08	77.72±6.22	94.63±1.63	93.23±2.43

Continued on next page

t	n	a	b	Accuracy	Precision	Recall	F1 score	AUROC	AUPRC
1	11	-1.00 🔥	-0.70 🔥	81.95±3.19	87.27±1.44	73.43±5.07	75.57±5.85	94.49±1.31	93.62±1.35
1	12	-1.00 ❄	-1.00 ❄	82.56±2.11	85.78±2.15	75.05±3.29	77.34±3.22	92.70±3.46	91.46±4.17
1	12	-1.00 🔥	-1.00 🔥	79.36±2.38	85.74±2.69	69.50±3.66	71.23±4.45	89.66±2.53	88.86±2.93
1	12	-1.00 ❄	-0.90 ❄	79.23±3.52	86.61±1.48	69.12±5.66	70.47±6.76	92.23±2.15	91.33±2.28
1	12	-1.00 🔥	-0.90 🔥	82.68±2.77	88.63±1.29	74.20±4.25	76.64±4.70	94.50±2.22	94.05±2.22
1	12	-1.00 ❄	-0.80 ❄	80.16±4.61	84.27±5.05	71.06±6.59	72.75±7.90	92.14±2.38	90.81±3.40
1	12	-1.00 🔥	-0.80 🔥	81.78±3.53	86.61±2.21	73.41±5.56	75.44±6.14	92.98±2.44	92.10±2.42
1	12	-1.00 ❄	-0.70 ❄	81.35±2.77	87.19±2.53	72.42±4.21	74.62±4.55	94.66±1.02	93.97±1.37
1	12	-1.00 🔥	-0.70 🔥	85.25±2.74	88.51±2.37	78.74±4.12	81.17±3.99	95.07±1.05	94.48±1.36

Table 14: Ablation study of CIF structure hyperparameters on APAVA dataset (16 Channels). We use 🔥 to represent learnable parameters, and ❄️ to represent non-learnable parameters.

t	n	a	b	Accuracy	Precision	Recall	F1 score	AUROC	AUPRC
-	-	-	-	82.49±1.40	82.38±1.79	81.20±1.32	81.60±1.39	91.10±1.63	91.30±1.71
-1	5	1 ❄️	1 ❄️	81.48±1.96	81.99±2.38	79.52±2.00	80.21±2.07	90.93±1.74	91.17±1.77
-1	6	1 🔥	1 🔥	84.00±2.37	84.33±2.61	82.37±2.44	83.02±2.50	92.67±2.57	92.87±2.55
-1	7	1 🔥	1 🔥	81.77±2.31	82.67±3.24	79.78±2.04	80.49±2.26	89.92±2.60	90.23±2.53
1	9	1 ❄️	1 ❄️	85.16±1.55	84.76±1.62	85.33±1.27	84.82±1.49	94.06±1.07	94.21±0.99
-1	10	1 🔥	1 🔥	82.60±1.82	82.30±2.04	81.92±2.29	81.92±1.95	91.94±1.55	92.16±1.50
-1	11	1 ❄️	2 ❄️	78.98±0.97	78.57±1.09	77.60±0.93	77.93±0.97	87.29±0.93	87.35±0.96
1	6	-1.00 ❄️	-1.00 ❄️	81.20±1.28	81.50±1.16	79.51±1.84	80.01±1.67	90.03±1.00	90.28±1.03
1	6	-1.00 🔥	-1.00 🔥	81.24±1.16	81.57±0.95	79.56±1.81	80.05±1.62	90.29±0.90	90.61±0.88
1	7	-1.00 ❄️	-1.00 ❄️	81.33±2.24	81.36±2.52	79.71±2.22	80.24±2.31	89.57±1.98	90.02±1.89
1	7	-1.00 ❄️	-1.00 ❄️	81.33±2.24	81.36±2.52	79.71±2.22	80.24±2.31	89.57±1.98	90.02±1.89
1	7	-1.00 🔥	-1.00 🔥	81.62±2.58	81.63±2.95	80.09±2.48	80.60±2.62	89.94±2.18	90.33±2.07
1	7	-1.00 ❄️	-0.90 ❄️	81.45±2.29	81.48±2.56	79.83±2.31	80.37±2.39	89.73±1.95	90.17±1.85
1	7	-1.00 🔥	-0.90 🔥	81.58±2.27	81.72±2.66	79.88±2.21	80.47±2.33	89.67±2.01	90.10±1.93
1	7	-1.00 ❄️	-0.80 ❄️	82.28±1.80	82.97±1.82	80.30±2.14	81.01±2.09	90.47±1.67	90.83±1.58
1	7	-1.00 🔥	-0.80 🔥	81.80±1.95	82.45±2.33	80.01±2.01	80.59±2.07	89.90±1.61	90.35±1.53
1	7	-1.00 ❄️	-0.70 ❄️	82.17±2.06	82.87±2.44	80.41±2.08	80.99±2.16	90.51±1.76	90.91±1.64
1	7	-1.00 🔥	-0.70 🔥	82.05±1.11	83.13±1.64	79.89±1.42	80.66±1.33	90.47±1.20	90.86±1.11
1	7	-1.00 ❄️	-0.60 ❄️	82.38±1.55	83.21±2.12	80.41±1.74	81.12±1.69	90.96±1.20	91.26±1.16
1	7	-1.00 🔥	-0.60 🔥	82.19±1.49	83.02±2.15	80.23±1.61	80.93±1.60	90.81±1.26	91.15±1.18
1	7	-1.00 ❄️	-0.50 ❄️	82.94±0.93	83.86±1.07	80.95±1.45	81.68±1.27	91.39±0.77	91.69±0.71
1	7	-1.00 🔥	-0.50 🔥	82.52±1.10	83.35±1.63	80.60±1.40	81.28±1.30	91.17±0.98	91.49±0.92
1	7	-1.00 ❄️	-0.40 ❄️	82.96±0.89	83.73±1.10	81.07±1.32	81.77±1.16	91.79±0.60	92.03±0.60
1	7	-1.00 🔥	-0.40 🔥	83.02±0.79	83.82±1.14	81.08±1.05	81.82±0.95	91.85±0.60	92.09±0.60
1	7	-1.00 ❄️	-0.30 ❄️	83.00±1.71	83.51±2.29	81.31±1.43	81.95±1.61	91.78±1.64	92.02±1.63
1	7	-1.00 🔥	-0.30 🔥	82.78±1.68	83.49±2.38	81.10±1.04	81.70±1.43	91.98±1.35	92.19±1.36
1	7	-1.00 ❄️	-0.20 ❄️	83.13±1.72	83.47±2.29	81.71±1.60	82.18±1.67	92.09±1.65	92.25±1.65
1	7	-1.00 🔥	-0.20 🔥	83.16±1.93	83.61±2.47	81.55±1.79	82.14±1.91	92.13±1.74	92.30±1.72
1	7	-1.00 ❄️	-0.10 ❄️	84.39±0.90	84.68±0.94	82.92±1.22	83.48±1.06	93.08±0.92	93.20±0.98
1	7	-1.00 🔥	-0.10 🔥	84.56±0.97	84.89±0.69	83.05±1.42	83.64±1.20	93.19±0.94	93.30±1.01
1	7	-1.00 ❄️	0.10 ❄️	84.25±1.46	84.47±1.37	82.77±1.79	83.33±1.64	92.77±1.08	92.90±1.13
1	7	-1.00 🔥	0.10 🔥	84.39±1.55	84.56±1.49	82.96±1.83	83.50±1.71	92.84±1.18	92.95±1.22
1	7	-1.00 ❄️	0.20 ❄️	84.02±1.48	84.15±1.52	82.56±1.61	83.12±1.60	92.51±1.21	92.66±1.20
1	7	-1.00 🔥	0.20 🔥	83.37±1.81	83.65±2.04	81.85±1.83	82.40±1.87	92.11±1.31	92.27±1.26
1	7	-1.00 ❄️	0.30 ❄️	82.95±2.19	82.86±2.64	81.70±1.98	82.11±2.18	91.84±1.67	92.01±1.62
1	7	-1.00 🔥	0.30 🔥	82.66±1.88	82.62±2.43	81.40±1.56	81.79±1.81	91.34±1.88	91.43±1.94
1	7	-1.00 ❄️	0.40 ❄️	82.33±1.91	82.35±2.29	80.91±1.87	81.38±1.97	91.20±1.98	91.32±2.00
1	7	-1.00 🔥	0.40 🔥	83.12±1.75	83.32±2.07	81.57±1.79	82.13±1.84	91.91±1.65	92.08±1.59
1	7	-1.00 ❄️	0.50 ❄️	82.07±1.77	82.32±2.31	80.33±1.61	80.96±1.78	90.99±1.65	91.21±1.59
1	7	-1.00 🔥	0.50 🔥	82.35±2.42	82.57±2.49	80.63±2.64	81.24±2.63	91.04±1.86	91.27±1.79
1	7	-1.00 ❄️	0.60 ❄️	82.03±2.11	82.19±2.65	80.39±2.01	80.97±2.16	90.74±1.94	90.95±1.87
1	7	-1.00 🔥	0.60 🔥	82.08±2.01	82.22±2.48	80.48±1.97	81.04±2.08	90.80±1.92	91.00±1.86
1	7	-1.00 ❄️	0.70 ❄️	81.73±2.22	81.66±2.39	80.24±2.36	80.72±2.38	90.43±1.90	90.63±1.82
1	7	-1.00 🔥	0.70 🔥	81.79±2.20	81.87±2.48	80.13±2.25	80.70±2.32	90.50±1.90	90.71±1.84
1	7	-1.00 ❄️	0.80 ❄️	81.37±1.94	81.69±2.61	79.56±1.75	80.19±1.94	90.28±2.07	90.50±2.00
1	7	-1.00 🔥	0.80 🔥	81.83±2.37	81.99±2.63	80.10±2.44	80.71±2.52	90.31±1.97	90.54±1.91
1	7	-1.00 ❄️	0.90 ❄️	81.72±1.73	82.11±2.28	79.84±1.62	80.52±1.76	90.29±1.72	90.49±1.67
1	7	-1.00 🔥	0.90 🔥	82.07±2.30	82.18±2.41	80.39±2.48	80.98±2.48	90.38±1.84	90.59±1.78
1	7	-1.00 ❄️	1.00 ❄️	81.29±1.73	81.08±1.65	79.84±2.05	80.27±1.93	89.88±1.38	90.09±1.36
1	7	-1.00 🔥	1.00 🔥	81.31±2.34	82.15±2.11	79.34±3.26	79.89±2.98	89.94±1.88	90.14±1.84

Continued on next page

t	n	a	b	Accuracy	Precision	Recall	F1 score	AUROC	AUPRC
1	7	-0.90 ❄	-1.00 ❄	81.34±2.29	81.35±2.56	79.74±2.33	80.26±2.41	89.54±2.01	89.96±1.97
1	7	-0.90 🔥	-1.00 🔥	81.30±2.17	81.41±2.48	79.59±2.20	80.16±2.28	89.53±1.99	89.96±1.95
1	7	-0.90 ❄	-0.90 ❄	81.58±2.33	81.58±2.82	80.05±2.21	80.56±2.36	89.96±2.13	90.33±2.04
1	7	-0.90 🔥	-0.90 🔥	81.89±2.19	82.12±2.15	80.15±2.54	80.73±2.47	90.10±2.14	90.41±2.09
1	7	-0.90 ❄	-0.80 ❄	82.00±1.62	82.67±1.83	80.05±1.93	80.73±1.86	90.12±1.47	90.49±1.41
1	7	-0.90 🔥	-0.80 🔥	81.75±1.77	82.20±2.33	80.00±1.77	80.58±1.82	89.88±1.42	90.30±1.36
1	7	-0.90 ❄	-0.70 ❄	81.31±1.74	81.92±2.21	79.29±1.77	79.99±1.84	89.40±1.63	89.88±1.52
1	7	-0.90 🔥	-0.70 🔥	81.87±2.08	82.28±2.50	80.18±2.09	80.74±2.16	90.02±1.74	90.44±1.63
1	7	-0.90 ❄	-0.60 ❄	81.98±1.47	82.62±1.97	80.09±1.50	80.75±1.54	90.37±1.07	90.73±1.03
1	7	-0.90 🔥	-0.60 🔥	81.93±1.35	82.56±2.14	80.08±0.93	80.73±1.17	90.09±1.10	90.49±1.07
1	7	-0.90 ❄	-0.50 ❄	81.72±1.50	82.60±2.15	79.70±1.32	80.40±1.44	90.11±1.68	90.46±1.61
1	7	-0.90 🔥	-0.50 🔥	81.33±1.40	81.65±2.17	79.66±1.26	80.19±1.32	90.08±1.36	90.45±1.21
1	7	-0.90 ❄	-0.40 ❄	82.35±0.75	82.80±1.60	80.67±0.25	81.25±0.47	91.06±0.76	91.35±0.71
1	7	-0.90 🔥	-0.40 🔥	82.45±0.46	82.95±1.18	80.68±0.54	81.31±0.41	91.13±0.59	91.40±0.55
1	7	-0.90 ❄	-0.30 ❄	81.38±1.83	81.35±2.47	80.09±1.34	80.46±1.64	90.22±1.37	90.48±1.47
1	7	-0.90 🔥	-0.30 🔥	81.31±1.88	81.24±2.53	80.15±1.24	80.44±1.63	90.21±1.42	90.47±1.52
1	7	-0.90 ❄	-0.20 ❄	82.01±1.85	81.92±2.42	80.77±1.62	81.13±1.79	90.86±1.71	91.07±1.77
1	7	-0.90 🔥	-0.20 🔥	82.42±1.76	82.42±2.22	80.98±1.67	81.47±1.77	91.10±1.67	91.28±1.72
1	7	-0.90 ❄	-0.10 ❄	83.94±0.79	84.11±0.90	82.51±1.01	83.04±0.89	92.50±0.78	92.65±0.83
1	7	-0.90 🔥	-0.10 🔥	82.92±1.67	83.22±1.78	81.44±2.00	81.92±1.87	91.66±1.60	91.82±1.62
1	7	-0.90 ❄	0.10 ❄	83.61±1.65	83.89±1.99	82.02±1.54	82.64±1.67	92.12±1.49	92.28±1.51
1	7	-0.90 🔥	0.10 🔥	83.75±2.23	84.27±2.21	81.95±2.53	82.66±2.49	92.21±2.01	92.36±1.99
1	7	-0.90 ❄	0.20 ❄	83.37±1.46	83.92±2.01	81.60±1.40	82.29±1.47	92.18±1.65	92.33±1.64
1	7	-0.90 🔥	0.20 🔥	83.51±1.25	84.15±1.64	81.66±1.33	82.40±1.32	92.33±1.47	92.47±1.48
1	7	-0.90 ❄	0.30 ❄	82.99±1.52	83.25±1.74	81.45±1.87	81.98±1.70	92.01±1.52	92.15±1.50
1	7	-0.90 🔥	0.30 🔥	81.62±1.47	81.77±2.19	80.25±1.19	80.64±1.34	90.76±1.81	90.98±1.74
1	7	-0.90 ❄	0.40 ❄	81.50±1.62	81.95±2.46	79.67±1.41	80.30±1.57	90.76±1.91	90.97±1.86
1	7	-0.90 🔥	0.40 🔥	81.59±1.74	81.90±2.32	79.81±1.63	80.43±1.76	90.73±1.84	90.94±1.79
1	7	-0.90 ❄	0.50 ❄	81.68±1.91	81.84±2.40	80.16±2.12	80.62±2.04	90.85±1.90	91.04±1.84
1	7	-0.90 🔥	0.50 🔥	81.71±1.71	82.05±2.40	79.99±1.72	80.56±1.76	90.82±1.98	91.01±1.93
1	7	-0.90 ❄	0.60 ❄	81.45±2.07	81.58±2.65	79.96±2.13	80.41±2.16	90.34±1.90	90.54±1.86
1	7	-0.90 🔥	0.60 🔥	81.52±1.84	81.68±2.44	80.00±1.89	80.47±1.90	90.34±1.84	90.55±1.79
1	7	-0.90 ❄	0.70 ❄	81.44±2.60	81.43±2.92	79.84±2.66	80.37±2.75	89.97±2.15	90.19±2.10
1	7	-0.90 🔥	0.70 🔥	81.02±1.46	81.49±2.75	79.19±1.13	79.80±1.29	90.21±2.15	90.38±2.09
1	7	-0.90 ❄	0.80 ❄	81.05±1.88	81.28±2.59	79.29±1.71	79.88±1.87	89.82±2.03	89.96±2.01
1	7	-0.90 🔥	0.80 🔥	81.41±2.61	81.44±2.87	79.75±2.70	80.31±2.77	89.82±2.10	90.00±2.05
1	7	-0.90 ❄	0.90 ❄	81.23±1.87	81.02±1.80	79.77±2.18	80.21±2.08	89.72±1.71	89.91±1.67
1	7	-0.90 🔥	0.90 🔥	81.59±2.37	81.53±2.33	80.01±2.69	80.52±2.60	89.95±1.92	90.17±1.87
1	7	-0.90 ❄	1.00 ❄	81.26±2.06	81.47±2.19	79.39±2.20	80.03±2.23	89.73±1.76	89.91±1.74
1	7	-0.90 🔥	1.00 🔥	80.78±1.60	80.71±1.59	79.13±1.81	79.65±1.76	89.51±1.56	89.63±1.48
1	7	-0.80 ❄	-1.00 ❄	81.24±2.14	81.34±2.24	79.59±2.40	80.11±2.36	89.28±1.74	89.65±1.80
1	7	-0.80 🔥	-1.00 🔥	81.24±1.98	81.67±2.43	79.34±2.05	79.98±2.11	89.23±1.77	89.63±1.83
1	7	-0.80 ❄	-0.90 ❄	81.44±2.14	81.48±2.46	79.88±2.12	80.38±2.22	89.56±1.82	89.93±1.83
1	7	-0.80 🔥	-0.90 🔥	81.12±1.93	81.32±2.23	79.44±1.93	79.97±2.01	89.23±1.52	89.66±1.56
1	7	-0.80 ❄	-0.80 ❄	81.22±1.66	81.38±2.25	79.53±1.40	80.09±1.59	89.32±1.30	89.77±1.30
1	7	-0.80 🔥	-0.80 🔥	80.96±1.29	81.22±2.05	79.24±1.08	79.79±1.18	88.96±1.01	89.44±1.05
1	7	-0.80 ❄	-0.70 ❄	81.73±1.63	82.03±2.08	80.00±1.63	80.59±1.66	89.71±1.26	90.08±1.25
1	7	-0.80 🔥	-0.70 🔥	81.93±1.59	82.45±2.15	80.08±1.61	80.73±1.64	89.96±1.34	90.30±1.33
1	7	-0.80 ❄	-0.60 ❄	81.73±1.42	81.72±1.72	80.22±1.34	80.71±1.42	89.55±1.25	89.95±1.21
1	7	-0.80 🔥	-0.60 🔥	81.52±1.45	81.87±2.22	79.83±1.16	80.39±1.31	89.60±1.05	90.00±1.04
1	7	-0.80 ❄	-0.50 ❄	81.40±1.46	81.51±1.70	79.76±1.51	80.29±1.52	89.54±1.56	89.88±1.47
1	7	-0.80 🔥	-0.50 🔥	80.99±1.82	81.09±1.84	79.30±2.07	79.83±2.03	89.14±1.94	89.44±1.89
1	7	-0.80 ❄	-0.40 ❄	81.09±1.65	81.21±1.75	79.40±1.80	79.94±1.79	89.26±1.86	89.49±1.78

Continued on next page

t	n	a	b	Accuracy	Precision	Recall	F1 score	AUROC	AUPRC
1	7	-0.80 🔥	-0.40 🔥	80.98±1.50	81.04±1.59	79.32±1.68	79.84±1.65	89.21±1.65	89.48±1.66
1	7	-0.80 ❄	-0.30 ❄	82.03±1.41	82.48±2.02	80.30±1.15	80.90±1.31	90.40±1.25	90.68±1.21
1	7	-0.80 🔥	-0.30 🔥	82.08±1.29	82.60±1.95	80.30±0.89	80.93±1.12	90.39±1.17	90.69±1.14
1	7	-0.80 ❄	-0.20 ❄	81.93±1.35	82.02±1.85	80.40±0.99	80.91±1.21	90.31±1.25	90.60±1.27
1	7	-0.80 🔥	-0.20 🔥	81.33±1.84	81.22±2.32	79.94±1.59	80.36±1.77	89.96±1.68	90.25±1.72
1	7	-0.80 ❄	-0.10 ❄	82.59±1.87	82.58±2.35	81.24±1.57	81.68±1.79	91.01±1.85	91.20±1.87
1	7	-0.80 🔥	-0.10 🔥	81.73±1.76	81.47±2.19	80.55±1.54	80.88±1.72	90.39±1.72	90.60±1.76
1	7	-0.80 ❄	0.10 ❄	82.89±1.77	83.56±2.02	81.01±1.90	81.72±1.91	91.67±1.74	91.83±1.74
1	7	-0.80 🔥	0.10 🔥	82.25±1.79	82.78±2.06	80.35±1.89	81.04±1.91	91.08±1.69	91.28±1.69
1	7	-0.80 ❄	0.20 ❄	82.03±2.50	82.65±2.68	80.14±2.73	80.78±2.76	90.83±2.46	91.04±2.40
1	7	-0.80 🔥	0.20 🔥	82.70±1.52	83.16±2.03	80.95±1.45	81.59±1.52	91.58±1.60	91.73±1.62
1	7	-0.80 ❄	0.30 ❄	82.07±1.68	82.51±2.06	80.25±1.76	80.89±1.80	90.43±2.29	90.65±2.22
1	7	-0.80 🔥	0.30 🔥	81.27±1.65	81.43±2.11	79.82±1.66	80.23±1.70	90.11±2.22	90.33±2.14
1	7	-0.80 ❄	0.40 ❄	81.23±1.54	81.37±2.17	79.65±1.41	80.15±1.51	90.19±1.80	90.43±1.75
1	7	-0.80 🔥	0.40 🔥	82.29±1.25	82.70±1.85	80.50±1.06	81.16±1.18	90.92±1.67	91.11±1.64
1	7	-0.80 ❄	0.50 ❄	80.92±1.92	81.08±2.68	79.51±1.75	79.89±1.85	89.95±2.06	90.15±2.03
1	7	-0.80 🔥	0.50 🔥	80.94±1.93	80.81±2.53	79.72±1.83	80.01±1.91	89.87±2.00	90.07±1.99
1	7	-0.80 ❄	0.60 ❄	80.92±1.66	80.55±1.65	79.75±1.98	80.02±1.85	89.67±1.66	89.82±1.68
1	7	-0.80 🔥	0.60 🔥	80.99±1.90	80.75±2.03	79.70±2.09	80.04±2.04	89.65±1.59	89.87±1.57
1	8	-1.00 ❄	-1.00 ❄	84.12±1.05	84.18±1.59	82.90±0.95	83.32±1.01	92.68±0.93	92.78±0.89
1	8	-1.00 🔥	-1.00 🔥	84.91±0.96	85.15±1.53	83.57±0.62	84.09±0.85	93.08±0.98	93.16±0.87
1	8	-1.00 ❄	-0.90 ❄	84.32±1.62	84.10±1.90	83.36±1.39	83.64±1.57	92.63±1.28	92.79±1.21
1	8	-1.00 🔥	-0.90 🔥	84.89±1.03	85.03±1.45	83.63±0.85	84.11±0.98	92.88±1.08	93.06±1.05
1	8	-1.00 ❄	-0.80 ❄	85.27±0.85	85.49±1.00	84.10±1.06	84.51±0.90	93.30±0.76	93.44±0.74
1	8	-1.00 🔥	-0.80 🔥	85.10±0.87	85.61±1.22	83.72±1.26	84.24±1.03	93.38±0.90	93.52±0.86
1	8	-1.00 ❄	-0.70 ❄	84.91±0.91	85.51±1.65	83.42±0.99	84.00±0.91	93.67±1.08	93.80±1.07
1	8	-1.00 🔥	-0.70 🔥	84.56±0.64	85.52±1.80	82.89±0.74	83.55±0.52	93.70±1.03	93.81±1.03
1	8	-1.00 ❄	-0.60 ❄	84.40±0.69	85.27±1.55	82.70±0.97	83.37±0.77	93.56±1.25	93.70±1.19
1	8	-1.00 🔥	-0.60 🔥	84.98±0.66	85.65±1.36	83.45±1.01	84.05±0.77	93.82±1.08	93.95±1.03
1	8	-1.00 ❄	-0.50 ❄	85.21±0.92	85.91±1.28	83.61±1.16	84.28±1.02	93.70±1.11	93.83±1.07
1	8	-1.00 🔥	-0.50 🔥	85.34±0.93	85.35±0.76	84.18±1.28	84.60±1.09	93.49±0.94	93.63±0.90
1	8	-1.00 ❄	-0.40 ❄	84.98±0.90	85.77±1.28	83.22±1.02	83.97±0.97	93.80±0.85	93.92±0.84
1	8	-1.00 🔥	-0.40 🔥	84.47±1.51	85.36±1.72	82.54±1.64	83.37±1.65	93.27±1.55	93.45±1.46
1	8	-1.00 ❄	-0.30 ❄	84.25±1.35	85.00±1.36	82.38±1.61	83.16±1.53	93.02±1.34	93.17±1.26
1	8	-1.00 🔥	-0.30 🔥	84.56±0.86	85.30±0.89	82.75±1.15	83.51±1.02	93.59±0.72	93.72±0.69
1	8	-1.00 ❄	-0.20 ❄	83.35±2.14	83.95±2.93	81.69±1.57	82.34±1.96	92.57±2.06	92.73±1.95
1	8	-1.00 🔥	-0.20 🔥	83.87±1.29	84.91±1.72	81.79±1.22	82.67±1.33	93.04±1.41	93.18±1.31
1	8	-1.00 ❄	-0.10 ❄	83.47±2.14	83.80±2.53	81.93±2.24	82.49±2.21	92.22±1.91	92.39±1.80
1	8	-1.00 🔥	-0.10 🔥	83.58±2.04	83.92±2.43	81.99±2.02	82.60±2.09	92.37±1.95	92.53±1.84
1	8	-1.00 ❄	0.10 ❄	83.59±1.46	83.74±1.51	82.09±1.67	82.65±1.60	92.21±1.25	92.36±1.22
1	8	-1.00 🔥	0.10 🔥	82.91±2.16	83.13±2.21	81.23±2.38	81.85±2.36	91.17±2.32	91.37±2.17
1	8	-1.00 ❄	0.20 ❄	81.31±2.64	81.25±2.71	79.83±2.89	80.27±2.87	90.09±2.07	90.27±2.07
1	8	-1.00 🔥	0.20 🔥	80.77±2.03	80.77±2.39	79.25±2.13	79.69±2.16	89.65±2.12	89.73±2.13
1	8	-1.00 ❄	0.30 ❄	81.29±2.45	81.41±2.65	79.66±2.56	80.17±2.60	89.46±2.36	89.71±2.24
1	8	-1.00 🔥	0.30 🔥	81.30±2.50	81.36±2.75	79.72±2.57	80.21±2.63	89.43±2.52	89.69±2.40
1	8	-1.00 ❄	0.40 ❄	80.31±2.06	80.88±2.68	78.15±1.95	78.87±2.09	89.10±2.26	89.35±2.17
1	8	-1.00 🔥	0.40 🔥	80.17±2.20	80.59±2.73	78.06±2.13	78.76±2.28	88.60±2.62	88.90±2.50
1	8	-1.00 ❄	0.50 ❄	79.04±2.24	79.87±3.14	76.60±2.07	77.34±2.24	87.44±2.78	87.79±2.67
1	8	-1.00 🔥	0.50 🔥	79.40±2.11	79.94±2.83	77.16±1.89	77.86±2.08	88.00±2.29	88.35±2.21
1	8	-1.00 ❄	0.60 ❄	78.32±2.40	78.88±2.95	76.20±2.09	76.76±2.29	86.79±2.20	87.16±2.11
1	8	-1.00 🔥	0.60 🔥	78.53±2.37	79.03±2.94	76.44±2.10	77.01±2.29	87.11±2.10	87.48±2.06
1	8	-1.00 ❄	0.70 ❄	78.16±2.00	78.58±2.40	75.89±1.95	76.51±2.07	86.46±2.07	86.89±2.01
1	8	-1.00 🔥	0.70 🔥	77.83±1.94	78.63±2.46	75.29±1.89	75.96±2.01	85.92±2.25	86.34±2.19

Continued on next page

t	n	a	b	Accuracy	Precision	Recall	F1 score	AUROC	AUPRC
1	8	-1.00 ❄️	0.80 ❄️	77.23±1.36	77.84±1.99	74.72±1.32	75.35±1.38	85.34±1.85	85.69±1.77
1	8	-1.00 🔥	0.80 🔥	77.23±1.63	78.03±2.45	74.63±1.34	75.29±1.49	85.38±2.03	85.82±2.03
1	8	-1.00 ❄️	0.90 ❄️	76.79±1.74	77.49±2.37	74.23±1.77	74.82±1.83	84.53±2.01	85.01±2.00
1	8	-1.00 🔥	0.90 🔥	76.52±1.27	76.86±1.96	74.11±1.03	74.68±1.13	84.70±1.39	85.11±1.30
1	8	-1.00 ❄️	1.00 ❄️	77.04±1.46	77.68±2.25	74.54±0.97	75.16±1.16	84.76±1.19	85.27±1.21
1	8	-1.00 🔥	1.00 🔥	76.90±1.48	77.73±2.41	74.32±0.83	74.94±1.05	84.52±1.16	85.02±1.15
1	8	-0.90 ❄️	-1.00 ❄️	83.35±1.73	83.28±1.97	82.35±1.80	82.59±1.79	92.15±0.89	92.26±0.86
1	8	-0.90 🔥	-1.00 🔥	83.07±1.89	82.95±2.03	82.08±2.08	82.30±2.01	91.80±1.12	91.91±1.09
1	8	-0.90 ❄️	-0.90 ❄️	83.58±1.84	83.36±2.19	82.69±1.73	82.88±1.84	92.20±1.08	92.31±1.04
1	8	-0.90 🔥	-0.90 🔥	84.43±1.40	84.28±1.65	83.42±1.39	83.72±1.43	92.62±0.87	92.67±0.85
1	8	-0.90 ❄️	-0.80 ❄️	83.86±2.07	83.70±2.40	82.92±1.89	83.16±2.04	92.31±1.21	92.44±1.21
1	8	-0.90 🔥	-0.80 🔥	83.70±1.81	83.76±2.48	82.63±1.49	82.94±1.69	92.52±1.24	92.64±1.27
1	8	-0.90 ❄️	-0.70 ❄️	84.36±0.98	84.79±1.91	82.93±0.80	83.47±0.86	92.78±1.16	92.93±1.16
1	8	-0.90 🔥	-0.70 🔥	83.97±1.05	84.46±2.13	82.56±0.81	83.06±0.88	92.77±1.07	92.92±1.07
1	8	-0.90 ❄️	-0.60 ❄️	84.74±1.29	84.95±1.72	83.49±1.01	83.94±1.21	93.28±0.90	93.38±0.89
1	8	-0.90 🔥	-0.60 🔥	84.58±1.37	85.19±2.20	83.14±0.87	83.70±1.18	93.33±1.18	93.43±1.16
1	8	-0.90 ❄️	-0.50 ❄️	84.64±1.22	84.72±1.40	83.44±1.35	83.86±1.29	93.01±1.12	93.17±1.07
1	8	-0.90 🔥	-0.50 🔥	84.72±1.08	85.00±1.39	83.29±1.05	83.86±1.10	93.01±1.17	93.17±1.12
1	8	-0.90 ❄️	-0.40 ❄️	84.75±1.32	84.76±1.42	83.51±1.45	83.97±1.41	93.01±1.02	93.14±1.02
1	8	-0.90 🔥	-0.40 🔥	84.57±0.89	84.90±1.15	83.05±0.96	83.66±0.94	93.08±0.92	93.20±0.93
1	8	-0.90 ❄️	-0.30 ❄️	84.92±1.28	85.22±1.41	83.47±1.46	84.05±1.40	93.35±1.01	93.45±1.02
1	8	-0.90 🔥	-0.30 🔥	84.25±1.82	84.32±2.00	82.91±1.89	83.41±1.90	92.82±1.33	92.92±1.37
1	8	-0.90 ❄️	-0.20 ❄️	84.44±1.35	84.82±1.20	82.87±1.72	83.49±1.56	92.75±1.31	92.89±1.26
1	8	-0.90 🔥	-0.20 🔥	83.97±1.12	84.59±1.12	82.14±1.29	82.89±1.26	92.55±1.22	92.71±1.14
1	8	-0.90 ❄️	-0.10 ❄️	83.90±0.94	84.18±0.92	82.35±1.26	82.94±1.10	92.53±0.92	92.69±0.88
1	8	-0.90 🔥	-0.10 🔥	83.61±0.93	84.06±1.27	81.91±1.05	82.57±1.00	92.44±1.04	92.60±1.03
1	8	-0.90 ❄️	0.10 ❄️	82.14±2.78	82.44±3.33	80.65±2.35	81.15±2.65	91.02±2.35	91.26±2.25
1	8	-0.90 🔥	0.10 🔥	82.38±1.98	82.59±2.42	80.78±1.74	81.35±1.94	91.09±2.04	91.31±1.97
1	8	-0.90 ❄️	0.20 ❄️	82.18±2.34	82.46±2.89	80.66±2.11	81.16±2.29	90.44±2.32	90.70±2.24
1	8	-0.90 🔥	0.20 🔥	81.24±2.99	81.32±3.43	79.81±2.77	80.24±2.98	89.57±2.76	89.77±2.69
1	8	-0.90 ❄️	0.30 ❄️	80.75±2.19	80.96±2.76	79.06±2.09	79.59±2.20	88.97±2.63	89.23±2.54
1	8	-0.90 🔥	0.30 🔥	80.66±2.40	80.85±2.84	78.97±2.38	79.49±2.46	89.08±2.65	89.35±2.56
1	8	-0.90 ❄️	0.40 ❄️	79.64±2.51	79.80±3.08	77.79±2.29	78.35±2.48	88.31±2.32	88.62±2.25
1	8	-0.90 🔥	0.40 🔥	79.76±2.79	79.68±3.28	78.15±2.63	78.62±2.80	88.16±2.37	88.48±2.32
1	8	-0.90 ❄️	0.50 ❄️	78.55±2.61	78.46±3.01	76.71±2.53	77.22±2.67	86.46±2.46	86.85±2.44
1	8	-0.90 🔥	0.50 🔥	78.46±2.48	78.51±2.87	76.57±2.47	77.08±2.57	86.58±2.23	86.96±2.21
1	8	-0.90 ❄️	0.60 ❄️	77.90±1.95	77.77±2.17	76.02±2.07	76.51±2.11	85.68±2.56	86.09±2.56
1	8	-0.90 🔥	0.60 🔥	78.36±1.87	78.18±2.15	76.55±1.86	77.05±1.93	86.32±1.81	86.69±1.86
1	8	-0.90 ❄️	0.70 ❄️	78.03±1.81	78.65±2.39	75.67±1.81	76.29±1.89	85.96±2.14	86.36±2.11
1	8	-0.90 🔥	0.70 🔥	77.76±1.79	78.52±2.30	75.11±1.76	75.83±1.87	85.64±2.09	86.08±2.07
1	8	-0.90 ❄️	0.80 ❄️	77.64±2.23	77.93±2.83	75.36±2.06	75.98±2.20	85.53±1.89	85.99±1.91
1	8	-0.90 🔥	0.80 🔥	77.41±1.95	78.00±2.28	74.82±2.10	75.49±2.15	85.18±2.41	85.53±2.47
1	8	-0.90 ❄️	0.90 ❄️	76.72±2.13	77.53±2.91	74.22±1.95	74.77±2.11	84.26±2.17	84.69±2.23
1	8	-0.90 🔥	0.90 🔥	76.70±1.98	77.20±2.64	74.36±1.82	74.89±1.95	84.27±2.06	84.68±2.15
1	8	-0.90 ❄️	1.00 ❄️	77.01±1.66	77.79±2.43	74.34±1.23	75.02±1.41	84.23±1.65	84.73±1.64
1	8	-0.90 🔥	1.00 🔥	77.09±1.36	77.87±2.13	74.47±1.04	75.12±1.18	84.27±1.44	84.70±1.52
1	8	-0.80 ❄️	-1.00 ❄️	83.51±1.91	83.37±1.61	82.43±2.47	82.70±2.24	91.74±1.31	91.81±1.33
1	8	-0.80 🔥	-1.00 🔥	83.33±1.98	83.22±1.60	82.31±2.64	82.51±2.38	91.59±1.46	91.68±1.46
1	8	-0.80 ❄️	-0.90 ❄️	83.44±1.35	83.84±2.08	82.11±1.44	82.52±1.37	92.12±0.96	92.23±1.04
1	8	-0.80 🔥	-0.90 🔥	83.72±1.48	83.55±1.62	82.97±1.74	83.05±1.58	92.21±0.94	92.26±0.98
1	8	-0.80 ❄️	-0.80 ❄️	83.86±1.36	84.20±2.17	82.59±1.33	83.00±1.30	92.50±1.00	92.58±1.04
1	8	-0.80 🔥	-0.80 🔥	83.87±1.40	83.95±1.92	82.76±1.41	83.08±1.38	92.48±1.02	92.57±1.05
1	8	-0.80 ❄️	-0.70 ❄️	83.89±1.05	84.03±2.00	82.76±0.86	83.10±0.91	92.50±1.13	92.62±1.15

Continued on next page

t	n	a	b	Accuracy	Precision	Recall	F1 score	AUROC	AUPRC
1	8	-0.80 🔥	-0.70 🔥	83.72±1.05	83.94±2.00	82.58±0.99	82.91±0.93	92.52±1.11	92.63±1.14
1	8	-0.80 ❄️	-0.60 ❄️	84.30±1.36	84.49±2.21	83.14±0.97	83.53±1.21	92.69±1.25	92.78±1.28
1	8	-0.80 🔥	-0.60 🔥	84.29±1.12	84.50±1.95	83.16±0.81	83.52±0.95	92.73±1.18	92.81±1.21
1	8	-0.80 ❄️	-0.50 ❄️	84.33±1.52	84.47±2.04	83.07±1.26	83.53±1.45	92.61±1.20	92.72±1.16
1	8	-0.80 🔥	-0.50 🔥	84.28±1.48	84.19±1.77	83.14±1.37	83.52±1.48	92.58±1.10	92.71±1.06
1	8	-0.80 ❄️	-0.40 ❄️	84.01±1.26	83.98±1.67	82.81±1.01	83.22±1.19	92.53±0.98	92.69±0.96
1	8	-0.80 🔥	-0.40 🔥	83.86±1.77	83.75±2.12	82.70±1.70	83.08±1.79	92.17±1.43	92.34±1.40
1	8	-0.80 ❄️	-0.30 ❄️	83.84±1.98	83.97±2.53	82.59±2.03	83.01±2.02	92.42±1.58	92.54±1.61
1	8	-0.80 🔥	-0.30 🔥	83.98±1.79	84.35±1.64	82.36±2.16	82.98±2.04	92.34±1.49	92.50±1.45
1	8	-0.80 ❄️	-0.20 ❄️	83.82±1.36	83.99±1.36	82.28±1.54	82.87±1.49	92.19±1.17	92.35±1.16
1	8	-0.80 🔥	-0.20 🔥	83.40±1.55	83.71±1.40	81.74±1.88	82.36±1.78	91.81±1.25	91.99±1.18
1	8	-0.80 ❄️	-0.10 ❄️	83.61±1.09	83.97±1.26	81.94±1.17	82.59±1.17	92.05±1.05	92.19±1.09
1	8	-0.80 🔥	-0.10 🔥	83.49±1.10	83.75±1.18	81.86±1.18	82.49±1.18	92.00±1.16	92.16±1.18
1	8	-0.80 ❄️	0.10 ❄️	80.88±2.92	81.02±3.31	79.41±2.37	79.85±2.74	89.83±2.36	90.14±2.27
1	8	-0.80 🔥	0.10 🔥	81.72±3.09	81.92±3.52	80.36±2.59	80.77±2.93	90.46±2.33	90.72±2.27
1	8	-0.80 ❄️	0.20 ❄️	81.36±1.99	81.66±2.51	79.67±1.84	80.22±1.97	89.72±2.24	89.99±2.21
1	8	-0.80 🔥	0.20 🔥	81.06±2.13	81.59±2.58	79.18±2.12	79.79±2.19	89.30±2.43	89.60±2.33
1	8	-0.80 ❄️	0.30 ❄️	79.82±2.62	80.09±3.48	78.20±2.10	78.66±2.42	88.38±2.57	88.69±2.51
1	8	-0.80 🔥	0.30 🔥	80.84±2.17	81.23±2.76	79.13±1.84	79.66±2.06	89.12±2.10	89.41±2.09
1	8	-0.80 ❄️	0.40 ❄️	79.54±2.09	79.91±2.97	77.54±1.65	78.17±1.91	87.71±2.30	88.05±2.27
1	8	-0.80 🔥	0.40 🔥	79.50±2.29	79.84±3.09	77.50±1.94	78.12±2.17	87.79±2.39	88.12±2.34
1	8	-0.80 ❄️	0.50 ❄️	78.56±2.26	78.97±3.48	76.50±1.65	77.11±1.97	86.58±2.73	86.88±2.66
1	8	-0.80 🔥	0.50 🔥	78.18±2.26	78.50±3.41	76.17±1.67	76.74±1.97	86.59±2.73	86.97±2.71
1	8	-0.80 ❄️	0.60 ❄️	77.86±1.91	77.81±2.33	75.84±1.89	76.39±1.99	85.38±2.65	85.79±2.67
1	8	-0.80 🔥	0.60 🔥	78.25±1.87	78.47±2.91	76.18±1.47	76.77±1.69	86.13±2.27	86.51±2.29
1	9	-1.00 ❄️	-1.00 ❄️	86.16±1.34	85.62±1.38	86.00±1.37	85.77±1.37	94.32±1.02	94.47±0.99
1	9	-1.00 🔥	-1.00 🔥	86.07±1.14	85.54±1.21	86.20±1.51	85.73±1.24	94.53±1.28	94.66±1.22
1	9	-1.00 ❄️	-0.90 ❄️	85.48±2.00	85.21±1.97	85.39±1.57	85.08±1.92	94.20±1.28	94.35±1.23
1	9	-1.00 🔥	-0.90 🔥	85.70±2.10	85.35±2.03	85.65±1.80	85.32±2.06	94.25±1.28	94.40±1.24
1	9	-1.00 ❄️	-0.80 ❄️	85.81±1.73	85.47±1.72	85.78±1.38	85.44±1.67	94.35±1.09	94.48±1.05
1	9	-1.00 🔥	-0.80 🔥	85.37±2.62	85.34±2.22	85.34±1.87	84.97±2.49	94.12±1.18	94.27±1.15
1	9	-1.00 ❄️	-0.70 ❄️	82.91±4.09	83.81±3.21	83.49±2.51	82.57±3.81	93.75±1.11	93.92±1.09
1	9	-1.00 🔥	-0.70 🔥	84.01±3.68	84.45±2.76	84.01±2.30	83.57±3.44	93.89±1.01	94.04±0.99
1	9	-1.00 ❄️	-0.60 ❄️	85.31±1.43	84.94±1.55	85.29±1.13	84.93±1.35	94.10±0.93	94.26±0.87
1	9	-1.00 🔥	-0.60 🔥	86.26±0.76	85.84±0.76	86.17±0.49	85.88±0.67	94.49±0.44	94.62±0.42
1	9	-1.00 ❄️	-0.50 ❄️	86.54±1.55	86.33±1.88	86.10±1.11	86.08±1.46	94.43±0.70	94.57±0.67
1	9	-1.00 🔥	-0.50 🔥	86.39±1.06	86.04±1.20	86.14±0.66	85.97±0.96	94.53±0.50	94.66±0.49
1	9	-1.00 ❄️	-0.40 ❄️	85.74±1.00	85.57±1.09	85.18±1.26	85.20±1.07	94.29±0.59	94.43±0.57
1	9	-1.00 🔥	-0.40 🔥	85.77±1.17	85.60±1.22	85.19±1.35	85.23±1.24	94.19±0.58	94.34±0.54
1	9	-1.00 ❄️	-0.30 ❄️	85.56±1.36	85.57±1.26	84.83±1.99	84.93±1.62	93.99±0.82	94.14±0.78
1	9	-1.00 🔥	-0.30 🔥	85.34±1.66	85.45±1.64	84.50±2.06	84.67±1.87	93.87±0.82	94.03±0.76
1	9	-1.00 ❄️	-0.20 ❄️	85.31±0.85	85.05±1.04	84.51±0.82	84.70±0.84	93.58±0.71	93.75±0.67
1	9	-1.00 🔥	-0.20 🔥	85.52±1.39	85.49±1.78	84.50±1.14	84.85±1.34	93.65±0.88	93.81±0.82
1	9	-1.00 ❄️	-0.10 ❄️	84.65±0.96	84.43±1.24	83.79±0.92	84.00±0.94	93.34±0.74	93.51±0.72
1	9	-1.00 🔥	-0.10 🔥	85.03±1.42	85.30±2.07	83.69±1.03	84.23±1.32	93.62±0.93	93.77±0.88
1	9	-1.00 ❄️	0.10 ❄️	83.35±0.99	84.57±1.70	81.21±0.99	82.07±1.03	92.63±1.25	92.79±1.15
1	9	-1.00 🔥	0.10 🔥	83.65±1.32	84.36±1.72	81.81±1.37	82.54±1.38	92.57±1.34	92.74±1.25
1	9	-1.00 ❄️	0.20 ❄️	83.90±2.14	84.40±2.06	82.13±2.45	82.83±2.39	92.65±1.78	92.81±1.66
1	9	-1.00 🔥	0.20 🔥	83.41±1.93	83.88±1.94	81.62±2.15	82.32±2.14	92.21±1.67	92.38±1.52
1	9	-1.00 ❄️	0.30 ❄️	83.16±2.07	83.70±1.92	81.31±2.47	82.01±2.38	92.20±1.86	92.34±1.73
1	9	-1.00 🔥	0.30 🔥	83.10±1.87	83.90±1.95	81.06±2.07	81.87±2.08	92.02±1.84	92.18±1.72
1	9	-1.00 ❄️	0.40 ❄️	82.84±1.76	83.51±1.33	80.89±2.31	81.60±2.16	91.59±1.89	91.73±1.73
1	9	-1.00 🔥	0.40 🔥	81.84±1.34	82.72±1.52	79.61±1.45	80.44±1.49	90.87±1.86	91.04±1.66

Continued on next page

t	n	a	b	Accuracy	Precision	Recall	F1 score	AUROC	AUPRC
1	9	-1.00 ❄	0.50 ❄	81.91±2.08	81.99±2.27	80.27±2.18	80.84±2.20	91.05±2.02	91.20±1.78
1	9	-1.00 🔥	0.50 🔥	81.50±1.66	81.65±1.87	79.77±1.79	80.35±1.77	90.67±1.72	90.79±1.47
1	9	-1.00 ❄	0.60 ❄	81.38±1.09	81.89±1.47	79.36±1.06	80.08±1.11	90.67±1.42	90.73±1.33
1	9	-1.00 🔥	0.60 🔥	81.44±0.93	82.07±1.00	79.32±1.10	80.08±1.07	90.78±1.29	90.84±1.22
1	9	-1.00 ❄	0.70 ❄	81.09±0.90	82.04±0.97	78.79±1.28	79.57±1.15	90.33±1.26	90.35±1.10
1	9	-1.00 🔥	0.70 🔥	81.23±0.71	81.92±0.61	79.07±1.05	79.82±0.95	90.42±1.15	90.46±1.03
1	9	-1.00 ❄	0.80 ❄	80.52±0.98	81.47±1.32	78.10±1.03	78.92±1.06	89.87±1.24	89.80±1.24
1	9	-1.00 🔥	0.80 🔥	80.17±1.14	81.05±1.37	77.76±1.33	78.54±1.32	89.68±1.13	89.65±1.09
1	9	-1.00 ❄	0.90 ❄	79.92±0.64	80.92±0.83	77.36±0.64	78.19±0.68	89.39±1.07	89.30±1.05
1	9	-1.00 🔥	0.90 🔥	79.99±0.84	80.70±1.14	77.66±0.97	78.41±0.95	89.50±1.11	89.37±1.07
1	9	-1.00 ❄	1.00 ❄	79.27±0.64	79.94±1.08	76.90±0.67	77.62±0.66	88.76±1.02	88.54±1.14
1	9	-1.00 🔥	1.00 🔥	78.91±1.49	80.03±1.67	76.16±1.62	76.97±1.69	88.21±2.36	88.14±2.21
1	9	-0.90 ❄	-1.00 ❄	85.58±2.16	85.25±1.89	85.67±1.94	85.22±2.14	93.97±1.34	94.13±1.32
1	9	-0.90 🔥	-1.00 🔥	85.76±2.20	85.40±2.06	85.78±2.04	85.39±2.20	94.03±1.44	94.18±1.41
1	9	-0.90 ❄	-0.90 ❄	85.81±1.11	85.23±1.13	85.83±1.19	85.46±1.15	94.12±0.98	94.29±0.94
1	9	-0.90 🔥	-0.90 🔥	85.65±1.63	85.48±1.80	85.39±1.02	85.20±1.49	94.14±0.90	94.29±0.87
1	9	-0.90 ❄	-0.80 ❄	85.39±2.84	85.26±2.48	85.48±1.93	85.04±2.68	94.04±1.05	94.18±1.05
1	9	-0.90 🔥	-0.80 🔥	85.26±3.24	85.15±2.81	85.33±2.33	84.90±3.09	94.01±1.18	94.15±1.18
1	9	-0.90 ❄	-0.70 ❄	85.23±2.83	85.34±2.47	85.06±2.08	84.78±2.67	94.23±1.11	94.38±1.07
1	9	-0.90 🔥	-0.70 🔥	85.23±2.88	85.30±2.44	85.09±2.07	84.79±2.71	94.23±1.16	94.38±1.14
1	9	-0.90 ❄	-0.60 ❄	84.00±3.17	84.01±2.61	84.68±2.39	83.76±3.04	93.89±1.28	94.04±1.22
1	9	-0.90 🔥	-0.60 🔥	85.74±2.99	85.56±2.43	85.91±2.20	85.42±2.86	94.44±1.14	94.58±1.10
1	9	-0.90 ❄	-0.50 ❄	86.01±0.83	85.89±1.17	85.53±0.97	85.50±0.82	94.34±0.45	94.49±0.42
1	9	-0.90 🔥	-0.50 🔥	84.85±2.47	85.08±2.36	84.56±1.95	84.34±2.34	94.14±0.89	94.29±0.85
1	9	-0.90 ❄	-0.40 ❄	85.45±1.78	85.68±2.13	84.67±2.06	84.80±1.87	93.88±1.21	94.04±1.16
1	9	-0.90 🔥	-0.40 🔥	85.46±1.62	85.56±1.93	84.80±1.90	84.86±1.70	93.92±1.26	94.08±1.22
1	9	-0.90 ❄	-0.30 ❄	85.59±1.58	85.46±1.68	85.02±1.71	85.04±1.63	93.95±0.86	94.11±0.81
1	9	-0.90 🔥	-0.30 🔥	85.14±1.96	84.89±2.06	84.51±2.26	84.56±2.08	93.45±1.52	93.62±1.45
1	9	-0.90 ❄	-0.20 ❄	85.00±1.14	85.29±1.28	84.03±1.91	84.25±1.49	93.49±0.63	93.66±0.59
1	9	-0.90 🔥	-0.20 🔥	84.40±2.40	84.20±2.47	83.33±2.64	83.66±2.57	92.83±1.83	93.07±1.77
1	9	-0.90 ❄	-0.10 ❄	84.89±0.93	85.20±1.54	83.66±1.03	84.09±0.95	93.41±0.79	93.58±0.75
1	9	-0.90 🔥	-0.10 🔥	84.79±1.06	84.88±1.53	83.67±0.82	84.05±0.97	93.44±0.72	93.60±0.69
1	9	-0.90 ❄	0.10 ❄	84.21±1.85	84.73±2.37	82.51±1.67	83.22±1.85	92.75±1.64	92.94±1.55
1	9	-0.90 🔥	0.10 🔥	84.04±1.91	84.66±2.38	82.26±1.84	83.00±1.96	92.82±1.64	93.01±1.55
1	9	-0.90 ❄	0.20 ❄	83.82±1.99	84.27±2.17	82.10±2.16	82.78±2.16	92.62±1.74	92.80±1.64
1	9	-0.90 🔥	0.20 🔥	83.93±2.12	84.38±2.25	82.22±2.30	82.90±2.30	92.63±1.80	92.82±1.69
1	9	-0.90 ❄	0.30 ❄	83.06±1.92	83.52±1.95	81.26±2.20	81.94±2.16	92.13±1.86	92.29±1.73
1	9	-0.90 🔥	0.30 🔥	83.91±1.34	84.43±1.38	82.20±1.62	82.87±1.52	92.59±1.48	92.71±1.35
1	9	-0.90 ❄	0.40 ❄	82.99±1.07	83.76±1.19	81.01±1.36	81.77±1.24	91.72±1.28	91.82±1.25
1	9	-0.90 🔥	0.40 🔥	83.45±1.14	84.40±1.42	81.39±1.19	82.23±1.21	92.28±1.39	92.41±1.32
1	9	-0.90 ❄	0.50 ❄	82.73±1.34	83.39±1.40	80.72±1.49	81.49±1.48	91.71±1.39	91.77±1.37
1	9	-0.90 🔥	0.50 🔥	82.71±1.31	83.34±1.55	80.75±1.39	81.51±1.40	91.80±1.40	91.85±1.34
1	9	-0.90 ❄	0.60 ❄	82.03±1.18	82.84±1.20	79.86±1.37	80.66±1.34	91.20±1.10	91.20±1.06
1	9	-0.90 🔥	0.60 🔥	81.97±1.26	82.81±1.29	79.79±1.48	80.59±1.45	91.15±1.22	91.12±1.18
1	9	-0.90 ❄	0.70 ❄	81.58±1.13	82.53±1.21	79.32±1.44	80.12±1.35	90.72±1.24	90.70±1.19
1	9	-0.90 🔥	0.70 🔥	80.92±0.64	81.94±0.93	78.50±0.63	79.35±0.66	90.35±1.14	90.30±1.10
1	9	-0.90 ❄	0.80 ❄	79.69±1.67	80.50±2.38	77.32±1.40	78.08±1.57	88.77±1.94	88.78±1.85
1	9	-0.90 🔥	0.80 🔥	80.03±1.27	80.91±1.87	77.60±1.08	78.40±1.21	89.27±1.66	89.27±1.60
1	9	-0.90 ❄	0.90 ❄	79.80±0.84	81.00±1.11	77.13±0.84	77.99±0.89	89.43±1.03	89.35±1.03
1	9	-0.90 🔥	0.90 🔥	79.82±0.94	81.20±1.20	77.06±0.97	77.94±1.02	89.43±1.15	89.24±1.17
1	9	-0.90 ❄	1.00 ❄	79.36±0.74	80.15±1.22	76.89±0.67	77.66±0.71	88.77±1.28	88.57±1.26
1	9	-0.90 🔥	1.00 🔥	79.23±0.91	80.23±0.95	76.59±1.04	77.40±1.07	88.79±1.17	88.64±1.18
1	9	-0.80 ❄	-1.00 ❄	85.37±1.64	85.90±0.60	84.34±2.90	84.54±2.30	93.82±1.30	94.00±1.21

Continued on next page

t	n	a	b	Accuracy	Precision	Recall	F1 score	AUROC	AUPRC
1	9	-0.80 🔥	-1.00 🔥	84.46±1.74	85.26±1.23	83.67±2.36	83.67±2.05	93.72±1.05	93.92±1.00
1	9	-0.80 ❄	-0.90 ❄	85.65±1.36	86.08±0.56	84.55±2.41	84.86±1.86	93.96±0.79	94.13±0.76
1	9	-0.80 🔥	-0.90 🔥	85.95±1.70	86.43±0.92	84.76±2.68	85.14±2.19	94.10±0.89	94.27±0.86
1	9	-0.80 ❄	-0.80 ❄	85.95±1.20	86.05±0.99	85.26±1.92	85.34±1.51	94.28±0.77	**94.44±0.72**
1	9	-0.80 🔥	-0.80 🔥	86.00±1.20	86.01±1.14	85.32±1.74	85.40±1.42	94.20±0.76	94.36±0.72
1	9	-0.80 ❄	-0.70 ❄	85.19±2.09	85.57±2.04	84.32±1.74	84.50±2.02	94.10±0.86	94.26±0.83
1	9	-0.80 🔥	-0.70 🔥	85.41±2.39	85.68±2.21	84.70±2.05	84.79±2.33	93.98±0.91	94.14±0.87
1	9	-0.80 ❄	-0.60 ❄	86.23±1.17	**86.35±1.35**	85.14±1.24	85.55±1.22	94.09±0.81	94.27±0.75
1	9	-0.80 🔥	-0.60 🔥	**86.30±1.05**	86.16±1.09	**85.47±1.12**	**85.71±1.09**	**94.26±0.54**	94.42±0.49
1	9	-0.80 ❄	-0.50 ❄	85.67±2.74	85.40±2.42	85.61±2.03	85.30±2.60	94.18±1.24	94.34±1.20
1	9	-0.80 🔥	-0.50 🔥	85.67±1.39	85.34±1.59	85.20±1.02	85.18±1.30	94.07±0.66	94.24±0.63
1	9	-0.80 ❄	-0.40 ❄	86.08±1.04	85.69±1.09	85.51±1.17	85.57±1.09	93.97±0.94	94.14±0.89
1	9	-0.80 🔥	-0.40 🔥	86.18±0.77	85.81±0.86	85.74±0.91	85.70±0.79	94.14±0.70	94.30±0.65
1	9	-0.80 ❄	-0.30 ❄	85.49±1.89	85.45±2.18	84.68±2.02	84.87±1.94	93.73±1.45	93.87±1.37
1	9	-0.80 🔥	-0.30 🔥	85.02±0.76	84.90±0.99	84.06±0.84	84.34±0.76	93.43±0.63	93.63±0.60
1	9	-0.80 ❄	-0.20 ❄	84.84±2.03	85.20±2.56	83.38±1.87	83.98±2.02	93.22±1.64	93.44±1.57
1	9	-0.80 🔥	-0.20 🔥	84.28±1.67	84.97±2.20	82.55±1.54	83.26±1.65	93.04±1.47	93.26±1.41
1	9	-0.80 ❄	-0.10 ❄	84.07±1.50	84.56±1.98	82.37±1.38	83.07±1.51	92.70±1.15	92.96±1.05
1	9	-0.80 🔥	-0.10 🔥	83.83±2.37	84.58±3.02	81.99±2.32	82.75±2.44	92.33±1.96	92.60±1.88
1	9	-0.80 ❄	0.10 ❄	84.21±1.34	85.39±1.96	82.14±1.24	83.03±1.33	92.98±1.31	93.20±1.20
1	9	-0.80 🔥	0.10 🔥	84.29±1.48	85.49±1.95	82.23±1.52	83.11±1.57	92.95±1.33	93.17±1.23
1	9	-0.80 ❄	0.20 ❄	84.32±1.36	84.94±1.39	82.54±1.57	83.28±1.51	92.76±1.43	92.97±1.32
1	9	-0.80 🔥	0.20 🔥	83.83±1.93	84.13±2.52	82.35±1.71	82.91±1.88	92.37±1.75	92.57±1.66
1	9	-0.80 ❄	0.30 ❄	83.48±1.29	84.23±1.50	81.54±1.39	82.32±1.39	92.28±1.43	92.47±1.33
1	9	-0.80 🔥	0.30 🔥	83.44±1.09	84.45±1.17	81.33±1.28	82.19±1.23	92.35±1.32	92.53±1.23
1	9	-0.80 ❄	0.40 ❄	82.66±1.24	83.38±1.47	80.65±1.39	81.41±1.36	91.36±1.59	91.50±1.43
1	9	-0.80 🔥	0.40 🔥	83.05±1.19	83.81±1.18	81.04±1.42	81.82±1.36	91.86±1.36	91.94±1.24
1	9	-0.80 ❄	0.50 ❄	82.63±1.22	83.53±1.38	80.47±1.32	81.31±1.34	91.70±1.26	91.70±1.33
1	9	-0.80 🔥	0.50 🔥	82.35±1.09	83.13±1.13	80.25±1.30	81.04±1.25	91.58±1.31	91.57±1.33
1	9	-0.80 ❄	0.60 ❄	81.38±1.59	82.08±1.55	79.21±1.89	79.97±1.84	90.25±2.10	90.37±1.94
1	9	-0.80 🔥	0.60 🔥	81.75±0.95	82.79±1.28	79.46±1.20	80.29±1.12	90.97±1.32	91.01±1.29
1	10	-1.00 ❄	-1.00 ❄	82.39±1.78	82.06±1.69	81.98±1.15	81.83±1.61	91.79±0.89	91.99±0.84
1	10	-1.00 🔥	-1.00 🔥	82.10±1.92	81.76±1.63	81.89±1.15	81.60±1.73	91.81±0.77	92.01±0.74
1	10	-1.00 ❄	-0.90 ❄	83.10±2.42	83.35±2.48	82.35±1.46	82.41±2.15	92.36±1.11	92.55±1.08
1	10	-1.00 🔥	-0.90 🔥	82.92±1.43	83.61±1.93	81.32±1.96	81.82±1.76	91.78±1.19	92.04±1.07
1	10	-1.00 ❄	-0.80 ❄	84.00±1.41	84.69±0.61	82.39±2.37	82.93±2.02	92.73±1.12	92.93±1.00
1	10	-1.00 🔥	-0.80 🔥	83.13±1.40	83.55±1.35	81.69±2.11	82.12±1.85	91.99±0.97	92.24±0.85
1	10	-1.00 ❄	-0.70 ❄	83.02±1.22	83.67±1.74	81.51±1.96	81.96±1.56	91.92±1.09	92.20±0.97
1	10	-1.00 🔥	-0.70 🔥	83.93±1.30	84.13±1.04	82.68±2.01	83.05±1.67	92.64±1.28	92.86±1.15
1	10	-1.00 ❄	-0.60 ❄	83.09±1.47	83.24±1.73	81.98±1.92	82.24±1.66	92.03±1.14	92.31±0.99
1	10	-1.00 🔥	-0.60 🔥	83.31±1.34	83.63±1.34	82.04±2.18	82.38±1.72	91.86±1.11	92.16±0.95
1	10	-1.00 ❄	-0.50 ❄	83.63±1.38	83.31±1.76	83.30±1.35	83.12±1.32	92.94±1.13	93.05±1.07
1	10	-1.00 🔥	-0.50 🔥	83.84±1.54	83.50±1.90	83.36±1.48	83.29±1.50	92.92±1.14	93.04±1.07
1	10	-1.00 ❄	-0.40 ❄	83.44±1.22	83.16±1.60	82.60±1.28	82.76±1.23	92.10±0.94	92.32±0.86
1	10	-1.00 🔥	-0.40 🔥	83.68±1.47	83.26±1.69	82.90±1.40	83.04±1.48	92.41±1.30	92.60±1.17
1	10	-1.00 ❄	-0.30 ❄	84.14±1.54	84.13±1.65	83.02±1.94	83.35±1.70	92.59±1.25	92.85±1.10
1	10	-1.00 🔥	-0.30 🔥	84.14±1.51	84.26±1.76	82.97±1.83	83.33±1.63	92.54±1.17	92.80±1.02
1	10	-1.00 ❄	-0.20 ❄	84.49±1.39	84.53±1.51	83.19±1.53	83.67±1.48	92.77±1.18	92.96±0.97
1	10	-1.00 🔥	-0.20 🔥	84.99±1.11	84.68±1.17	84.10±1.17	84.35±1.17	93.07±1.01	93.22±0.88
1	10	-1.00 ❄	-0.10 ❄	85.12±1.28	84.99±1.30	84.03±1.45	84.40±1.38	93.20±1.06	93.40±0.90
1	10	-1.00 🔥	-0.10 🔥	85.07±1.18	84.90±1.22	84.03±1.31	84.38±1.26	93.20±0.98	93.41±0.84
1	10	-1.00 ❄	0.10 ❄	85.20±1.27	85.52±1.67	83.79±1.30	84.36±1.31	93.83±0.98	93.95±0.84
1	10	-1.00 🔥	0.10 🔥	85.39±0.95	85.67±1.26	84.03±1.05	84.58±1.01	93.85±0.93	93.96±0.81

Continued on next page

t	n	a	b	Accuracy	Precision	Recall	F1 score	AUROC	AUPRC
1	10	-1.00 ❄️	0.20 ❄️	84.61±2.08	84.76±2.42	83.28±2.06	83.79±2.13	93.05±1.55	93.15±1.51
1	10	-1.00 🔥	0.20 🔥	83.96±1.32	84.31±1.63	82.40±1.41	83.00±1.38	92.88±1.26	92.97±1.16
1	10	-1.00 ❄️	0.30 ❄️	82.95±1.59	84.10±1.90	80.95±2.19	81.65±2.02	92.40±1.45	92.51±1.41
1	10	-1.00 🔥	0.30 🔥	82.36±1.83	83.87±2.10	80.25±2.70	80.91±2.54	92.27±1.35	92.38±1.32
1	10	-1.00 ❄️	0.40 ❄️	82.33±1.92	84.13±2.36	79.84±2.27	80.75±2.23	91.95±1.82	92.11±1.74
1	10	-1.00 🔥	0.40 🔥	82.08±1.93	84.03±2.22	79.57±2.57	80.41±2.50	91.87±1.80	92.03±1.74
1	10	-1.00 ❄️	0.50 ❄️	81.20±2.56	83.46±2.24	78.47±3.40	79.26±3.51	91.14±2.18	91.32±2.13
1	10	-1.00 🔥	0.50 🔥	82.10±2.55	84.46±1.10	79.38±3.61	80.21±3.66	92.01±1.75	92.19±1.77
1	10	-1.00 ❄️	0.60 ❄️	82.56±2.79	84.15±3.28	80.11±2.92	81.05±3.03	91.53±3.05	91.68±2.95
1	10	-1.00 🔥	0.60 🔥	82.43±2.81	83.64±3.29	80.12±2.90	81.01±3.01	90.84±3.48	91.09±3.34
1	10	-1.00 ❄️	0.70 ❄️	82.85±1.77	84.55±1.60	80.32±2.11	81.30±2.12	91.51±2.11	91.75±2.01
1	10	-1.00 🔥	0.70 🔥	82.01±2.88	83.43±3.38	79.59±2.98	80.49±3.10	90.63±3.37	90.85±3.24
1	10	-1.00 ❄️	0.80 ❄️	82.50±1.48	84.59±1.19	79.75±1.79	80.80±1.81	90.85±2.07	91.15±1.98
1	10	-1.00 🔥	0.80 🔥	82.63±1.73	84.52±1.40	79.98±2.10	80.99±2.11	90.85±2.43	91.08±2.44
1	10	-1.00 ❄️	0.90 ❄️	81.82±2.02	83.59±2.26	79.11±2.16	80.11±2.26	90.07±3.10	90.44±2.88
1	10	-1.00 🔥	0.90 🔥	81.59±1.80	83.13±2.47	79.02±1.71	79.96±1.84	89.65±3.19	90.07±2.93
1	10	-1.00 ❄️	1.00 ❄️	81.13±1.69	82.88±1.79	78.36±1.88	79.32±1.95	89.14±2.90	89.58±2.66
1	10	-1.00 🔥	1.00 🔥	81.10±1.70	82.79±1.98	78.36±1.83	79.32±1.90	89.02±3.03	89.47±2.76
1	10	-0.90 ❄️	-1.00 ❄️	82.59±2.68	82.56±2.82	81.84±1.90	81.91±2.44	91.85±1.39	92.04±1.33
1	10	-0.90 🔥	-1.00 🔥	83.28±2.87	83.28±2.41	82.93±1.80	82.75±2.62	92.44±0.97	92.59±1.00
1	10	-0.90 ❄️	-0.90 ❄️	83.91±2.02	83.97±2.62	83.04±1.41	83.23±1.82	92.80±1.18	92.94±1.19
1	10	-0.90 🔥	-0.90 🔥	83.90±1.48	84.63±1.54	82.33±2.23	82.86±1.93	92.59±1.29	92.79±1.19
1	10	-0.90 ❄️	-0.80 ❄️	83.69±1.20	84.52±1.09	82.10±2.17	82.61±1.76	92.59±0.84	92.78±0.76
1	10	-0.90 🔥	-0.80 🔥	83.72±1.01	83.93±0.61	82.53±1.91	82.84±1.51	92.38±1.01	92.60±0.91
1	10	-0.90 ❄️	-0.70 ❄️	83.52±1.21	83.79±0.44	82.42±2.31	82.64±1.83	92.53±1.04	92.74±0.93
1	10	-0.90 🔥	-0.70 🔥	83.02±2.15	83.25±2.19	82.83±1.28	82.49±1.88	92.67±0.95	92.83±0.95
1	10	-0.90 ❄️	-0.60 ❄️	84.05±1.60	84.14±2.22	83.16±1.74	83.34±1.63	92.85±1.20	93.01±1.16
1	10	-0.90 🔥	-0.60 🔥	83.55±1.59	83.72±2.20	82.50±1.81	82.75±1.65	92.31±1.35	92.57±1.21
1	10	-0.90 ❄️	-0.50 ❄️	83.41±1.23	83.06±1.42	82.63±1.44	82.74±1.31	92.32±0.92	92.53±0.92
1	10	-0.90 🔥	-0.50 🔥	84.28±1.78	84.12±2.11	83.44±2.07	83.60±1.90	92.76±1.27	92.91±1.20
1	10	-0.90 ❄️	-0.40 ❄️	83.73±1.30	84.51±1.75	82.02±1.61	82.66±1.45	92.44±1.13	92.73±1.01
1	10	-0.90 🔥	-0.40 🔥	83.58±1.75	83.79±2.16	82.18±1.77	82.67±1.79	92.26±1.36	92.52±1.26
1	10	-0.90 ❄️	-0.30 ❄️	83.02±1.73	83.49±1.89	81.56±2.52	81.98±2.15	92.01±1.34	92.28±1.26
1	10	-0.90 🔥	-0.30 🔥	83.30±2.09	83.70±2.11	81.87±2.82	82.29±2.48	92.21±1.43	92.46±1.34
1	10	-0.90 ❄️	-0.20 ❄️	84.79±1.35	84.91±1.27	83.52±1.79	83.98±1.56	92.90±1.31	93.16±1.15
1	10	-0.90 🔥	-0.20 🔥	84.93±1.34	85.25±1.30	83.45±1.62	84.05±1.50	92.89±1.25	93.15±1.08
1	10	-0.90 ❄️	-0.10 ❄️	84.75±1.72	84.97±1.26	83.42±2.34	83.88±2.08	93.04±1.28	93.26±1.20
1	10	-0.90 🔥	-0.10 🔥	85.28±0.92	85.48±0.80	83.97±1.31	84.48±1.10	93.47±0.87	93.67±0.76
1	10	-0.90 ❄️	0.10 ❄️	85.17±1.27	85.83±1.30	83.45±1.48	84.20±1.42	93.55±1.07	93.71±0.95
1	10	-0.90 🔥	0.10 🔥	85.26±1.33	86.12±1.10	83.45±1.76	84.23±1.59	93.62±1.02	93.79±0.90
1	10	-0.90 ❄️	0.20 ❄️	84.40±1.92	85.22±2.03	82.53±2.18	83.31±2.12	93.24±1.44	93.38±1.36
1	10	-0.90 🔥	0.20 🔥	84.64±1.99	85.41±2.03	82.81±2.26	83.58±2.21	93.42±1.53	93.54±1.45
1	10	-0.90 ❄️	0.30 ❄️	83.79±2.29	84.16±2.57	82.12±2.35	82.79±2.41	92.42±2.07	92.59±2.04
1	10	-0.90 🔥	0.30 🔥	84.09±1.92	84.88±2.27	82.26±2.09	83.01±2.06	92.83±1.68	92.96±1.57
1	10	-0.90 ❄️	0.40 ❄️	83.35±2.22	84.75±2.58	81.09±2.41	82.00±2.42	92.22±2.03	92.41±1.94
1	10	-0.90 🔥	0.40 🔥	83.19±2.04	84.21±2.33	81.16±2.40	81.93±2.30	92.01±1.82	92.19±1.72
1	10	-0.90 ❄️	0.50 ❄️	82.78±2.16	83.87±2.50	80.63±2.41	81.45±2.40	91.52±2.15	91.72±2.05
1	10	-0.90 🔥	0.50 🔥	82.80±2.00	84.12±2.53	80.49±2.06	81.39±2.13	91.62±2.16	91.81±2.05
1	10	-0.90 ❄️	0.60 ❄️	83.05±2.85	84.44±3.08	80.73±3.14	81.63±3.19	91.27±3.08	91.47±2.97
1	10	-0.90 🔥	0.60 🔥	82.81±3.02	84.38±3.45	80.40±3.21	81.33±3.31	91.19±3.06	91.42±2.94
1	10	-0.90 ❄️	0.70 ❄️	81.83±2.43	83.46±2.89	79.29±2.59	80.21±2.69	90.11±3.29	90.38±3.17
1	10	-0.90 🔥	0.70 🔥	81.98±2.43	83.45±2.84	79.49±2.55	80.42±2.65	90.19±3.28	90.46±3.15
1	10	-0.90 ❄️	0.80 ❄️	82.12±1.91	83.59±2.32	79.61±1.95	80.57±2.05	90.15±2.89	90.52±2.76

Continued on next page

t	n	a	b	Accuracy	Precision	Recall	F1 score	AUROC	AUPRC
1	10	-0.90 🔥	0.80 🔥	82.57±1.51	84.47±1.03	79.92±1.91	80.92±1.91	90.53±2.37	90.85±2.32
1	10	-0.90 ❄	0.90 ❄	81.33±2.10	82.93±2.05	78.65±2.43	79.58±2.46	89.00±2.80	89.45±2.63
1	10	-0.90 🔥	0.90 🔥	81.22±2.00	82.72±2.31	78.57±2.11	79.50±2.21	88.90±3.00	89.35±2.80
1	10	-0.90 ❄	1.00 ❄	80.70±2.22	82.20±2.75	78.02±2.29	78.93±2.39	88.22±3.63	88.72±3.36
1	10	-0.90 🔥	1.00 🔥	80.84±2.14	82.29±2.62	78.19±2.19	79.10±2.30	88.31±3.29	88.81±3.03
1	10	-0.80 ❄	-1.00 ❄	82.64±3.04	82.99±2.51	82.27±1.67	82.05±2.71	92.09±0.93	92.24±0.97
1	10	-0.80 🔥	-1.00 🔥	82.47±2.87	83.03±2.53	82.02±1.49	81.83±2.51	92.11±0.90	92.25±0.94
1	10	-0.80 ❄	-0.90 ❄	82.07±2.68	82.37±3.01	81.16±1.80	81.28±2.39	91.27±1.31	91.53±1.19
1	10	-0.80 🔥	-0.90 🔥	82.43±2.88	82.81±3.05	81.66±2.12	81.69±2.63	91.91±1.28	92.11±1.22
1	10	-0.80 ❄	-0.80 ❄	83.51±1.48	83.71±1.00	82.42±2.24	82.65±1.93	92.39±1.38	92.59±1.28
1	10	-0.80 🔥	-0.80 🔥	83.77±1.48	84.19±1.37	82.44±2.02	82.84±1.81	92.45±1.33	92.65±1.24
1	10	-0.80 ❄	-0.70 ❄	83.03±1.77	83.59±2.51	82.29±1.90	82.26±1.80	92.56±0.98	92.73±0.99
1	10	-0.80 🔥	-0.70 🔥	83.02±1.81	83.61±2.58	82.29±1.82	82.26±1.79	92.59±1.03	92.75±1.05
1	10	-0.80 ❄	-0.60 ❄	84.28±1.33	84.09±1.49	83.34±1.59	83.58±1.43	92.56±1.14	92.74±1.10
1	10	-0.80 🔥	-0.60 🔥	83.80±1.20	84.28±1.81	82.55±1.97	82.89±1.55	92.78±1.16	92.94±1.13
1	10	-0.80 ❄	-0.50 ❄	83.84±1.44	83.72±1.74	82.79±1.55	83.09±1.50	92.19±1.06	92.40±1.09
1	10	-0.80 🔥	-0.50 🔥	83.87±1.89	83.54±1.91	83.09±2.22	83.21±2.04	92.40±1.36	92.57±1.29
1	10	-0.80 ❄	-0.40 ❄	83.96±1.86	83.83±2.24	83.00±1.66	83.25±1.80	92.54±1.42	92.73±1.41
1	10	-0.80 🔥	-0.40 🔥	83.96±1.79	83.97±2.33	83.00±1.53	83.24±1.68	92.50±1.40	92.69±1.38
1	10	-0.80 ❄	-0.30 ❄	83.79±1.79	84.27±2.40	82.24±1.80	82.82±1.83	92.62±1.39	92.83±1.36
1	10	-0.80 🔥	-0.30 🔥	83.91±1.84	84.44±2.58	82.34±1.79	82.94±1.84	92.46±1.59	92.71±1.51
1	10	-0.80 ❄	-0.20 ❄	84.07±1.86	84.76±2.30	82.25±1.93	83.00±1.97	92.69±1.80	92.93±1.69
1	10	-0.80 🔥	-0.20 🔥	84.39±2.20	84.78±2.25	82.77±2.45	83.42±2.40	92.80±1.70	93.03±1.61
1	10	-0.80 ❄	-0.10 ❄	84.91±1.21	85.39±1.19	83.33±1.56	83.97±1.40	93.02±1.31	93.28±1.16
1	10	-0.80 🔥	-0.10 🔥	85.03±1.17	85.57±0.97	83.41±1.55	84.08±1.37	93.22±1.11	93.46±0.99
1	10	-0.80 ❄	0.10 ❄	85.05±1.42	86.16±1.20	83.04±1.73	83.93±1.66	93.39±1.18	93.60±1.09
1	10	-0.80 🔥	0.10 🔥	84.81±1.82	85.62±1.86	82.99±2.13	83.76±2.04	93.32±1.34	93.48±1.29
1	10	-0.80 ❄	0.20 ❄	84.86±2.12	85.58±2.18	83.14±2.48	83.85±2.37	93.29±1.67	93.43±1.60
1	10	-0.80 🔥	0.20 🔥	84.91±1.94	85.70±2.08	83.17±2.28	83.89±2.16	93.28±1.60	93.43±1.54
1	10	-0.80 ❄	0.30 ❄	83.83±2.15	84.81±2.52	81.92±2.43	82.67±2.38	92.32±1.75	92.47±1.68
1	10	-0.80 🔥	0.30 🔥	84.18±2.32	85.02±2.50	82.32±2.62	83.07±2.55	92.58±1.94	92.76±1.88
1	10	-0.80 ❄	0.40 ❄	83.80±2.71	84.93±2.96	81.71±2.94	82.56±2.96	92.10±2.30	92.30±2.22
1	10	-0.80 🔥	0.40 🔥	82.77±2.13	84.13±2.48	80.54±2.53	81.36±2.42	91.49±1.87	91.71±1.78
1	10	-0.80 ❄	0.50 ❄	82.92±2.35	84.52±2.66	80.48±2.54	81.44±2.61	91.33±2.48	91.54±2.42
1	10	-0.80 🔥	0.50 🔥	82.75±2.39	84.39±2.53	80.27±2.69	81.22±2.72	91.14±2.45	91.38±2.39
1	10	-0.80 ❄	0.60 ❄	82.82±2.70	84.30±2.92	80.42±2.94	81.35±3.00	90.82±2.86	91.08±2.77
1	10	-0.80 🔥	0.60 🔥	82.70±2.69	84.47±2.95	80.17±2.96	81.13±3.02	90.79±2.98	91.05±2.90
1	11	-1.00 ❄	-1.00 ❄	79.22±1.88	79.78±2.26	77.02±1.89	77.66±1.98	87.90±2.48	87.61±2.56
1	11	-1.00 🔥	-1.00 🔥	78.95±2.00	79.44±2.13	76.75±2.24	77.36±2.30	87.35±2.75	87.03±2.91
1	11	-1.00 ❄	-0.90 ❄	80.32±1.48	80.55±1.47	78.51±2.08	79.03±1.80	88.71±2.44	88.42±2.46
1	11	-1.00 🔥	-0.90 🔥	79.55±1.68	80.46±1.44	77.03±2.11	77.79±2.10	87.82±2.48	87.56±2.60
1	11	-1.00 ❄	-0.80 ❄	80.14±3.22	80.91±2.61	77.92±4.12	78.49±4.09	88.18±3.57	87.92±3.74
1	11	-1.00 🔥	-0.80 🔥	80.95±2.34	81.48±1.94	78.87±2.97	79.52±2.83	89.08±2.46	88.89±2.49
1	11	-1.00 ❄	-0.70 ❄	80.50±2.96	81.16±2.38	78.33±3.71	78.94±3.70	88.26±3.57	88.11±3.71
1	11	-1.00 🔥	-0.70 🔥	80.69±2.81	81.34±2.24	78.50±3.52	79.15±3.50	88.48±3.45	88.33±3.59
1	11	-1.00 ❄	-0.60 ❄	80.80±2.83	80.97±2.55	79.02±3.42	79.52±3.37	88.66±3.59	88.57±3.74
1	11	-1.00 🔥	-0.60 🔥	80.60±2.85	80.78±2.74	78.74±3.32	79.30±3.32	88.66±3.45	88.57±3.59
1	11	-1.00 ❄	-0.50 ❄	81.15±3.63	81.83±1.84	79.62±5.33	79.70±5.11	89.42±3.83	89.32±3.93
1	11	-1.00 🔥	-0.50 🔥	81.54±2.37	81.54±1.82	80.24±3.35	80.49±2.99	89.61±3.25	89.50±3.33
1	11	-1.00 ❄	-0.40 ❄	81.54±2.67	81.72±2.38	79.89±3.50	80.35±3.16	89.57±3.11	89.58±3.15
1	11	-1.00 🔥	-0.40 🔥	81.33±3.16	81.79±2.42	79.45±4.14	79.95±3.95	89.35±3.30	89.37±3.31
1	11	-1.00 ❄	-0.30 ❄	82.12±1.82	82.48±1.78	80.38±2.26	80.96±2.13	90.11±2.71	90.25±2.84
1	11	-1.00 🔥	-0.30 🔥	81.01±3.27	82.10±2.88	78.56±3.96	79.31±4.08	89.49±3.67	89.35±4.16

Continued on next page

t	n	a	b	Accuracy	Precision	Recall	F1 score	AUROC	AUPRC
1	11	-1.00 ❄	-0.20 ❄	83.20±1.45	83.60±1.84	81.46±1.37	82.14±1.48	91.53±1.64	91.71±1.66
1	11	-1.00 🔥	-0.20 🔥	83.10±1.53	83.60±1.87	81.27±1.50	81.99±1.58	91.58±1.63	91.77±1.63
1	11	-1.00 ❄	-0.10 ❄	84.37±1.54	84.57±2.01	82.99±1.33	83.53±1.50	92.48±1.38	92.56±1.54
1	11	-1.00 🔥	-0.10 🔥	84.46±1.33	84.87±1.86	82.99±1.31	83.56±1.35	92.81±1.37	92.88±1.51
1	11	-1.00 ❄	0.10 ❄	83.73±1.69	84.85±2.98	82.21±1.05	82.73±1.36	93.46±1.44	93.53±1.44
1	11	-1.00 🔥	0.10 🔥	82.74±2.32	84.99±2.84	80.43±2.60	81.21±2.61	93.20±1.45	93.22±1.50
1	11	-1.00 ❄	0.20 ❄	83.62±2.29	84.44±3.21	82.16±1.83	82.66±2.13	92.80±1.99	92.81±2.07
1	11	-1.00 🔥	0.20 🔥	83.89±2.04	84.90±2.93	82.32±1.74	82.88±1.92	93.41±1.67	93.48±1.65
1	11	-1.00 ❄	0.30 ❄	83.82±2.04	84.80±2.93	82.24±1.38	82.82±1.79	93.31±1.81	93.37±1.80
1	11	-1.00 🔥	0.30 🔥	82.96±1.90	84.00±2.84	81.31±1.82	81.85±1.84	92.42±2.02	92.52±1.95
1	11	-1.00 ❄	0.40 ❄	83.59±2.03	84.92±3.01	81.71±1.68	82.43±1.93	93.09±2.10	93.15±2.08
1	11	-1.00 🔥	0.40 🔥	83.72±2.15	85.07±3.14	81.84±1.68	82.57±2.00	93.11±2.17	93.17±2.14
1	11	-1.00 ❄	0.50 ❄	81.58±2.82	83.88±2.85	79.04±3.47	79.77±3.58	92.37±1.95	92.40±1.99
1	11	-1.00 🔥	0.50 🔥	81.38±2.67	83.85±2.80	78.72±3.23	79.50±3.40	92.17±1.82	92.21±1.85
1	11	-1.00 ❄	0.60 ❄	81.27±2.91	83.59±3.45	78.66±3.11	79.46±3.33	91.70±2.11	91.73±2.11
1	11	-1.00 🔥	0.60 🔥	81.64±3.07	83.33±3.43	79.29±3.24	80.05±3.46	91.73±2.16	91.77±2.16
1	11	-1.00 ❄	0.70 ❄	82.84±1.59	85.24±1.04	80.22±2.58	81.13±2.37	92.97±0.53	93.03±0.47
1	11	-1.00 🔥	0.70 🔥	83.37±1.53	85.39±1.02	80.92±2.38	81.83±2.19	93.12±0.44	93.17±0.41
1	11	-1.00 ❄	0.80 ❄	83.21±1.26	85.12±1.01	80.78±2.07	81.69±1.82	92.67±0.56	92.72±0.50
1	11	-1.00 🔥	0.80 🔥	81.71±2.85	84.43±1.93	78.82±3.93	79.66±3.81	91.85±1.61	91.91±1.67
1	11	-1.00 ❄	0.90 ❄	81.12±1.64	83.78±1.27	78.20±2.68	79.06±2.50	91.78±0.87	91.84±0.80
1	11	-1.00 🔥	0.90 🔥	82.00±1.53	83.96±1.20	79.41±2.35	80.28±2.18	91.47±0.66	91.56±0.56
1	11	-1.00 ❄	1.00 ❄	81.36±1.50	83.66±1.26	78.52±2.24	79.43±2.21	91.25±0.61	91.32±0.55
1	11	-1.00 🔥	1.00 🔥	80.85±1.66	83.29±1.40	77.91±2.43	78.80±2.42	91.21±0.51	91.29±0.49
1	11	-0.90 ❄	-1.00 ❄	80.14±1.22	80.37±1.18	78.14±1.45	78.78±1.41	87.82±2.40	87.65±2.41
1	11	-0.90 🔥	-1.00 🔥	79.36±2.28	79.55±2.03	77.39±2.81	77.92±2.81	87.28±2.79	87.05±2.90
1	11	-0.90 ❄	-0.90 ❄	79.34±1.81	80.12±2.30	77.02±2.02	77.70±2.04	87.42±3.02	87.18±3.21
1	11	-0.90 🔥	-0.90 🔥	79.64±1.46	80.28±2.29	77.48±1.31	78.13±1.38	87.80±2.46	87.62±2.54
1	11	-0.90 ❄	-0.80 ❄	79.99±1.70	80.35±2.32	78.03±1.33	78.65±1.54	88.22±2.41	88.02±2.55
1	11	-0.90 🔥	-0.80 🔥	80.08±1.43	80.51±2.03	78.05±1.27	78.70±1.37	88.32±2.07	88.16±2.20
1	11	-0.90 ❄	-0.70 ❄	80.13±1.81	80.51±2.14	78.09±2.04	78.72±2.02	88.30±3.05	88.19±3.26
1	11	-0.90 🔥	-0.70 🔥	80.46±1.64	81.08±1.97	78.33±1.94	79.01±1.88	88.73±2.75	88.60±2.93
1	11	-0.90 ❄	-0.60 ❄	80.95±2.47	81.47±2.49	78.90±2.85	79.56±2.88	89.18±2.81	89.13±2.98
1	11	-0.90 🔥	-0.60 🔥	81.15±1.86	81.78±1.94	79.03±2.12	79.75±2.13	89.45±1.97	89.39±2.06
1	11	-0.90 ❄	-0.50 ❄	81.48±1.97	81.81±2.02	80.02±2.69	80.37±2.37	89.74±2.37	89.70±2.46
1	11	-0.90 🔥	-0.50 🔥	81.48±2.50	82.06±2.28	79.74±3.32	80.20±3.09	89.57±2.98	89.54±3.09
1	11	-0.90 ❄	-0.40 ❄	81.22±3.24	81.77±2.51	79.45±4.52	79.83±4.12	89.10±3.93	89.12±3.95
1	11	-0.90 🔥	-0.40 🔥	81.10±3.01	81.01±2.73	79.59±3.72	79.98±3.54	88.97±3.37	89.03±3.47
1	11	-0.90 ❄	-0.30 ❄	82.32±1.46	82.67±1.14	80.71±2.18	81.21±1.87	90.17±1.98	90.32±1.97
1	11	-0.90 🔥	-0.30 🔥	82.77±2.66	82.67±2.04	81.85±3.76	81.91±3.29	90.29±3.45	90.29±3.53
1	11	-0.90 ❄	-0.20 ❄	82.33±1.09	83.49±1.87	80.24±1.52	80.98±1.30	90.80±1.66	90.96±1.71
1	11	-0.90 🔥	-0.20 🔥	82.77±1.68	83.45±1.65	80.87±2.20	81.55±2.01	90.88±1.98	91.04±2.08
1	11	-0.90 ❄	-0.10 ❄	84.37±1.46	84.89±1.69	82.85±1.56	83.43±1.53	92.36±1.32	92.45±1.49
1	11	-0.90 🔥	-0.10 🔥	84.14±1.71	84.40±2.14	82.80±1.63	83.28±1.71	92.31±1.42	92.40±1.58
1	11	-0.90 ❄	0.10 ❄	85.19±1.31	86.08±1.29	83.39±1.68	84.16±1.53	93.98±0.84	94.08±0.91
1	11	-0.90 🔥	0.10 🔥	84.25±2.52	85.39±2.50	82.41±2.92	83.10±2.90	93.15±2.03	93.18±2.23
1	11	-0.90 ❄	0.20 ❄	83.24±1.93	84.15±2.38	81.61±2.19	82.15±2.14	92.52±1.61	92.61±1.56
1	11	-0.90 🔥	0.20 🔥	82.68±1.90	83.89±2.25	80.90±2.49	81.43±2.29	92.36±1.49	92.42±1.43
1	11	-0.90 ❄	0.30 ❄	81.52±1.86	83.80±2.72	79.08±2.15	79.83±2.12	92.12±1.77	92.19±1.72
1	11	-0.90 🔥	0.30 🔥	81.72±2.91	84.83±3.05	79.04±3.60	79.77±3.77	93.15±1.85	93.18±1.85
1	11	-0.90 ❄	0.40 ❄	82.68±2.38	84.76±3.01	80.42±2.63	81.19±2.65	92.73±1.87	92.79±1.89
1	11	-0.90 🔥	0.40 🔥	82.33±2.22	84.56±2.94	79.99±2.52	80.75±2.53	92.73±1.87	92.79±1.89
1	11	-0.90 ❄	0.50 ❄	80.22±2.26	83.74±3.01	77.06±2.85	77.86±3.00	91.89±1.90	91.96±1.91

Continued on next page

t	n	a	b	Accuracy	Precision	Recall	F1 score	AUROC	AUPRC
1	11	-0.90 🔥	0.50 🔥	82.25±1.63	84.45±2.98	79.83±1.60	80.67±1.67	92.55±1.83	92.59±1.80
1	11	-0.90 ❄️	0.60 ❄️	81.94±3.27	85.51±1.67	78.75±4.37	79.66±4.48	93.08±1.12	93.08±1.12
1	11	-0.90 🔥	0.60 🔥	80.59±3.45	83.82±3.66	77.69±4.10	78.38±4.36	91.83±2.16	91.87±2.14
1	11	-0.90 ❄️	0.70 ❄️	81.48±3.27	84.64±1.36	78.39±4.45	79.21±4.53	92.24±1.32	92.25±1.22
1	11	-0.90 🔥	0.70 🔥	81.65±2.80	85.06±1.38	78.49±3.90	79.40±3.87	92.44±1.43	92.47±1.41
1	11	-0.90 ❄️	0.80 ❄️	82.43±2.13	84.70±1.00	79.76±3.07	80.65±2.99	92.18±0.69	92.20±0.61
1	11	-0.90 🔥	0.80 🔥	82.38±1.89	84.62±1.17	79.77±2.88	80.63±2.75	92.13±0.82	92.19±0.77
1	11	-0.90 ❄️	0.90 ❄️	80.80±1.61	83.74±1.34	77.75±2.67	78.60±2.53	91.39±1.01	91.46±0.95
1	11	-0.90 🔥	0.90 🔥	80.20±1.74	83.09±2.11	77.10±2.67	77.93±2.53	90.86±1.74	90.93±1.78
1	11	-0.90 ❄️	1.00 ❄️	80.77±1.59	83.06±1.41	77.92±2.45	78.76±2.39	90.62±0.65	90.70±0.66
1	11	-0.90 🔥	1.00 🔥	80.71±1.75	83.07±1.14	77.87±2.78	78.67±2.76	90.46±0.67	90.55±0.62
1	11	-0.80 ❄️	-1.00 ❄️	80.31±0.95	80.70±1.70	78.46±1.16	79.01±1.05	88.49±1.64	88.43±1.68
1	11	-0.80 🔥	-1.00 🔥	80.07±0.97	80.54±1.85	78.10±0.62	78.71±0.75	88.22±1.85	88.17±1.95
1	11	-0.80 ❄️	-0.90 ❄️	79.85±1.16	80.44±1.54	77.69±1.39	78.34±1.35	88.06±2.13	87.98±2.23
1	11	-0.80 🔥	-0.90 🔥	79.93±1.22	80.24±1.97	78.05±1.05	78.62±1.11	88.02±2.16	87.92±2.29
1	11	-0.80 ❄️	-0.80 ❄️	80.31±1.34	81.35±1.74	77.82±1.43	78.64±1.47	88.31±2.37	88.23±2.52
1	11	-0.80 🔥	-0.80 🔥	80.10±1.45	80.86±1.73	77.87±1.73	78.55±1.69	88.30±2.41	88.17±2.58
1	11	-0.80 ❄️	-0.70 ❄️	80.22±2.11	80.68±2.41	78.13±2.34	78.80±2.32	88.09±3.14	87.99±3.35
1	11	-0.80 🔥	-0.70 🔥	80.42±2.33	80.79±2.78	78.45±2.48	79.08±2.49	88.28±3.28	88.18±3.51
1	11	-0.80 ❄️	-0.60 ❄️	80.50±2.06	81.00±2.64	78.55±2.19	79.16±2.15	88.78±3.01	88.71±3.22
1	11	-0.80 🔥	-0.60 🔥	80.75±2.27	81.63±2.17	78.52±2.94	79.20±2.85	88.94±2.83	88.92±3.00
1	11	-0.80 ❄️	-0.50 ❄️	80.99±2.48	81.13±2.94	79.36±2.54	79.87±2.56	88.87±3.30	88.92±3.45
1	11	-0.80 🔥	-0.50 🔥	81.01±2.16	81.34±2.34	79.36±2.66	79.81±2.52	89.09±2.76	89.15±2.86
1	11	-0.80 ❄️	-0.40 ❄️	81.15±2.14	81.62±2.19	79.36±2.79	79.87±2.60	88.92±2.87	89.03±2.99
1	11	-0.80 🔥	-0.40 🔥	81.19±2.06	81.17±1.63	79.70±2.78	80.08±2.59	88.93±2.74	89.02±2.80
1	11	-0.80 ❄️	-0.30 ❄️	82.22±1.90	82.63±1.73	80.62±2.50	81.10±2.32	89.95±2.94	90.08±3.07
1	11	-0.80 🔥	-0.30 🔥	82.14±1.92	82.55±1.57	80.49±2.58	80.98±2.40	89.90±2.73	90.08±2.81
1	11	-0.80 ❄️	-0.20 ❄️	82.18±1.22	83.92±1.86	79.72±1.70	80.60±1.58	90.70±2.02	90.93±2.10
1	11	-0.80 🔥	-0.20 🔥	82.71±1.97	83.36±2.01	80.95±2.45	81.54±2.33	90.79±2.29	90.95±2.37
1	11	-0.80 ❄️	-0.10 ❄️	83.70±1.39	84.68±1.85	81.92±1.80	82.58±1.61	92.13±1.48	92.33±1.54
1	11	-0.80 🔥	-0.10 🔥	83.87±1.55	84.82±1.89	82.23±1.91	82.80±1.74	92.14±1.53	92.36±1.56
1	11	-0.80 ❄️	0.10 ❄️	84.17±1.31	85.52±2.56	82.50±1.43	83.09±1.31	93.34±1.36	93.43±1.40
1	11	-0.80 🔥	0.10 🔥	84.50±1.85	85.22±2.27	83.16±2.08	83.60±2.00	93.11±1.23	93.21±1.27
1	11	-0.80 ❄️	0.20 ❄️	84.18±2.35	85.30±2.13	82.11±2.81	82.96±2.71	93.22±1.82	93.26±1.85
1	11	-0.80 🔥	0.20 🔥	83.61±1.84	85.27±2.07	81.21±2.10	82.19±2.08	93.07±1.62	93.11±1.65
1	11	-0.80 ❄️	0.30 ❄️	81.97±3.23	83.74±2.62	79.74±4.14	80.34±4.16	92.14±1.82	92.17±1.83
1	11	-0.80 🔥	0.30 🔥	82.22±2.81	83.93±2.42	80.01±3.62	80.66±3.54	92.15±1.74	92.19±1.75
1	11	-0.80 ❄️	0.40 ❄️	82.52±2.69	85.46±1.58	79.52±3.50	80.54±3.50	93.40±1.17	93.43±1.26
1	11	-0.80 🔥	0.40 🔥	82.52±2.69	85.44±1.65	79.53±3.48	80.54±3.56	93.48±1.00	93.50±1.10
1	11	-0.80 ❄️	0.50 ❄️	82.04±2.79	84.87±1.69	79.13±3.81	80.02±3.81	92.83±0.97	92.87±1.01
1	11	-0.80 🔥	0.50 🔥	82.19±3.01	85.03±1.60	79.33±4.16	80.18±4.12	92.96±0.94	93.00±0.99
1	12	-1.00 ❄️	-1.00 ❄️	84.18±2.02	84.30±2.64	83.31±1.89	83.49±1.94	92.87±1.55	92.95±1.61
1	12	-1.00 🔥	-1.00 🔥	83.59±1.61	83.64±1.85	83.17±0.85	83.02±1.36	92.53±1.00	92.60±1.04
1	12	-1.00 ❄️	-0.90 ❄️	84.30±1.87	84.23±2.35	83.67±1.63	83.71±1.77	92.93±1.25	92.99±1.35
1	12	-1.00 🔥	-0.90 🔥	84.46±2.02	84.24±2.35	83.84±1.87	83.88±1.99	92.75±1.60	92.86±1.59
1	12	-1.00 ❄️	-0.80 ❄️	84.88±2.12	84.88±2.73	84.08±2.16	84.24±2.13	93.34±1.55	93.42±1.62
1	12	-1.00 🔥	-0.80 🔥	84.58±2.26	84.43±2.63	83.82±2.08	83.97±2.22	92.96±1.41	93.06±1.46
1	12	-1.00 ❄️	-0.70 ❄️	85.19±1.93	85.16±2.35	84.34±1.91	84.55±1.93	93.39±1.39	93.46±1.47
1	12	-1.00 🔥	-0.70 🔥	85.19±1.78	85.04±2.09	84.32±1.84	84.55±1.83	93.24±1.39	93.32±1.47
1	12	-1.00 ❄️	-0.60 ❄️	85.35±1.94	85.64±2.67	84.55±2.14	84.69±1.99	93.76±1.56	93.90±1.56
1	12	-1.00 🔥	-0.60 🔥	85.41±1.65	85.79±2.22	84.48±2.21	84.69±1.83	93.77±1.35	93.93±1.34
1	12	-1.00 ❄️	-0.50 ❄️	85.14±1.30	85.62±1.70	83.78±1.67	84.29±1.43	93.52±1.33	93.70±1.27
1	12	-1.00 🔥	-0.50 🔥	85.52±1.80	85.49±1.87	84.52±2.07	84.83±1.94	93.54±1.44	93.71±1.39

Continued on next page

t	n	a	b	Accuracy	Precision	Recall	F1 score	AUROC	AUPRC
1	12	-1.00 ❄	-0.40 ❄	84.03±1.12	84.71±2.00	82.58±1.36	83.07±1.19	93.14±0.98	93.30±0.95
1	12	-1.00 🔥	-0.40 🔥	83.98±1.14	84.70±2.22	82.42±0.60	83.01±0.88	92.91±1.18	93.09±1.13
1	12	-1.00 ❄	-0.30 ❄	84.05±1.06	84.61±1.59	82.58±1.51	83.09±1.28	92.92±0.78	93.08±0.78
1	12	-1.00 🔥	-0.30 🔥	83.97±1.24	84.45±1.65	82.61±1.74	83.04±1.51	92.91±0.79	93.06±0.79
1	12	-1.00 ❄	-0.20 ❄	85.24±0.88	85.64±1.45	83.77±0.73	84.39±0.83	93.51±0.87	93.67±0.82
1	12	-1.00 🔥	-0.20 🔥	85.19±1.04	85.49±1.37	83.76±0.98	84.35±1.05	93.45±0.89	93.61±0.84
1	12	-1.00 ❄	-0.10 ❄	83.69±1.77	84.82±1.96	81.70±2.22	82.46±2.15	92.87±1.30	93.03±1.28
1	12	-1.00 🔥	-0.10 🔥	83.62±2.13	85.05±1.89	81.46±2.78	82.27±2.63	92.81±1.47	92.96±1.46
1	12	-1.00 ❄	0.10 ❄	84.25±1.76	84.32±2.16	82.92±1.65	83.42±1.79	92.53±1.45	92.65±1.46
1	12	-1.00 🔥	0.10 🔥	84.33±1.73	84.54±2.03	82.88±1.72	83.45±1.80	92.63±1.45	92.74±1.46
1	12	-1.00 ❄	0.20 ❄	82.74±1.78	83.24±1.66	80.88±2.12	81.57±2.03	91.24±1.56	91.40±1.55
1	12	-1.00 🔥	0.20 🔥	82.21±1.51	82.63±1.77	80.39±1.64	81.04±1.63	90.98±1.67	91.05±1.76
1	12	-1.00 ❄	0.30 ❄	80.52±2.72	80.56±3.10	79.14±2.51	79.49±2.72	89.65±2.26	89.66±2.42
1	12	-1.00 🔥	0.30 🔥	80.64±2.87	80.62±3.13	79.39±2.69	79.68±2.89	89.80±2.23	89.80±2.44
1	12	-1.00 ❄	0.40 ❄	79.37±2.80	79.60±2.74	78.00±2.38	78.26±2.69	88.59±2.08	88.71±2.21
1	12	-1.00 🔥	0.40 🔥	79.55±2.75	79.95±3.15	77.86±2.33	78.30±2.64	88.76±2.13	88.87±2.26
1	12	-1.00 ❄	0.50 ❄	77.61±2.79	78.16±3.04	75.85±2.19	76.17±2.56	86.92±1.93	87.05±2.14
1	12	-1.00 🔥	0.50 🔥	77.75±2.77	78.29±2.93	76.01±2.18	76.33±2.56	87.06±1.87	87.16±2.12
1	12	-1.00 ❄	0.60 ❄	76.59±2.74	76.89±2.96	74.58±2.54	74.97±2.77	85.51±1.86	85.68±2.08
1	12	-1.00 🔥	0.60 🔥	76.80±2.77	77.22±3.10	74.67±2.60	75.11±2.83	85.64±1.94	85.82±2.16
1	12	-1.00 ❄	0.70 ❄	74.58±1.66	75.08±1.90	72.82±1.73	72.87±1.76	83.55±0.69	83.69±0.95
1	12	-1.00 🔥	0.70 🔥	74.14±2.41	75.06±1.99	72.17±3.45	72.02±3.77	83.26±1.57	83.38±1.80
1	12	-1.00 ❄	0.80 ❄	72.86±0.93	73.07±1.82	70.88±1.55	70.94±1.47	81.88±0.69	81.97±0.94
1	12	-1.00 🔥	0.80 🔥	72.38±1.91	72.81±1.18	70.22±3.39	70.05±3.82	81.26±1.44	81.39±1.58
1	12	-1.00 ❄	0.90 ❄	72.69±1.54	72.52±1.88	70.35±1.86	70.63±1.91	80.94±1.12	81.00±1.17
1	12	-1.00 🔥	0.90 🔥	72.30±1.19	72.15±1.49	69.91±1.78	70.14±1.79	80.65±1.03	80.73±1.06
1	12	-1.00 ❄	1.00 ❄	72.82±1.82	72.76±1.85	70.16±2.39	70.48±2.47	80.34±1.35	80.52±1.41
1	12	-1.00 🔥	1.00 🔥	72.30±2.14	72.34±2.32	69.73±2.70	69.93±2.98	79.28±2.79	79.61±2.69
1	12	-0.90 ❄	-1.00 ❄	82.81±2.69	83.16±3.15	81.99±2.68	82.04±2.64	91.96±2.05	92.09±2.05
1	12	-0.90 🔥	-1.00 🔥	84.29±1.64	83.94±1.78	83.60±1.85	83.68±1.73	92.44±1.44	92.58±1.41
1	12	-0.90 ❄	-0.90 ❄	84.19±1.82	84.06±2.20	83.58±1.73	83.60±1.78	92.65±1.14	92.73±1.19
1	12	-0.90 🔥	-0.90 🔥	84.12±1.68	84.03±2.13	83.37±1.63	83.48±1.64	92.39±1.34	92.52±1.33
1	12	-0.90 ❄	-0.80 ❄	84.10±1.29	84.81±2.47	82.86±1.63	83.21±1.28	93.24±1.59	93.30±1.67
1	12	-0.90 🔥	-0.80 🔥	84.47±1.62	84.60±2.31	83.65±1.61	83.80±1.57	93.11±1.30	93.18±1.39
1	12	-0.90 ❄	-0.70 ❄	84.56±1.58	85.14±2.61	83.39±1.79	83.74±1.57	92.90±1.45	93.07±1.46
1	12	-0.90 🔥	-0.70 🔥	84.51±2.21	84.74±2.93	83.60±2.04	83.82±2.14	92.89±1.70	93.04±1.69
1	12	-0.90 ❄	-0.60 ❄	84.65±2.23	85.00±2.71	83.52±2.45	83.86±2.34	93.03±1.75	93.21±1.71
1	12	-0.90 🔥	-0.60 🔥	85.00±1.91	85.23±2.24	83.81±2.17	84.22±2.04	93.19±1.58	93.34±1.56
1	12	-0.90 ❄	-0.50 ❄	85.51±1.90	85.74±1.89	84.36±2.36	84.74±2.14	93.45±1.53	93.61±1.50
1	12	-0.90 🔥	-0.50 🔥	85.13±1.85	85.42±1.88	83.84±2.27	84.31±2.07	93.20±1.51	93.33±1.42
1	12	-0.90 ❄	-0.40 ❄	85.13±2.39	85.22±2.55	83.93±2.63	84.36±2.56	93.20±1.56	93.33±1.46
1	12	-0.90 🔥	-0.40 🔥	85.55±2.00	85.49±2.36	84.69±2.00	84.92±2.02	93.40±1.36	93.52±1.28
1	12	-0.90 ❄	-0.30 ❄	84.57±1.39	85.00±2.08	83.07±1.20	83.67±1.35	93.11±1.20	93.28±1.14
1	12	-0.90 🔥	-0.30 🔥	83.90±1.33	85.12±1.39	81.87±1.84	82.67±1.66	92.70±0.87	92.85±0.85
1	12	-0.90 ❄	-0.20 ❄	84.49±1.17	84.66±1.76	83.14±0.85	83.66±1.08	92.85±0.96	93.03±0.90
1	12	-0.90 🔥	-0.20 🔥	84.72±1.32	84.68±1.71	83.55±1.11	83.97±1.29	93.13±1.09	93.25±1.04
1	12	-0.90 ❄	-0.10 ❄	83.91±1.50	84.79±1.54	82.10±1.97	82.79±1.81	92.70±1.23	92.86±1.19
1	12	-0.90 🔥	-0.10 🔥	84.15±1.58	84.99±1.58	82.26±1.89	83.03±1.82	92.89±1.28	93.00±1.24
1	12	-0.90 ❄	0.10 ❄	84.04±1.85	84.19±1.99	82.61±1.99	83.14±1.99	92.08±1.52	92.21±1.55
1	12	-0.90 🔥	0.10 🔥	83.41±2.31	83.47±2.29	81.95±2.59	82.47±2.51	91.81±1.88	91.93±1.93
1	12	-0.90 ❄	0.20 ❄	81.77±2.66	81.92±2.74	80.48±2.58	80.81±2.71	90.51±2.00	90.50±2.17
1	12	-0.90 🔥	0.20 🔥	80.66±1.85	80.78±1.60	79.51±2.69	79.64±2.31	89.94±1.79	89.97±1.88
1	12	-0.90 ❄	0.30 ❄	80.22±2.29	80.42±2.57	78.60±2.23	79.04±2.34	89.09±2.03	89.06±2.27

Continued on next page

t	n	a	b	Accuracy	Precision	Recall	F1 score	AUROC	AUPRC
1	12	-0.90 🔥	0.30 🔥	80.24±2.39	80.57±2.60	78.68±2.22	79.07±2.39	89.24±2.15	89.19±2.41
1	12	-0.90 ❄️	0.40 ❄️	78.23±3.06	78.77±2.11	76.39±4.18	76.58±4.21	87.60±2.29	87.70±2.39
1	12	-0.90 🔥	0.40 🔥	78.21±3.00	78.94±2.08	76.13±4.20	76.41±4.14	87.42±2.65	87.53±2.74
1	12	-0.90 ❄️	0.50 ❄️	77.44±2.18	77.78±2.37	75.35±2.23	75.82±2.33	86.03±1.63	86.14±1.89
1	12	-0.90 🔥	0.50 🔥	76.73±2.99	77.57±2.51	74.30±3.78	74.64±4.06	85.69±2.08	85.84±2.31
1	12	-0.90 ❄️	0.60 ❄️	76.27±2.64	76.83±2.90	74.00±2.56	74.42±2.76	84.85±1.71	84.99±1.96
1	12	-0.90 🔥	0.60 🔥	75.74±2.75	76.63±2.59	73.23±3.24	73.55±3.53	84.34±1.82	84.46±2.11
1	12	-0.90 ❄️	0.70 ❄️	75.22±2.41	75.97±2.68	72.67±2.36	73.07±2.61	83.65±1.55	83.67±1.87
1	12	-0.90 🔥	0.70 🔥	74.03±1.66	74.65±2.27	71.90±1.85	72.03±1.81	83.04±0.82	82.99±1.05
1	12	-0.90 ❄️	0.80 ❄️	73.00±1.76	73.29±2.36	70.68±1.86	70.87±1.92	81.77±0.94	81.75±1.20
1	12	-0.90 🔥	0.80 🔥	73.11±1.55	73.26±2.04	70.86±1.66	71.07±1.69	81.76±0.93	81.69±1.23
1	12	-0.90 ❄️	0.90 ❄️	73.24±1.86	73.84±2.05	70.25±2.31	70.57±2.50	81.18±1.01	81.02±1.42
1	12	-0.90 🔥	0.90 🔥	72.12±1.04	72.84±2.07	69.16±1.45	69.33±1.54	80.58±0.57	80.50±0.91
1	12	-0.90 ❄️	1.00 ❄️	72.33±1.92	73.19±1.90	68.99±2.68	69.16±2.95	79.75±1.64	79.69±1.81
1	12	-0.90 🔥	1.00 🔥	71.73±2.72	72.00±3.35	68.88±2.88	69.10±3.16	79.28±2.16	79.35±2.25
1	12	-0.80 ❄️	-1.00 ❄️	84.43±1.79	84.12±2.00	83.83±1.94	83.85±1.83	92.42±1.46	92.51±1.44
1	12	-0.80 🔥	-1.00 🔥	84.28±1.52	83.87±1.75	83.75±1.53	83.73±1.52	92.46±1.43	92.51±1.39
1	12	-0.80 ❄️	-0.90 ❄️	83.47±1.22	83.33±1.42	83.08±0.90	82.91±1.05	92.20±0.98	92.28±1.00
1	12	-0.80 🔥	-0.90 🔥	83.87±1.72	83.65±2.13	83.45±1.51	83.34±1.64	92.49±1.40	92.54±1.40
1	12	-0.80 ❄️	-0.80 ❄️	84.07±1.47	83.83±1.68	83.54±1.65	83.49±1.51	92.49±1.19	92.61±1.26
1	12	-0.80 🔥	-0.80 🔥	84.08±1.57	84.21±2.13	83.25±1.69	83.38±1.56	92.63±1.37	92.71±1.43
1	12	-0.80 ❄️	-0.70 ❄️	84.35±1.59	84.69±2.35	83.18±1.55	83.54±1.54	92.81±1.58	92.87±1.68
1	12	-0.80 🔥	-0.70 🔥	84.22±2.03	84.39±2.67	83.07±2.07	83.43±2.04	92.61±1.85	92.76±1.81
1	12	-0.80 ❄️	-0.60 ❄️	84.91±2.08	85.43±2.01	83.42±2.56	83.98±2.35	92.77±1.68	92.97±1.59
1	12	-0.80 🔥	-0.60 🔥	84.65±1.82	84.98±2.11	83.30±2.03	83.80±1.96	92.74±1.63	92.90±1.58
1	12	-0.80 ❄️	-0.50 ❄️	84.33±2.12	85.09±1.94	82.86±2.92	83.33±2.52	92.82±1.78	92.99±1.71
1	12	-0.80 🔥	-0.50 🔥	84.57±1.91	85.18±1.95	83.12±2.52	83.62±2.23	93.02±1.69	93.19±1.63
1	12	-0.80 ❄️	-0.40 ❄️	84.30±1.52	85.33±2.20	82.42±1.70	83.20±1.64	92.90±1.53	93.01±1.44
1	12	-0.80 🔥	-0.40 🔥	84.05±1.41	84.94±2.21	82.42±1.82	83.01±1.57	92.92±1.57	93.05±1.46
1	12	-0.80 ❄️	-0.30 ❄️	84.23±1.66	85.00±1.84	82.54±1.99	83.19±1.89	92.87±1.22	93.03±1.15
1	12	-0.80 🔥	-0.30 🔥	84.30±1.38	85.64±1.53	82.33±2.16	83.10±1.72	93.14±1.40	93.27±1.32
1	12	-0.80 ❄️	-0.20 ❄️	84.46±1.62	85.23±1.53	82.63±1.94	83.39±1.87	92.85±1.15	92.98±1.07
1	12	-0.80 🔥	-0.20 🔥	84.26±1.58	85.56±1.83	82.18±1.88	83.05±1.82	92.96±1.30	93.11±1.25
1	12	-0.80 ❄️	-0.10 ❄️	83.69±0.93	84.36±1.98	81.99±0.32	82.65±0.67	92.33±1.16	92.44±1.28
1	12	-0.80 🔥	-0.10 🔥	83.42±1.18	84.76±1.61	81.21±1.44	82.10±1.39	92.74±0.96	92.85±0.96
1	12	-0.80 ❄️	0.10 ❄️	81.87±1.80	82.34±2.45	80.32±1.48	80.80±1.69	90.48±2.20	90.59±2.21
1	12	-0.80 🔥	0.10 🔥	82.39±1.66	82.48±1.35	80.87±2.25	81.35±1.99	90.82±1.77	90.87±1.86
1	12	-0.80 ❄️	0.20 ❄️	81.33±2.44	81.99±2.04	79.28±3.06	79.92±3.00	90.08±1.91	90.21±1.93
1	12	-0.80 🔥	0.20 🔥	81.08±2.25	81.50±2.14	79.16±2.70	79.76±2.64	89.78±1.94	89.90±1.97
1	12	-0.80 ❄️	0.30 ❄️	80.32±1.87	80.76±2.18	78.45±1.95	79.00±1.98	88.72±1.82	88.61±2.11
1	12	-0.80 🔥	0.30 🔥	79.55±1.02	79.72±1.23	78.22±1.77	78.42±1.32	88.34±1.65	88.22±1.85
1	12	-0.80 ❄️	0.40 ❄️	77.65±3.37	78.93±1.57	75.15±4.83	75.37±5.30	86.89±1.51	87.04±1.63
1	12	-0.80 🔥	0.40 🔥	78.07±2.81	79.33±1.61	75.53±4.00	75.93±4.22	87.00±1.53	87.14±1.61
1	12	-0.80 ❄️	0.50 ❄️	77.51±2.91	78.32±3.86	75.04±2.90	75.65±3.12	86.13±3.08	86.21±3.24
1	12	-0.80 🔥	0.50 🔥	77.33±2.74	77.67±2.78	75.09±3.15	75.59±3.17	85.76±2.27	85.88±2.52

J.2 GENERALIZABILITY OF HYPERPARAMETERS

We transfer the key hyperparameters obtained from HM-BiTCN—such as the fusion coefficients (a, b), and segment length (n)—to other baseline models. This experiment evaluates whether these hyperparameters retain effectiveness when applied to different architectures, indicating their robustness and broader applicability.

Table 15: **Results of Subject-Independent Setup.** Green cells indicate performance improvement with CIF.

Datasets	Models	Accuracy	Precision	Recall	F1 score	AUROC	AUPRC
APAVA (2-Classes) Reproduced	Autoformer	73.18±7.33	73.87±6.72	73.01±6.10	72.40±7.03	81.64±7.24	81.10±7.75
	Autoformer + CIF	75.96±2.68	76.33±3.47	75.11±1.10	74.97±1.90	83.42±1.99	83.15±2.63
	Crossformer	72.76±2.04	79.64±2.45	67.41±2.62	66.88±3.61	71.81±4.06	71.64±3.74
	Crossformer + CIF	82.32±2.60	85.35±1.83	79.21±3.17	80.29±3.30	90.39±1.58	90.02±1.47
	FEDformer	75.16±1.67	74.98±0.69	73.34±2.97	73.50±2.90	83.89±1.54	83.27±1.62
	FEDformer + CIF	77.20±2.17	76.97±2.07	77.02±2.60	76.55±2.40	86.70±1.73	86.53±1.76
	Informer	72.20±2.78	73.92±4.80	68.48±2.51	68.74±2.70	70.14±3.43	70.84±3.80
	Informer + CIF	79.78±2.07	82.29±3.03	76.55±2.05	77.53±2.23	78.56±1.33	78.58±1.14
	iTransformer	74.55±1.66	74.77±2.10	71.76±1.72	72.30±1.79	85.59±1.55	84.39±1.57
	iTransformer + CIF	74.95±0.87	74.40±0.75	73.79±1.78	73.81±1.43	84.30±0.88	82.49±0.96
	MTST	69.24±1.24	75.87±2.80	63.28±1.81	61.62±2.75	66.09±3.27	68.08±2.93
	MTST + CIF	76.20±2.39	81.46±1.11	71.67±3.06	72.06±3.73	77.65±3.37	77.98±2.73
	Nonformer	71.81±4.20	71.31±4.40	70.15±3.38	70.38±3.74	71.54±2.73	72.79±2.50
	Nonformer + CIF	71.89±3.81	71.80±4.58	69.44±3.56	69.74±3.84	70.55±2.96	70.78±4.08
	Reformer	78.42±2.85	80.89±4.52	75.20±2.28	76.09±2.54	75.48±2.79	77.52±2.64
	Reformer + CIF	81.51±0.57	**84.90±0.86**	78.18±0.60	79.32±0.64	79.10±2.50	80.77±2.21
	Transformer	75.53±4.28	76.90±5.05	72.14±4.87	72.64±5.44	72.30±6.04	73.04±7.15
	Transformer + CIF	77.96±2.82	79.34±3.86	75.07±2.52	75.87±2.73	74.75±1.62	74.76±2.33
	Medformer	77.85±2.42	80.31±3.21	74.38±2.49	75.21±2.67	80.85±3.80	81.62±3.24
	Medformer + CIF	81.06±1.58	82.97±2.23	78.26±1.52	79.23±1.65	85.74±1.85	86.32±1.48
	MedGNN	77.40±5.77	82.77±4.46	73.24±7.06	73.29±9.01	81.31±2.94	82.80±2.91
	MedGNN + CIF	81.02±1.51	84.21±2.62	77.76±1.52	78.83±1.64	86.27±2.79	87.45±2.40
	HM-BiTCN	82.49±1.40	82.38±1.79	81.20±1.32	81.60±1.39	91.10±1.63	91.30±1.71
	HM-BiTCN + CIF	**85.16±1.55**	84.76±1.62	**85.33±1.27**	**84.82±1.49**	**94.06±1.07**	**94.21±0.99**

Table 16: **Results of Subject-Independent Setup.** Green cells indicate performance improvement with CIF.

Datasets	Models	Accuracy	Precision	Recall	F1 score	AUROC	AUPRC
TDBrain (2-Classes) Reproduced	Autoformer	90.38±3.03	91.16±2.42	90.38±3.03	90.31±3.09	95.83±2.14	95.43±2.31
	Autoformer + CIF	**93.42±2.49**	**93.71±2.27**	**93.42±2.49**	**93.40±2.51**	97.46±1.08	97.21±1.15
	Crossformer	82.15±2.60	82.81±2.11	82.15±2.60	82.04±2.70	91.20±2.23	91.47±2.16
	Crossformer + CIF	89.40±1.26	89.83±1.18	89.40±1.26	89.37±1.27	96.76±0.62	96.80±0.62
	FEDformer	77.60±1.23	78.25±1.52	77.60±1.23	77.48±1.19	86.31±1.23	86.48±1.36
	FEDformer + CIF	78.87±1.94	79.19±2.00	78.88±1.94	78.82±1.94	88.12±1.87	88.39±1.92
	Informer	88.42±2.99	89.01±2.45	88.42±2.99	88.36±3.05	96.54±0.90	96.66±0.85
	Informer + CIF	89.38±1.66	89.71±1.37	89.38±1.66	89.35±1.68	96.92±0.66	97.03±0.64
	iTransformer	74.69±1.02	74.76±1.04	74.69±1.02	74.67±1.02	83.35±1.24	83.65±1.41
	iTransformer + CIF	72.79±1.12	72.89±1.16	72.79±1.12	72.76±1.11	81.08±1.03	81.31±0.93
	MTST	77.67±3.58	78.97±4.37	77.67±3.58	77.45±3.55	86.47±4.84	84.99±6.43
	MTST + CIF	87.21±1.99	87.30±2.06	87.21±1.99	87.20±1.99	94.14±1.83	93.24±2.63
	Nonformer	88.10±2.39	88.76±1.74	88.10±2.39	88.04±2.47	96.56±0.91	96.36±1.21
	Nonformer + CIF	88.00±2.06	88.91±1.68	88.00±2.06	87.92±2.12	97.10±1.10	97.17±1.09
	PatchTST	77.98±2.64	79.30±3.73	77.98±2.64	77.76±2.65	86.67±4.03	84.93±5.47
	PatchTST + CIF	79.58±0.86	80.22±0.82	79.58±0.86	79.47±0.88	87.20±1.57	85.81±1.17
	Reformer	88.50±2.30	89.01±1.80	88.50±2.30	88.45±2.35	96.10±0.63	96.19±0.55
	Reformer + CIF	89.08±1.19	89.47±0.70	89.08±1.19	89.05±1.23	96.88±0.35	97.00±0.35
	Transformer	85.13±1.86	86.39±1.56	85.13±1.86	84.99±1.93	95.61±1.05	95.63±0.91
	Transformer + CIF	89.96±1.57	90.53±1.26	89.96±1.57	89.92±1.60	97.73±0.45	97.77±0.46
	Medformer	88.77±1.24	88.91±1.11	88.77±1.24	88.76±1.25	96.38±0.34	96.44±0.30
	Medformer + CIF	90.88±0.87	90.94±0.81	90.88±0.87	90.87±0.87	97.39±0.30	97.46±0.28
	HM-BiTCN	84.90±2.60	86.02±2.00	84.90±2.60	84.76±2.74	93.94±1.92	94.20±1.85
	HM-BiTCN + CIF	93.13±1.41	93.33±1.37	93.13±1.41	93.12±1.42	**98.62±0.66**	**98.68±0.63**

Table 17: **Results of Subject-Independent Setup.** Green cells indicate performance improvement with CIF.

Datasets	Models	Accuracy	Precision	Recall	F1 score	AUROC	AUPRC
ADFTD (3-Classes) Reproduced	Autoformer	46.90±2.89	45.59±2.37	44.91±2.23	44.34±2.52	63.49±2.44	45.63±2.29
	Autoformer + CIF	45.92±2.78	44.81±2.44	44.66±2.25	44.26±2.38	62.69±2.21	44.93±2.68
	Crossformer	50.18±1.97	45.97±1.84	46.30±1.73	45.90±1.84	66.68±1.67	48.65±1.89
	Crossformer + CIF	54.58±1.22	47.85±0.67	48.96±0.89	48.22±0.72	69.10±1.05	52.23±0.98
	FEDformer	45.75±0.78	45.71±1.29	44.27±1.28	43.51±1.00	62.64±1.64	45.88±1.35
	FEDformer + CIF	48.63±1.99	46.97±1.58	46.87±1.63	46.69±1.54	65.56±2.14	48.30±2.30
	Informer	48.42±1.99	46.94±1.60	46.41±0.99	45.76±0.43	65.99±1.14	47.49±1.07
	Informer + CIF	50.12±0.66	47.23±0.47	46.77±0.39	46.62±0.38	65.13±0.52	46.84±0.54
	iTransformer	52.85±1.36	46.97±1.05	47.31±1.03	46.84±0.78	67.46±0.96	49.90±0.89
	iTransformer + CIF	50.76±0.50	47.11±0.67	47.29±0.59	47.10±0.66	67.00±0.55	49.60±0.69
	MTST	45.77±1.70	44.39±1.73	43.70±1.82	43.36±1.98	61.38±1.57	44.01±1.60
	MTST + CIF	46.36±0.93	45.04±0.65	45.47±0.88	44.87±0.81	63.57±1.24	47.35±1.36
	Nonformer	50.81±1.06	48.71±1.40	48.55±1.47	48.36±1.38	66.95±1.54	48.08±1.82
	Nonformer + CIF	51.81±2.11	49.93±0.81	49.66±0.36	49.10±0.57	68.59±0.60	50.44±0.94
	Reformer	51.28±2.60	49.68±2.75	49.64±2.02	48.45±2.06	69.20±2.53	51.74±3.24
	Reformer + CIF	52.50±0.91	52.10±2.91	49.01±2.74	47.53±4.23	68.25±1.79	50.44±2.59
	Transformer	50.53±0.94	49.31±0.87	48.57±1.23	48.42±1.28	67.98±0.90	49.07±1.35
	Transformer + CIF	52.84±2.50	51.27±2.33	51.53±2.37	51.10±2.21	70.25±2.42	52.35±2.94
	Medformer	53.70±1.18	51.51±1.32	50.49±1.48	50.35±1.53	70.48±1.17	50.91±1.13
	Medformer + CIF	55.88±0.82	51.91±1.90	50.80±1.63	50.29±1.92	70.45±1.33	53.73±1.70
	MedGNN	50.22±3.21	48.65±3.72	47.50±4.57	47.33±4.40	67.18±4.39	48.84±4.11
	MedGNN + CIF	54.89±1.23	51.57±1.57	51.46±1.68	50.85±2.05	71.98±1.59	53.89±1.73
	HM-BiTCN	52.05±2.22	50.45±3.00	50.40±2.55	49.48±2.70	69.43±2.84	50.99±3.15
	HM-BiTCN + CIF	**58.56±0.93**	**55.65±0.81**	**55.86±0.79**	**55.42±0.82**	**76.07±0.59**	**59.75±0.67**

Table 18: **Results of Subject-Independent Setup.** Green cells indicate performance improvement with CIF.

Datasets	Models	Accuracy	Precision	Recall	F1 score	AUROC	AUPRC
PTB (2-Classes)	**Autoformer**	71.99±2.74	69.60±3.85	61.50±4.23	61.43±5.07	74.29±1.89	70.26±2.00
	Autoformer + CIF	77.71±0.63	77.15±1.29	70.32±1.62	71.77±1.60	81.20±4.15	78.13±4.80
	Crossformer	78.06±3.44	81.53±3.13	68.62±5.63	69.76±6.53	88.31±2.07	85.81±2.43
	Crossformer + CIF	84.55±4.80	85.96±3.63	78.64±7.49	80.25±7.89	92.17±2.99	91.16±3.70
	FEDformer	74.54±2.27	77.99±4.10	63.14±3.29	63.28±4.36	84.63±4.27	80.91±5.55
	FEDformer + CIF	77.93±1.86	80.65±3.50	68.59±2.20	70.23±2.63	86.00±3.51	83.42±4.76
	Informer	79.59±0.65	83.33±0.77	70.58±0.95	72.58±1.08	92.77±0.48	90.89±0.57
	Informer + CIF	83.63±2.32	85.31±1.80	77.28±3.67	79.37±3.45	93.87±0.48	92.29±0.63
	iTransformer	83.43±1.19	88.06±1.47	75.64±1.55	78.29±1.70	91.38±1.41	91.08±1.30
	iTransformer + CIF	81.62±2.96	87.48±2.03	72.74±4.41	74.99±4.91	90.25±3.29	89.80±3.28
	MTST	75.53±2.45	78.72±1.87	64.78±4.06	65.30±4.81	87.76±4.09	83.60±3.92
	MTST + CIF	81.80±1.60	84.19±2.05	74.28±2.05	76.52±2.25	91.30±2.48	88.41±3.30
	Nonformer	78.93±1.46	82.48±1.53	69.68±2.15	71.50±2.56	90.54±0.59	87.78±1.46
	Nonformer + CIF	71.89±3.81	71.80±4.58	69.44±3.56	69.74±3.84	70.55±2.96	70.78±4.08
	PatchTST	75.28±2.44	77.05±2.44	64.86±4.05	65.41±5.28	88.11±2.59	82.65±2.87
	PatchTST + CIF	80.80±1.90	82.46±1.75	73.23±2.81	75.24±2.95	92.45±0.91	88.23±1.61
	Reformer	78.11±1.65	82.70±0.80	68.17±2.68	69.68±3.34	90.77±1.56	88.14±1.20
	Reformer + CIF	81.95±2.09	84.63±1.07	74.44±3.53	76.55±3.64	93.36±0.87	91.53±1.05
	Transformer	76.43±1.98	81.25±1.15	65.64±3.29	66.44±4.39	90.21±1.24	87.28±1.49
	Transformer + CIF	78.80±2.44	82.45±2.36	69.42±3.62	71.10±4.33	92.50±1.17	89.07±1.39
	Medformer	80.99±0.75	83.01±0.72	73.35±1.16	75.47±1.21	93.10±1.18	90.69±1.04
	Medformer + CIF	78.74±0.64	81.11±0.84	75.40±0.66	76.31±0.71	83.20±0.91	83.66±0.92
	HM-BiTCN	81.87±1.87	86.50±1.24	73.49±2.90	75.84±3.20	94.20±0.29	93.04±0.45
	HM-BiTCN + CIF	**88.29±1.45**	**90.66±1.48**	**83.21±2.02**	**85.59±1.96**	**94.28±0.93**	**93.78±1.11**

During the process of transferring the optimized CIF hyperparameter configurations from the HM-BiTCN architecture to other model structures, we observed significant improvements in performance across most models and evaluation metrics. This result strongly demonstrates that the CIF module not only exhibits high generalizability but also possesses well-transferable hyperparameters that can be effectively adapted to various architectures. These hyperparameters enhance feature extraction and representation capabilities across different model designs. This finding further highlights the potential of the CIF architecture in diverse tasks and provides valuable insights for future model design and parameter sharing.

J.3 Fine-tuning Transferred Parameters

For models where the transferred hyperparameters from HM-BiTCN do not yield optimal results, we perform additional fine-tuning. This step investigates the adaptability of CIF-related parameters and explores how they can be optimized for other model structures.

Table 19: **Results of Subject-Independent Setup.** Green cells indicate performance improvement with CIF.

Datasets	Models	Accuracy	Precision	Recall	F1 score	AUROC	AUPRC
TDBrain (2-Classes) Reproduced	iTransformer	74.69±1.02	74.76±1.04	74.69±1.02	74.67±1.02	83.35±1.24	83.65±1.41
	iTransformer + CIF(HM-BiTCN)	72.79±1.12	72.89±1.16	72.79±1.12	72.76±1.11	81.08±1.03	81.31±0.93
	iTransformer + CIF(New)	76.10±0.76	76.16±0.75	76.10±0.76	76.09±0.76	84.79±1.15	85.13±1.11
	Nonformer	88.10±2.39	88.76±1.74	88.10±2.39	88.04±2.47	96.56±0.91	96.36±1.21
	Nonformer + CIF(HM-BiTCN)	88.00±2.06	88.91±1.68	88.00±2.06	87.92±2.12	97.10±1.10	97.17±1.09
	Nonformer + CIF (New)	88.67±1.30	89.34±0.93	88.67±1.30	88.61±1.33	96.89±0.31	96.91±0.37

Table 20: **Results of Subject-Independent Setup.** Green cells indicate performance improvement with CIF.

Datasets	Models	Accuracy	Precision	Recall	F1 score	AUROC	AUPRC
ADFTD (3-Classes) Reproduced	Autoformer	46.90±2.89	45.59±2.37	44.91±2.23	44.34±2.52	63.49±2.44	45.63±2.29
	Autoformer + CIF((HM-BiTCN))	45.92±2.78	44.81±2.44	44.66±2.25	44.26±2.38	62.69±2.21	44.93±2.68
	Autoformer + CIF(New)	48.49±1.31	46.42±1.07	45.39±1.80	44.94±1.97	63.75±1.46	46.10±1.84
	iTransformer	52.85±1.36	46.97±1.05	47.31±1.03	46.84±0.78	67.46±0.96	49.90±0.89
	iTransformer + CIF(HM-BiTCN)	50.76±0.50	47.11±0.67	47.29±0.59	47.10±0.66	67.00±0.55	49.60±0.69
	iTransformer + CIF(New)	53.93±1.52	48.44±0.89	49.13±1.17	48.56±0.84	68.70±0.94	50.88±1.20
	Reformer	51.28±2.60	49.68±2.75	49.64±2.02	48.45±2.06	69.20±2.53	51.74±3.24
	Reformer + CIF(HM-BiTCN)	52.50±0.91	52.10±2.91	49.01±2.74	47.53±4.23	68.25±1.79	50.44±2.59
	Reformer + CIF(New)	53.11±1.71	52.14±1.42	52.42±1.90	51.73±2.01	70.47±1.64	51.88±1.92
	Medformer	53.70±1.18	51.51±1.32	50.49±1.48	50.35±1.53	70.48±1.17	50.91±1.13
	Medformer + CIF(HM-BiTCN)	55.88±0.82	51.91±1.90	50.80±1.63	50.29±1.92	70.45±1.33	53.73±1.70
	Medformer + CIF(New)	55.21±1.42	52.84±2.36	52.60±2.26	52.43±2.65	72.11±2.42	54.10±3.09

Table 21: **Results of Subject-Independent Setup.** Green cells indicate performance improvement with CIF.

Datasets	Models	Accuracy	Precision	Recall	F1 score	AUROC	AUPRC
PTB (2-Classes) Reproduced	iTransformer	83.43±1.19	88.06±1.47	75.64±1.55	78.29±1.70	91.38±1.41	91.08±1.30
	iTransformer + CIF(HM-BiTCN)	81.62±2.96	87.48±2.03	72.74±4.41	74.99±4.91	90.25±3.29	89.80±3.28
	iTransformer + CIF(New)	83.56±1.15	86.00±1.03	76.78±1.94	79.10±1.87	90.40±0.75	89.80±0.93
	Nonformer	78.93±1.46	82.48±1.53	69.68±2.15	71.50±2.56	90.54±0.59	87.78±1.46
	Nonformer + CIF(HM-BiTCN)	71.89±3.81	71.80±4.58	69.44±3.56	69.74±3.84	70.55±2.96	70.78±4.08
	Nonformer + CIF(New)	80.46±2.20	84.22±2.44	71.79±3.10	73.89±3.50	92.74±0.97	90.30±1.26
	Medformer	80.99±0.75	83.01±0.72	73.35±1.16	75.47±1.21	93.10±1.18	90.69±1.04
	Medformer + CIF(HM-BiTCN)	78.74±0.64	81.11±0.84	75.40±0.66	76.31±0.71	83.20±0.91	83.66±0.92
	Medformer + CIF(New)	83.98±0.81	85.21±0.62	78.00±1.30	80.11±1.22	93.32±0.97	90.97±1.69

For models that did not initially benefit from the direct transfer of CIF hyperparameters optimized for HM-BiTCN, we conducted further fine-tuning of the key CIF parameters. The results demonstrate that, after targeted adjustment, these models also achieved notable performance improvements. This process not only reinforces the adaptability of the CIF architecture across diverse models but also highlights the high tunability and flexibility of its hyperparameters. By appropriately modifying the number of selected channels, fusion direction, and scaling factors, as shown in Tables 15, 16, 17, 18 and Figures 11, 12, 13, 14, CIF can be effectively tailored to different network structures, thereby maximizing its strengths in feature modeling and discriminative capability.

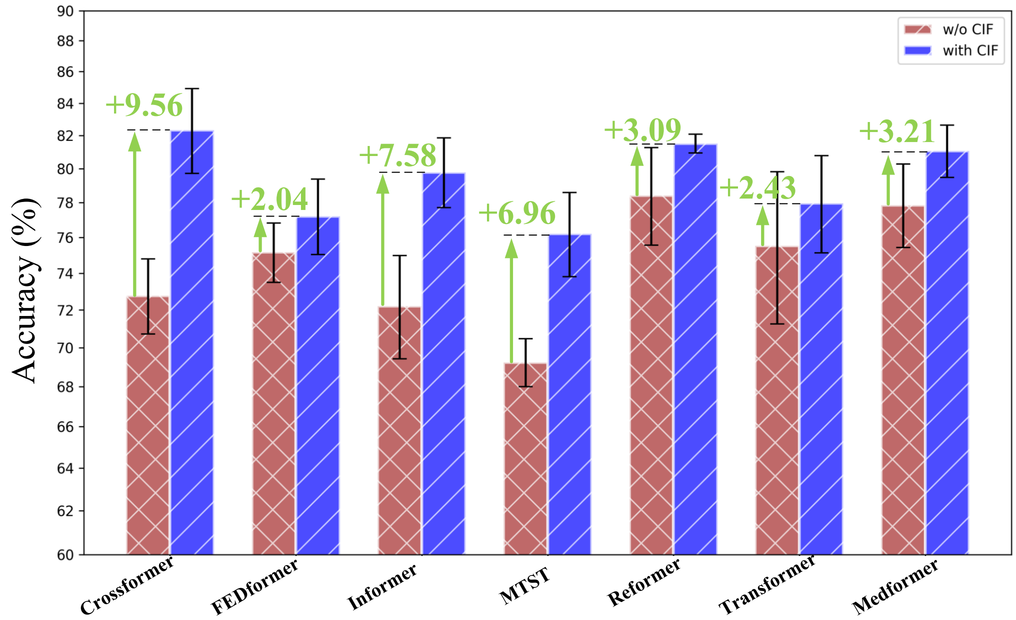

Figure 11: Performance improvement on the APAVA dataset using the CIF method.

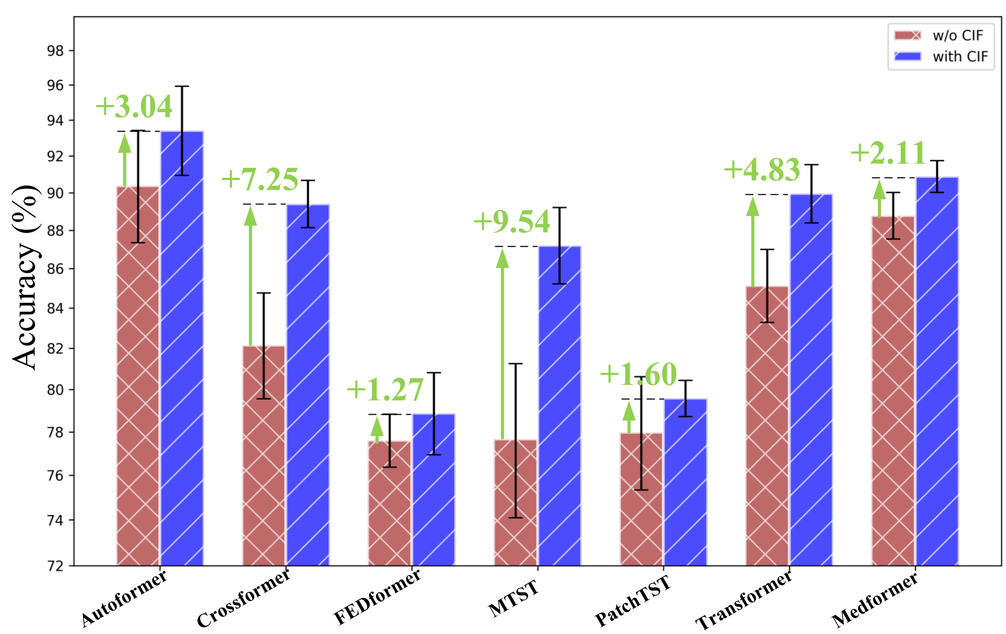

Figure 12: Performance improvement on the TDBRAIN dataset using the CIF method.

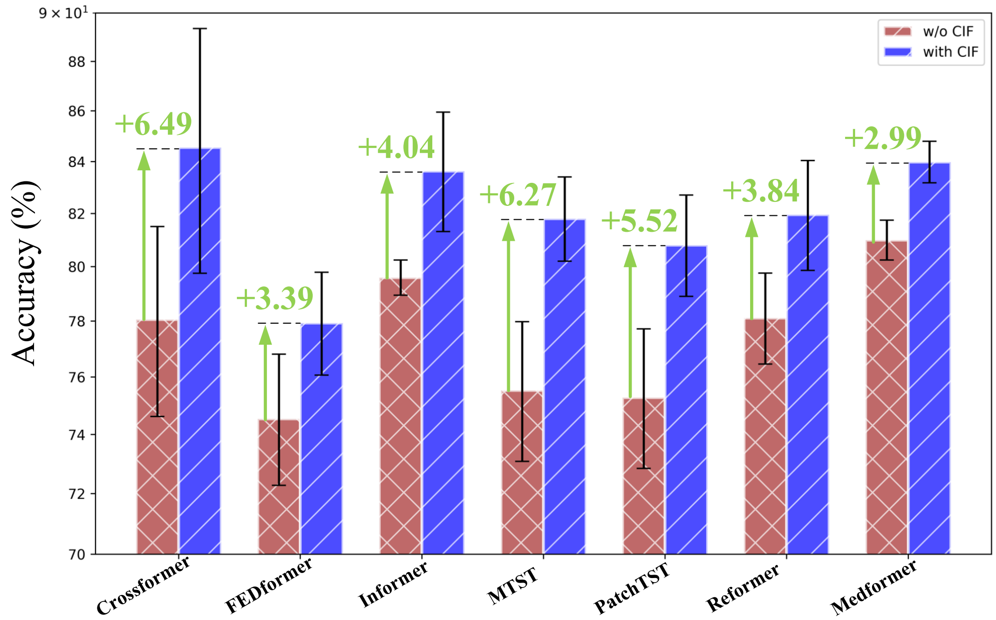

Figure 13: Performance improvement on the PTB dataset using the CIF method.

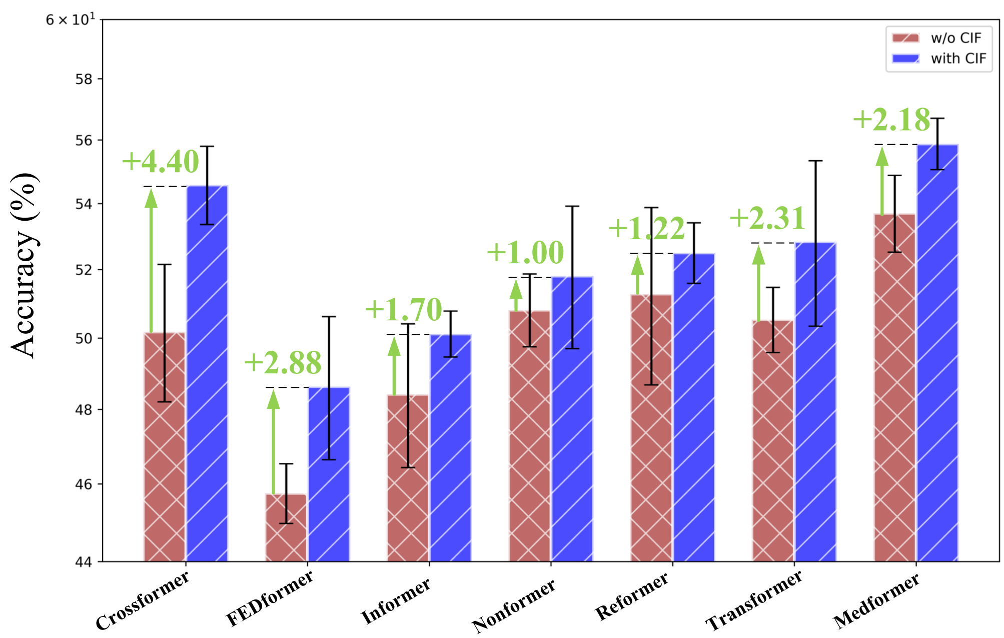

Figure 14: Performance improvement on the ADFTD dataset using the CIF method.

K LIMITATIONS AND FUTURE WORK

Limitations:

Biomedical time series exhibit complex modal characteristics, which lead to significant efficiency bottlenecks when manually adjusting the prior parameters (t, n, a, b) with clear medical interpretations in the CIF model based on empirical experience. This limitation highlights the urgent need for developing novel automated hyperparameter optimization frameworks.

Future Work:

We plan to explore a more universal and generalizable time-series analysis approach, incorporating domain knowledge, structural modeling, and automated hyperparameter optimization. This integration should foster both deeper theoretical insights and stronger practical applicability, providing robust solutions for real-world medical problems.

Furthermore, incorporating domain-specific prior knowledge into medical time-series analysis can more precisely reveal and model relationships between channels. By integrating medical expertise, clinical experience, and existing pathological data, the interpretability and predictive performance of models can be enhanced, thereby supporting clinical decision-making and interventions. On this basis, frequency-domain analysis Hu et al. (2025); Nason & Sachs (1999); Yi et al. (2025) offers an additional perspective: by applying Fourier transform or wavelet decomposition to the signals, physiological features at different frequency components can be identified, revealing patterns that are difficult to capture in the time domain. This is particularly valuable for noise reduction, extraction of periodic signals, and detection of pathological events, and can also provide richer feature representations for model inputs. Future research could further explore how to combine time-domain and frequency-domain information, integrating domain priors to improve the accuracy and robustness of intelligent medical analytics.

Finally, we must acknowledge that the development trends in the field of artificial intelligence highlight the importance of architectural innovation. Future research should focus on designing novel architectures that align more closely with the CIF method, combining the strengths of existing models. For example, the local feature extraction capabilities of CNNs LeCun et al. (1989), the temporal stability of TCNs Bai et al. (2018) for long sequences, the long-term dependency modeling of RNNs Rumelhart et al. (1986) and LSTMs Hochreiter & Schmidhuber (1997), the global modeling efficiency of Transformers Vaswani et al. (2017), the resource-efficient computation of Mamba Gu & Dao (2023), and the hybrid recurrence-attention structure of RWKV Peng et al. (2023). By adapting and integrating these methods, we aim to build a powerful model that is not only deeply compatible with the CIF framework but also capable of efficiently handling complex medical time-series data.

L BROADER IMPACTS

In this study, we take the first step toward a paradigm shift in medical time-series analysis, transitioning from a focus on model architecture improvements to emphasizing the intrinsic structure of the data. Our experimental results, which outperform several state-of-the-art methods across multiple datasets, validate the effectiveness of this approach. We emphasize that uncovering the essential characteristics in medical time-series data is a valuable research direction, particularly given the critical need for model interpretability in medical applications. However, practitioners should be cognizant of the method's limitations.